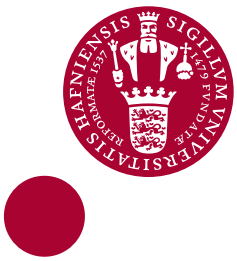

Structural Investigation of Photosynthetic Membrane Using Small-Angle Scattering

Jakubauskas, Dainius

Publication date:
2018

Document version
Publisher's PDF, also known as Version of record

UNIVERSITY OF COPENHAGEN
FACULTY OF SCIENCE

Dainius Jakubauskas

X-ray and neutron science
Niels Bohr Institute

Structural investigation of photosynthetic membranes using small-angle scattering

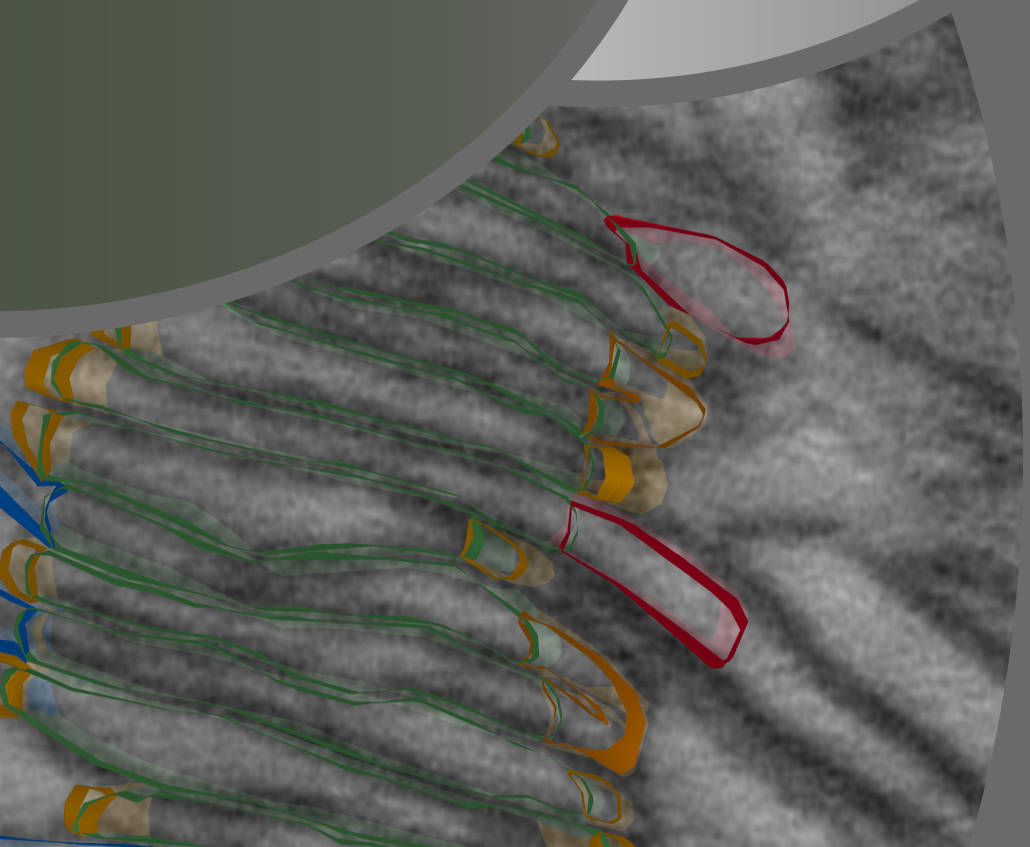

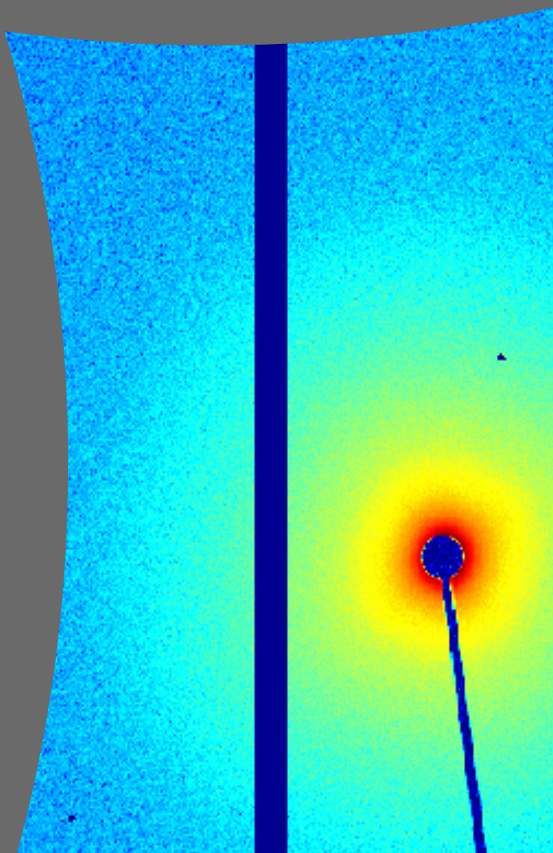

Structural investigation of photosynthetic membranes using small-angle scattering

Dainius Jakubauskas

X-ray and Neutron Science group, Niels Bohr Institute

Photosynthesis and Synthetic Biology group, Department of Plant and Environmental Sciences

University of Copenhagen

Dissertātiō quam in Facultas Naturalis Universitāte Hafniensi ad gradum PhD obtinendum publice defendet Dainius Jakubauskas

June 2018

This PhD thesis has been submitted to the PhD school of The Faculty of Science, University of Copenhagen

Preface

This thesis is submitted as a partial fulfilment of the requirements for the degree of philosophiae doctor (PhD) in Biophysics at the University of Copenhagen. This interdisciplinary doctoral work has been conducted from 2011 to 2018 in both X-ray and Neutron Scattering group (XNS), Niels Bohr Institute and in Photosynthesis and Synthetic Biology group (PLMOL), Department of Plant and Environmental Sciences at the University of Copenhagen under the supervision of professor Kell Mortensen (XNS), associate professor Jacob Judas Kain Kirkensgaard (XNS) and professor Poul Erik Jensen (PLMOL). I acknowledge financial support from the Center of Synethetic biology 'bioSYNergy' funded by the University of Copenhagen for Interdisciplinary research and the Copenhagen Plant Science Center.

Scattering experiments have been performed using our in-house X-ray scattering instrument 'Ganesha' (SAXSlab) and in the large-scale facilities: PETRAIII synchrotron (DESY, Hamburg), an experimental trial has also been performed in ESRF (Grenoble, France). Neutron scattering experiments were performed in Australian Neutron Science and Technology Organization (Sydney, Australia), Paul Scherrer Institute (Willigen, Switzerland) and Jülich Centre for Neutron Science (Munich, Germany). ESS, DanScatt and COST Action CM1101 are acknowledged for financial support.

Plant-based experimental work has been carried out in the photosynthesis group, University of Copenhagen, and in National Deuteration Facility (ANSTO, Sydney) laboratories as well as in the Centre for Carbon, Water and Food, Sydney University Institute of Agriculture (Camden, Sydney, Australia). Wild type cyanobacterial strains have been obtained from Brett Neilan's group, the School of Biotechnology and Biomolecular Sciences, University of New South Wales (Sydney, Australia) and Department of Chemistry and Biomolecular Science, Department of Molecular Sciences, Faculty of Science and Engineering, Macquarie University (Sydney, Australia). Cyanobacterial and plant mutants of CURT1 have been obtained from Plant Molecular biology group, Department of biology, Ludwig-Maximillians-Universität (Munich, Germany). *Arabidopsis thaliana* Col0 plants were obtained from Barry Pogson's group, ARC Centre of Excellence in Plant Energy Biology, Australian National University (Canberra, Australia). *Alocassia macrorhizzos* seedling has been provided by Wah Chow, Research School of Biology, Australian National University (Canberra, Australia). PLB and thylakoid tomography work has been performed in collaboration with Łucja Kowalewska in the Institute of

Experimental Plants Biology, Faculty of Biology, University of Warsaw.

When I started my PhD under the project 'Cubic membranes', the aim was to investigate scattering from prolamellar bodies, to obtain scattering curves in higher resolution and to confirm their cubic nature as well as to determine their space group more precisely by means of modelling and to follow the PLB-thylakoid development. Due to experimental practicalities and low scattering signal (*sic!* which was finally obtained), this gradually turned into a side project, the results of which are presented in Chapter 4. I therefore have shifted focus to thylakoid membrane investigations. Since the isolated thylakoid system is already well studied in different conditions, the main focus was shifted towards thylakoid system investigations *in vivo*. I have used three species of cyanobacteria with different thylakoid ultrastructures as well as high-/ordinary-grana containing plants. The results from this part of PhD work are presented as Manuscripts 1 and 2.

This PhD thesis is divided into two parts. In the first part of the thesis, background knowledge about photosynthesis (Chapter 1) and small angle scattering theory (Chapter 2) are presented. Coming from the biochemistry background, I had to grasp these physical concepts relatively early in the PhD. I therefore assume that scattering introduction is a sufficient primer for a biologist, who would want to expand one's method toolbox with scattering methods. Chapter 3 builds the mathematical apparatus required for modelling in a step-wise matter and derives estimates of scattering length densities of a thylakoid membrane. As I introduce many biological-biochemical assumptions in this work, some of my statements can be considered contradictory and are thus thoroughly evaluated. Furthermore, Chapter 4 contains a compilation of preliminary experimental results on prolamellar bodies and cyanobacterial membrane temperature and light-induced behaviour.

The second part of this PhD thesis contains three manuscripts, presenting and reviewing the results obtained during this PhD. Manuscript 1 presents the model of cyanobacterial scattering and extracts structural parameters of the thylakoid membrane just from the scattering curve. Up to my knowledge, this is the most comprehensive scattering model on biological system *in vivo* to date.

Manuscript 2 extends the modelling of cyanobacterial thylakoids towards higher-plant grana stacks and investigates light-induced thylakoid dynamics by a complex of complementary methods: TEM, CLSM and scattering. Additional experiments, conducted on plants having extensive network of grana stacks are currently performed and modelling scattering curves is in progress.

Manuscript 3 is a review, providing the most up-to-date understanding of scattering from photosynthetic organisms and the underlying biochemistry of ultrastructural changes. This review considers scattering with the underlying mathematical model as a complementary method to biological TEM analysis and discusses biological requirements of a successful scattering experiment. It also presents a concise overview of early scattering works and highlights important issues, regarding the interpretation of scattering data.

Summary

The investigation of ultrastructural development and dynamics of thylakoid membranes can provide a valuable information of photosynthetic organism adaptation in relation to environmental factors and stimuli - e.g. ion concentration, illumination or temperature changes. This knowledge, in perspective, can be employed to increase photosynthetic yield and biomass. Structural studies of thylakoid membrane development and their stacking in chloroplast native environment are most typically performed by means of microscopy. Microscopy, however, only allows capturing 'snapshots' of various dynamical stages. Furthermore, the changes of thylakoid states are of the Ångstrom scale and can appear in a matter of minutes, what makes microscopy analysis a burden.

The other common approach - dynamical studies of isolated thylakoid membranes, is sound biochemically, but such studies contain significantly lower structural information, as thylakoid membranes inherently loose their large-scale order upon isolation. Furthermore, thylakoid membrane stacking *in vitro* is predominantly determined by buffering conditions, therefore an ultrastructural correlation between the thylakoid state *in vitro* and *in vivo* is not straightforward.

In this PhD work, thylakoid stacking and dynamics is investigated *in vivo* by means of small-angle scattering and is correlated to the results of microscopy. Measuring small-angle scattering of cyanobacteria, a relative simple unicellular photosynthetic prokaryote, membrane content of which is 90 % thylakoids, enabled formulating a thylakoid form factor, containing a protein-rich membrane separated by two aqueuous compartments, and ultrastructurally arranged as stacked lamellae. This mathematical model has been implemented in the scattering curve-fitting framework 'WillItFit?', what now enables the fitting of experimental scattering data from photosynthetic organisms. Performing D_2O contrast variation study on cyanobacterial cells *in vivo* strengthens the evidence that scattering peaks origin from both proteins and lipids localized in thylakoid membranes.

Fitting this mathematical model to actual SANS scattering curves in their entirety brought the knowledge about cyanobacterial thylakoid membrane and lumen thicknesses, thylakoid-thylakoid repeat distance and related fitting uncertainty parameters (Manuscript 1). This experiment is, up to my knowledge, the first successful mathematical model application, when the entire scattering curve of a complex photosynthetic organism is investigated and system changes are followed *in vivo*. We are optimistic about, that this

scattering model will be applied in investigation of other photosynthetic organisms - both wild-types and functional thylakoid mutants - with the aim to pinpoint the key actors, governing structural thylakoid reorganization and dynamics in their native environments.

As an additional experiment, I was able to show that thylakoid repeat distance in wild-type cyanobacteria remains stable upon white light illumination up to 200 μmol photons $\cdot m^{-2} \cdot s^{-1}$ during the 1.5 h measurement timeframe. This result supports two previously published findings, that the dark-light thylakoid dynamics in wild type cyanobacterial cells is lower in comparison to thylakoid dynamics in phycobilisome-deficient mutant strains. Furthermore, I show that cyanobacterial thylakoid ultrastructure is impacted in higher temperatures. Scattering experiments suggest that the average thylakoid repeat distance decreases in 50-60 ° C, but that the overall lamellar thylakoid ultrastructure remains intact, this finding is also confirmed by electron microscopy. I hypothesize that the decrease of thylakoid repeat distance is caused by the increase of hydrophobic interactions between adjacent thylakoid membranes.

The knowledge obtained from relatively simple cyanobacterial system has been employed in scattering studies of higher plant thylakoids. I have investigated plants having both the extensive and typical grana systems (Manuscript 2). By extending the methodology of W. Kreutz and W. Menke to SANS experiments on variegated leaves, I have been able to obtain scattering curve of the thylakoid system directly from the plant leaf scattering measurements *in vivo* and to investigate thylakoid dynamics. Although this work is significantly less progressed in terms of scattering data analysis, by comparing scattering curves from dark-adapted and 500 μmol photons $\cdot m^{-2} \cdot s^{-1}$ white light illuminated plants, I show that shade-tolerant plants having high grana exhibit a smaller light-induced decrease of thylakoid repeat distance than plants with a typical grana-stroma thylakoid ultrastructure. This finding is complemented and supported both by transmission electron microscopy and confocal laser scanning microscopy studies of the same plant species in the same experimental conditions.

Overall, the results of this PhD thesis add an important commentary to the ongoing debate, namely that the statement 'lumen contracts/expands upon illumination' cannot be generalized. In my opinion, lumen behaviour is a secondary effect of the underlying biochemistry (which is barely understood), including ion redistribution, and the statement *per se* is only scientifically valid if supplemented with plant species, exact experimental conditions and spectral quality, as several outcomes of thylakoid behaviour have been observed - which all can be complementary and not contradictory. In a way, as the author of this PhD thesis has been living in Denmark for some time, he likes to put the following debate in a literature perspective: 'To shrink, or to expand: that is the question'. In my opinion, this biologically important question cannot be justifiably answered unless all biochemical circumstances and actors are known and accounted for.

Finally, a small angle neutron scattering study of maize prolamellar bodies is provided. Surprisingly, the intensity of scattering signal was low even in isolated and upconcentrated PLBs in 100% D_2O-based buffer, even though the paracrystalline structure of PLB was retained after isolation. Therefore the cubic nature of maize PLBs could not be confirmed

by scattering experiments, only by the electron tomography modelling of etioplasts. Importantly, the q position of a single scattering peak from three biological replicates of isolated etioplasts was consistent, which is promising. Scattering signal from PLBs in etiolated leaves *in vivo* had not been observed, but this 'blank' experiment made possible to directly subtract the biological background scattering from the *Arabidopsis thaliana* leaf, which did not otherwise have a scattering measurement of its variegated equivalent.

Finally, this thesis contains not only the stepwise mathematical derivation of the necessary mathematical apparatus, but also numerous biological considerations on protein volume fractions in different cellular compartments or issues with scattering length density derivations for a complex biological system - and a thorough discussion on their validity and limitations. For this reason, the first part of the thesis includes a concise X-ray and neutron scattering literature study dating back to 1953 - the very first small angle diffraction measurement of plant chloroplasts' A critical review on the development of the photosynthetic organism scattering field, together with a more personal reflection on its perspectives is given as a review (Manuscript 3).

Dansk Resume

Ultrastrukturel udvikling og dynamiske ændringer af thylakoidmembraner i en fotosyntetisk organisme kan tilvejebringe en værdifuld information om tilpasning miljø og stimuli - f.x. ionkoncentration, belysning eller temperaturændringer. Denne viden kan i på sigt anvendes til at øge cyanobakterie, algers og planters udbytte og biomasse. Strukturelle undersøgelser af thylakoidmembranudvikling og deres organisering i naturligt miljø udføres typisk ved hjælp af mikroskopi. Dette giver dog kun mulighed for at se 'snapshots' af de forskellige dynamiske faser. Endvidere er kortvarige ændringer i thylakoidtilstande i Ångstrøm-skala vanskelige at følge og dette gør mikroskopianalysen mindre anvendelig.

En anden almindelig tilgang giver væsentlig lavere strukturel information, da thylakoidmembraner mister deres overordende struktur ved isolation. Desuden bestemmes thylakoidmembran *in vitro* overvejende af buffringsbetingelserne, derfor kan en ultrastrukturel korrelation mellem *in vitro* og *in vivo* thylakoidtilstande ikke sammenlignes.

Dette PhD-arbejde undersøger thylakoid organisering og dynamik *in vivo* ved hjælp af småvinkelspredning og data korreleres med resultaterne fra mikroskopi. Småvinkelsprednings målinger af cyanobakterier, som er relativt simple encellede fotosyntetiske prokaryoter hvor 90 % af membranindholdet udgøres af thylakoider, tillader at formulere en model for thylakoid formfaktor. Modellen indeholder to proteinrige membraner adskilt af

to vandholdige kamre (lumen og inter-thylakoid rum) og membraner er ultrastrukturelt arrangeret som stakkede lameller. Denne matematiske model er implementeret i småvinkelspredningskurve-fitting programmet 'WillItFit?', hvilket gør det muligt at tilpasse og forklare eksperimentelle spredningsdata fra fotosyntetiske organismer. Udførelsen af D_2O kontrastvariantstudier på cyanobakterie celler *in vivo* forstærker beviset for, at spredning opstår fra både proteiner og lipider, som er lokaliseret i thylakoidmembranen.

Tilpasning af denne matematiske model til faktiske SANS-spredningskurver i deres helhed gav viden om thylakoidmembran- og lumentykkelser, thylakoid-thylakoid-gentagelsesafstand og relaterede ultrastrukturelle parametre i cyanobakterier (Manuskript 1). Dette eksperiment er, så vidt vides, den første succesfulde anvendelse af en matematiske model i en undersøgelse af spredningskurven for en kompleks fotosyntetisk organisme og dynamiske systemændringer *in vivo*. Vi mener, at denne spredningsmodel kan anvendes til at undersøge andre fotosyntetiske organismer - både vildtyper og mutanter med ændret thylakoidstruktur, med det formål at identificere de centrale aktører, som styrer reorganisering og dynamik *in vivo*.

Jeg var i stand til at vise, at thylakoid gentagelsesafstand i vildtype cyanobakterier forbliver stabil ved belysning med et hvidt lys op til 200 μmol fotoner $\cdot m^{-2} \cdot s^{-1}$ i løbet af 1,5 timers målingsperiode. Dette resultat understøtter to tidligere publicerede værker, at mørk-lys thylakoiddynamik i vildtype cyanobakterie celler er mindre, sammenlignet med thylakoiddynamik i phycobilisom-manglende cyanobakterie mutanter. Desuden viser jeg, at cyanobakterie thylakoid ultrastruktur er påvirket af høje temperaturer. Spredningseksperimenter tyder på, at den gennemsnitlige thylakoid gentagelsesafstand formindskes i 50-60 ° C, mens den samlede lamellære thylakoid ultrastruktur forbliver intakt. Dette bekræftes også ved elektronmikroskopi, og jeg antager, at gentagelsesafstandsformindskelsen skyldes øgede hydrofobiske interaktioner mellem tilstødende thylakoidmembraner.

Viden, der er opnået fra et relativt simpelt cyanobakterie system, er blevet anvendt i spredningsundersøgelser af thylakoider i højere-planter. Jeg undersøgte planter med både et øget og normalt grana system (Manuskript 2). Ved at udvide W. Kreutz og W. Menkes metodik til SANS-eksperimenter på grønne og variegated blade fra højere planter, har jeg fået en spredningskurve for thylakoidsystemet direkte fra bladmålinger *in vivo*. Selv om dette arbejde er mindre advanceret i spredningsdataanalysen, sammenlignet med spredningskurver fra mørke-tilpassede og hvidt lys af 500 μmol fotoner $\cdot m^{-2} \cdot s^{-1}$ belyste planter, viste undersøgelsen, at thylakoidgentagelsesafstand af belyste skyggetolerante planter skrumper mindre end i planter med normale grana. Dette resultat suppleres og understøttes af både transmissionselektronmikroskopi og konfokal laserscanningsmikroskopi målinger af de samme plantearter under tilsvarende forsøgsbetingelser.

Resultater af denne PhD-afhandling tilføjer derfor vigtig viden til den igangværende diskussion, om hvorvidt udsagnet 'lumen skrumper/udvider ved belysning' kan generaliseres eller ej. Efter min mening er den observerede dynamik en sekundær effekt af den underliggende biokemi. Derfor er udsagnet som sådan kun videnskabeligt gyldig, hvis planteart, eksakte forsøgsbetingelser og lys kvaliteten angives. Forskellige resultater af thylakoiddynamik er observeret gennem tiden - de kan være komplementære, men ikke

nødvendigvis. Forfatteren af denne PhD-afhandling har levet i Danmark i et stykke tid, han ville gerne omformulere den følgende debat med et uddrag fra literatur: 'at skrumpe eller øge, det er spørgsmålet'. Det vigstigste er dog, at dette biologisk vigtige spørgsmål ikke kan forsvarligt besvares, medmindre alle biokemiske tilstande og påvirkinger er kendte.

Endelig beskriver jeg en småvinkelneutronspredningsundersøgelse af majs prolamellarlegemer (PLBer). Overraskende viser dette, at spredningsignalsintensiteten fra prøver med koncentrerede isolerede PLBer i 100 % D_2O-baseret buffer var lav, uanset om parakrystallinske strukturer var bibeholdt efter isolering. Derfor kunne den kubiske natur af majs-PLB ikke bekræftes ved spredningseksperimenter, kun ved elektron-tomografi undersøgelse. Spredningsmålingene viste, at q-positionen af den enkelte spredningspeak fra tre biologiske replikater var konsistent. Spredningssignalet fra PLBer i D_2O-infiltrerede blader *in vivo* blev heller ikke observeret, men dette 'blanke' eksperiment muliggjorde at trække en biologisk baggrundsspredning direkte fra *Arabidopsis thaliana* blade, som ikke ellers havde en spredningsmåling af en variegated ækvivalent.

Denne afhandling indeholder udover en trinvis matematisk afledning af en nødvendig teori, men også adskillige biologiske overvejelser - fra proteinvolumenfraktioner i forskellige cellulære rum til problemer med beregning en spredninglængdendensitet for et komplekst biologisk system, samt en grundig diskussion om deres gyldighedsgrænser. Derfor indeholder den første del af afhandlingen en kortfattet røntgen- og neutronspredningslitteraturstudie, som starter i 1953 - fra den allerførste 'småvinkeldiffraktionsmåling af plantekloroplaster'. En kritisk gennemgang af fagområdet 'spredning fra fotosyntetiske organismer', samt en personlig refleksion om udviklingsperspektiver gives som en review (Manuskript 3).

Contents

Acknowledgements

Although this PhD started as an inter-laboratory project in University of Copenhagen, it soon changed to the inter-continental biological-mathematical-scattering project of all kinds. During the last three years I have met and contacted numerous people for advices or actions and I am greatly indebted for their inputs. Without you this project would be different and way less exciting. I therefore use the opportunity to say my sincere

Thanks

To my supervisors - Kell, Jacob and Poul Erik. Without your trust and support this project could not occur.

I am always fascinated by Kell's combination of his endless knowledge, ability to explain things and endless patience towards 'keen-to-learn-biologists'. He has always stimulated to look for a decision independently, but when I did not have a clue at all, a quick drop-by his office was usually enough to be put on a solid ground and to continue.

Among other things, which include Jacob's inherent ability to flash-freeze marshmallows in the lab and sing in a band, he has also taught me the correct pronunciation of 'halvfjerds' and 'øl magnet' vs. 'oljemagnat'. I also thank Kell and Jacob for the opportunity to be 'the-first-man-inside-SAXS-chamber'.

From the time of my master project, when Poul Erik said 'We are creative people, we will think of something', he had always been an impetus and encouraged not only to find a solution, but also to ask questions and present things in a positive and eloquent way.

To Łucja, Radek and Michał and their professor Agnieszka Mostowska (University of Warsaw, Poland). If one wishes to find a perfect collaborator, one does not need to look further. Thank You for being with me all the time no matter what; also for being the first members of anti-HK club: 'In models we trust...'.

To Mathias, Anurag and Omar (KU, Copenhagen, Denmark) for all CURT1-related plant, cyanobacterial, plant-physiological and theoretical matters. To Kamil for *Chlamydomonas* strains. For Artur for numerous cyanobacterial advices and luckily being wrong on the statement 'nobody grows cyanobacteria in Australia'. To Lisbeth and to Hanne for the danish resume, office talks and the out-of-office company. To the rest of Photosynthesis group for a creative environment.

To Søren Roi, Nicolai, Frederik, Viktor and Lasse (KU) for measuring my green

samples with me-present-remotely and for badminton mornings. To Grethe, who was the first who started 'danish-only' policy on me. To Anine and Simon for proofreading this PhD thesis, Aghiad for X-ray course together and the rest of X-ray and neutron group for integrating a biochemist.

To Christopher Garvey (ANSTO, Sydney, Australia) for numerous experimental ideas, help to organize beamtimes - from a lot of paperwork, buying seeds and plants to Al-sputtered quartz windows. Thanks for your film knowledge and your sense of humour during all these long measurement hours.

To Anna Sokolova (ANSTO, Sydney, Australia) for all her help both with BILBY with me on-site and me-remotely, presenting our scattering work to the kids, and for a phrase 'I have never thought you could even measure scattering on plant leaves'. Also for the unbeatable argument 'I don't work with hungry men' and all these delicious cakes. They were very useful during night measurements :).

To ANSTO instrument support team, lead by Andrew McGregor, for dedicating their weekend to start up BILBY and Andrew Eltobaji for all sample environment setups.

To Gergely Nagy (PSI) and Renáta Ünnep (Wigner Research Center for Physics, Budapest, Hungary) for almost infinite discussions on SANS-related matters, data sharing and numerous advices.

To Eva Selstam (Umeå University, Sweden) for teaching me PLB isolation technicalities, for your vast literature knowledge and inputs to my numerous questions as well as the attitude 'take everything you like with you' from your article library. To Katalin Solymosi (Eötvös Loránd University, Budapest, Hungary) and Michał Gabruk (Jagiellonian University, Krakow, Poland) for introducing me to PLB literature and answering endless structural-literature questions.

To Henrik Aronsson and Cornelia Spetea Wiklund (University of Gothenburg, Sweden) for providing my first PLBs and a genuine interest in thylakoid scattering works.

To Martin Cramer Pedersen for 'WillItFit?' adjustments and the fourth column.

To Søren Skou (SAXSlab) for keeping our 'Ganesha' awake at all times and to Jesper, who was the first one to introduce me to experimental SAXS practicalities.

To Stephen Hyde and the entire team from ANU Dept. of Applied Mathematics for my stay and trip to Tindibilla, for Mango (a software, not a fruit) and Ajay Limaye (Australian National University, Canberra) for Drishti.

To Robert Corkery (KTH, Stockholm, Sweden), for the statement 'I have tried using a lamellar model on those (read: cyanobacterial) curves, but it did not work'. It was a bit of a journey to understand what to improve.

To Catherine Nielsen (Center for Advanced Bioimaging, KU), Inger Margrethe Jensen (KU) and Beata Bieniak (University of Warsaw) for sample preparation

and TEM-use advices. And those numerous cuts made...

To Dariusz Lange, (Silesian Center for Heart Diseases in Zabrze, Poland) and Sebastian (technician) for allowing and helping to use their TEM facility for PLB tomography.

To Andres Käch, Ohad Medalia (University of Zurich, Switzerland), Eyal Shimoni (Weizmann Institute of Science, Israel) and Dganit Danino (Technion, Israel). For all your input on EM techniques.

To Waah Sooh Chow (Australian National University, Canberra) for a smallish *Alocassia* seedling I could put in a cardboard box and bring to ANSTO for measurements.

To Derek Collinge and Barry Pogson (Australian National University, Canberra) for growing and providing *Arabidopsis* Col0 plants for SANS measurements.

To Julie Dechorgnat, Hero Tahaei, Andrew Merchant and Brent Kaiser (Center for Carbon, Water and Food, University of Sydney, Australia) for the possibility to use your growth chambers and black boxes, agreed upon by mails. Yes, plants did contain paracrystalline PLBs during my scattering experiment!

To Sarah Ongley, Bakir Al-Sinawi, Angela Soeriyadi, Joao Pereyra and Brett Neilan (University of New South Wales, Sydney, Australia) for the 6803 and 7942 strains at that point I needed them very much.

To Amy Asher, Martin Ostrowski, Fallen Teoh and Ian Paulsen (Macquarie University, Sydney, Australia) for the 7002 strain at that point I needed it very much again.

To Olga Baulina (Lomonosov University, Moscow, Russia) for numerous papers with TEM images of cyanobacterial thylakoid ultrastructures in all conditions.

To Annegrete Wilde (Freiburg University, Germany) for the 6803 strain potent to grow in the dark.

To Eva Mari Aaro and Luca Bersanini (Turku University, Finland) for explaining idiosyncrasies of phycobilisome behaviour, cyanobacterial state transitions and lumen proteome.

To Tomas Morosinoto (University of Padova, Italy) for BBY isolation protocol and detergent matters.

To Tobias Schumann, Peter Jahns (Heinrich-Heine-University Dässeldorf, Germany) and William H. J. Wood (University of Sheffield, UK) for sharing their raw data on TEM picture statistics.

To Donald Bryant (Pennsylvania State University, USA) for a discussion on 7002 behaviour with the outcome 'Darkness in 7002 doesn't cause much change in anything'.

To Robert E. Blankenship (Washington University in St. Luis, USA) and Noam Adir (Technion, Israel) for a discussion on phycobilisome concentration.

To Jörg Pieper and Maksim Golub (University of Tartu, Estonia) for a discussion on phycobiliprotein SLD.

To Kresten Lindorff-Larsen, Kasper Dyrberg Rand (KU), Jeffrey Brender (University of Michigan, USA) and Zoë Fischer (European Spallation Source, Sweden) for deuteration advices.

To Nir Keren and Uri Raviv (Hebrew University Jerusalem, Israel) for a discussion on near-biological membrane behaviour in different temperatures and osmolarities and Anja Krieger-Liszkay (Paris South University, France) - for mentioning their work in the conference.

To David Kramer (Washington State University, USA), Radek Kaňa (Czech Academy of Sciences), Dušan Lazar (Palacky University Olomouc, Czech republic), Dimiry Zlenko, Ilya Kovalenko and Aleksander Tichonov (Lomonosov University) for a multi-faceted confirmation, that nobody knows what a thylakoid does upon dark-light transition and answering endless questions on 'modelling thylakoid' matters.

To Robert Russel, Peter Holden, Karyn Wilde (ANSTO, NDF, Sydney, Australia), Nick Timperon (ANSTO lab manager) for lab space, cyanobacterial incubators, dark cold room, *Chlamydomonas*, cyanobacteria in D_2O and 5 kg of salt to maintain a high humidity inside the incubator.

To Jade Li (Medical Research Council, Cambridge, UK) and Rapolas Žilionis (Harvard University, USA) for writing an important membrane work - as well as digging it up from the library archives.

To Zinaida Eltsova and Ekaterina Petuskova (Russian Academy of Sciences) for finding and sending articles from '70s in their original language. Also for the entire KU library for providing hard-copies or scans of a lot of original references.

To Robyn Margaret Stuart (KU Datalab) and Christian Ritz (NEXS, KU) for all statistic advices and teaching me *R*.

To Sten Ebbesen and all language teachers who taught me and those who had to listen me talking foreign languages (including all fødevarestuderende and their tutor Lars Øgendal).

To all people inviting me to participate or allowing to organize numerous extracurricular activities: from Cherry's Bubble, PLEN Christmas Choir, DKDM team, Kirsten Grønfeldt, Nicolai Elsberg, Elsebeth Dreisig and to our Protmūšis team.

To all my friends and family.

To my grandparents Alikas and Nijolė. I guess my physics education and endless

interest in understanding science started very early on in my life. I got many answers from You.

List of Abbreviations

ATP	Adenosine triphosphate
α-DM	n-dodecyl-α-D-maltoside
BBY particles	Berthold-Babcock-Yocum particles; PSII-LHCII containing grana fragments without lumen
B-S cells	Bundle-sheet cells. CO_2 fixation of C4 plants occurs here
CAM plants	Plants fixating CO_2 onto phosphoenolpyruvate. Malate stored in mesophyl cell vacuoles
C3 plants	Plants fixating CO_2 onto ribulose 1,5-bispohosphate
C4 plants	Plants fixating CO_2 onto phosphoenolpyruvate. Malate/aspartate shuttled to B-S cells
ChemF	Chemical fixation
Chl a	Chlorophyll a
Cyt b_6f	Cytochrome b_6f
CLSM	Confocal laser scanning microscopy
DGDG	Digalactosyl diacylglycerol
DMPC	1,2-Dimyristoyl-sn-glycero-3-phosphorylcholine
DPPE	1,2-Dipalmitoyl-sn-glycero-3-phosphoethanolamine
FFT	Fast Fourier Transformation
Gal	Galactose
HPF	High pressure freezing
kDa	kiloDalton
LHCII/LHC I	Light harvesting complex II / I
MCT	Modified Caillé Theory
MGDG	Monogalactosyl diacylglycerol
NPQ	Non-photochemical quenching
OD	Optical density (measured mostly at 730 nm in this PhD thesis)
OEC	Oxygen evolving complex in PSII
PBS	Phycobilisome
PC	Phosphatidylcholine
PChlide	Protochlorophyllide
PE	Phosphatidylethanolamine
PG	Phosphatidyldiacylglycerol
PI	Phosphatidylinositol
PLB	Prolamellar body
PMA	Phenylmercuric acetate
PMS	Phenazine methosulphate
POPC	1-palmitoyl-2-oleoyl-sn-glycero-3-phosphocholine

POR	Protochlorophyllide oxidoreductase
PS	Phosphatidylserine
PT	Prothylakoids
PQ and PQH_2	Plastoquinone
RD	Repeat distance
RT	Room temperature
SAXS	Small angle X-ray scattering
SANS	Small angle neutron scattering
SLD	Scattering length density
SQ	Sulfoquinovose
SQDG	Sulfoquinovosyl diacylglycerol
TEM	Transmission electron microscopy
UDP	Uridine diphosphate
WT	Wild type

γ	Euler's constant, $\gamma = 0.57721$
$\Delta\rho_H$	Scattering length density of lipid headgroups
$\Delta\rho_T$	Scattering length density of lipid tailgroups
$\Delta\rho_L$	Scattering length density of lumen
$\Delta\rho_S$	Scattering length density of stroma
η	Caillé parameter

D	Darkness
D Re-Ad	Dark re-adapted
FR	Far-red light
LL	Low light (below 10-25 μmol photons $\cdot m^{-2} \cdot s^{-1}$)
NL	Normal light (100 μmol photons $\cdot m^{-2} \cdot s^{-1}$)
NatL	Natural light (fluctuating: median around 130-150 μmol photons $\cdot m^{-2} \cdot s^{-1}$, maximum around 1200 μmol photons $\cdot m^{-2} \cdot s^{-1}$)
ML	Medium light (500 μmol photons $\cdot m^{-2} \cdot s^{-1}$)
HL	High light (above 500-700 μmol photons $\cdot m^{-2} \cdot s^{-1}$, most commonly 100-1500 μmol photons $\cdot m^{-2} \cdot s^{-1}$)
R	Red light

Chapter 1

Photosynthetic membrane ultrastuctures and development

1.1 Photosynthesis

Oxygenic photosynthesis evolved approximately 2.4 billion years ago in cyanobacteria [102]. Photosynthesis is the principal process, producing biochemical energy equivalents ATP and NADPH, oxygen and organic matter on Earth. In eukaryotic organisms, photosynthetic reactions take place in specialized organelles - chloroplasts, which contain thylakoids - closed membrane sacks, embedding photosynthetic protein complexes. In prokaryotic cyanobacteria, thylakoids are located in the cell cytoplasm and embed both the photosynthetic proteins and the cellular respiration proteins [201, 12]. Chloroplast ultrastructure and thylakoid arrangement is described in later sections.

The first light-dependent stage of photosynthetic reactions is the conversion of sunlight into a chemical energy by splitting water, transporting electrons and creating a proton gradient across the thylakoid membrane (Fig. 1.1). This chain of light-dependent processes (also called photosynthetic electron transport) is catalysed by four large multi-subunit membrane protein complexes, embedded in the thylakoid membrane: photosystem II (PSII), cytochrome b_6f complex, photosystem I (PSI) and CF_oCF_1-ATP synthase. As electrons are transferred from water to NADPH, protons are pumped into a lumenal compartment. Further light-independent photosynthetic reactions (upper part of Fig. 1.1), most importantly carbon fixation via Calvin-Benson cycle, take place inside chloroplast stroma (in C3 higher plants) or in the cytoplasm (cyanobacteria); in C4 and CAM plants, carbon fixation reactions and Calvin-Benson cycle are spatially separated.

The overall biochemistry of photosynthesis and most important anabolic reactions are schematically indicated in Fig. 1.1. During the light-dependent phase of photosynthesis, two water molecules are oxidized, 4 protons and 4 electrons are released, O_2 evolves as a side product of water cleavage. When photosystems are excited, two water molecules

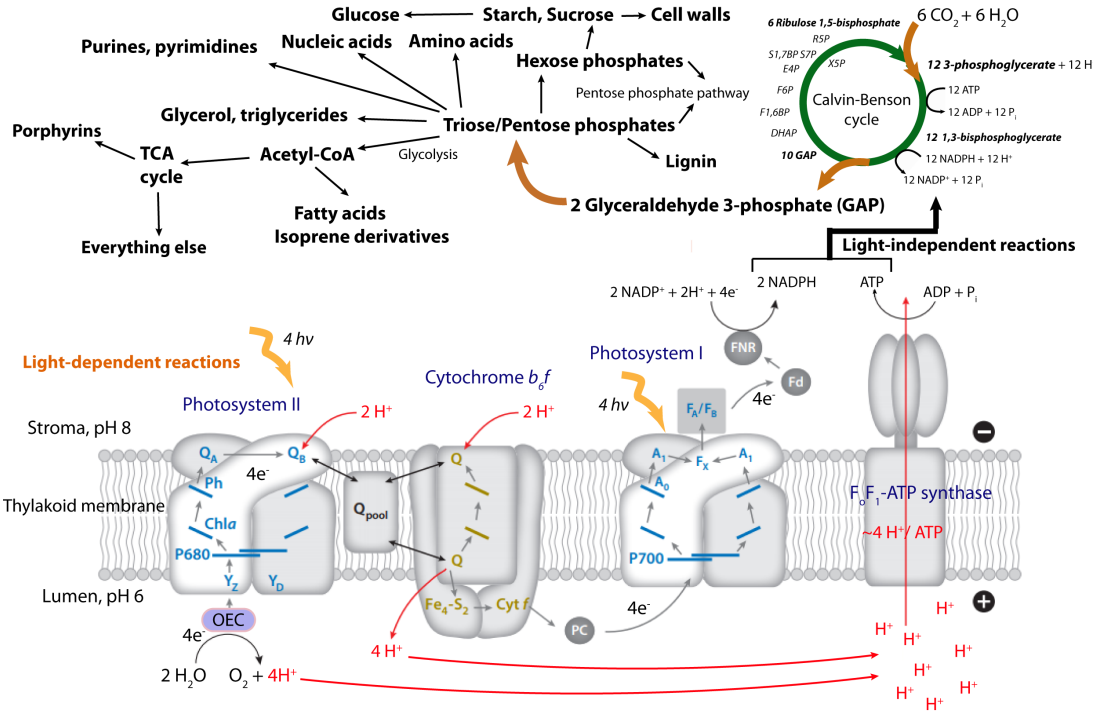

Figure 1.1: Linear electron transfer - two water molecules are split in the oxygen-evolving complex (OEC) of light-excited photosystem II, releasing 4 electrons, 1 oxygen molecule and 4 protons. These 4 electrons are sequentially transported to photosystem I via plastoquinone (PQH_2) molecule, cytochrome b_6f and plastocyanin (PC). Additional protons are pumped from the stroma side to the thylakoid lumen by plastoquinone (PQH_2) and the cytochrome b_6f complex. Light-excited photosystem I transfers electrons from plastocyanin through the thylakoid membrane to the stromal protein ferredoxin one at a time. Subsequently, these 4 electrons are taken up by ferredoxin-NADPH reductase and 2 NADPH molecules are synthesized. The proton gradient created by electron transport ($pH = 6$ vs. $pH = 8$) between the lumen and stroma is employed by the CF_oCF_1-ATP synthase to synthesize ATP. ATP and NADPH are the primary products of the photosynthetic light-dependent reactions, which are used in Calvin-Benson cycle (light-independent reactions). Carbon is fixated as CO_2 onto ribulose-1,5-bisphosphate (RuBP), eventually forming glyceraldehyde-3-phosphate (GAP). GAP molecules as well as pentose phosphates from RuBP regeneration phase are used as the precursors for all other molecules, including plant secondary metabolites. Figure adapted from [66].

are split and 4 electrons are released; 8 photons are required. Electrons reach ferredoxin NADPH reductase protein one at a time and two NADPH molecules are synthesized. Additional 4 protons are imported into a thylakoid lumen during the quinone cycle (Q cycle). A recurrent proton movement from lumen to stroma through the CF_oCF_1-ATP synthase complex is created due to the proton gradient, what drives the synthesis of ATP; around 4 protons are needed to synthesize 1 ATP molecule.

NADPH and ATP together with water and CO_2 are used during light-independent reactions in the stroma. Carbon is fixated during the Calvin-Benson cycle, where CO_2 and H_2O molecules are bound to six ribulose-1,5-bisphosphate (RuBP) molecules, forming twelve 3-phosphoglycerate (3-PG) molecules, this reaction is catalysed by a ribulose-1,5-bisphosphate carboxylase/oxygenase (Rubisco) enzyme. 3-PG molecules are phosphorylated to 1,3-bisphosphoglycerate molecules and finally reduced to glyceraldehyde-3-phosphate (GAP) molecules. Two GAP molecules are used as precursors for all other molecules, whereas remaining GAP molecules are used to regenerate RuBP molecules, various pentose phosphates are involved in regeneration reactions. Contrary to light-dependent reactions, the stoichiometry of thr light-independent reactions is less concise and is plant-type dependent. In C3 plants, Calvin-Benson cycle consumes eighteen ATP and twelve NADPH to assimilate 6 CO_2 molecules into two triose phosphates (3 ATP : 2 NADPH : 1 CO_2). In C4 plants, at least five molecules of ATP (due to C4/C3 shuttle action) are needed for the assimilation of one molecule of CO_2 (5 ATP : 2 NADPH : 1 CO_2) [39].

A stoichiometric summary of all photosynthetic reactions is (Eq. 1.1):

$$6CO_2 + 6H_2O \xrightarrow{8h\nu} (CH_2O)_6 + 6O_2 \tag{1.1}$$

where $(CH_2O)_6$ represents a 'hexose' molecule, produced by reduction of six CO_2 molecules. In summary, plants, algae and cyanobacteria are capable to carry out this complex sequence of endergonic reactions, which has a Gibbs free energy change of $\Delta G^{\circ\prime}$ = +2840 kJ/mol of hexose [39].

The maximum rate of photosynthesis, sustained for several hours in optimal conditions can reach 100 mmol of fixed CO_2/kg chlorophyll/s [17]. On an global scale photosynthetic pigments absorb around 5 % of incoming solar radiation and the total chemical energy stored in photosynthetic products amounts to 0.5-0.7 ‰ of total incoming solar radiation, or $4 \cdot 10^{21}$ J/year. For comparison, the global energy consumption in 2013 was $5 \cdot 10^{20}$ J/year, which is around 1/10 of the chemical energy stored as photosynthetic products (lignin, cellulose, sugars, amino acids, lipids, plant secondary metabolites etc.) [17]. Despite the overall energy redundancy, several world regions are affected by food deprivation. This underlines the enormous importance on current research in plant sciences improving photosynthesis and understanding the flexibility and adaptability of the photosynthetic apparatus to changing environmental conditions with the help of new techniques, in this case small angle scattering.

1.2 Chloroplast development. Photosynthetic membrane ultrastructures

Light-dependent photosynthetic reactions take place in thylakoids, located inside chloroplasts (in higher plants) or cytoplasm (in cyanobacteria). Chloroplast (Fig. 1.2) is an endosymbiotic organelle of cyanobacterial origin, it retains a functional genome (plastome), a double outer membrane (chloroplast envelope) and the photosynthetic apparatus (embedded in a thylakoid membrane). Chloroplasts belong to a diverse family of plastids, which, in addition to photosynthesis, are involved in the synthesis of amino acids, fatty acids, purine and pyrimidine bases, terpenoids, pigments, hormones as well as nitrogen and sulphur assimilation. Small undifferentiated proplastids, found in meristems and reproductive tissues, can differentiate and interconvert between several functional variants depending on developmental context: amyloplasts (starch storage), chromoplasts (carotenoid storage), elaioplasts (oil storage), etioplasts (chloroplast precursors, developed in the absence of light), chloroplasts (photosynthesis) and to gerontoplasts (aging chloroplasts) (Fig. 1.3 a) [111, 203, 219, 9, 273].

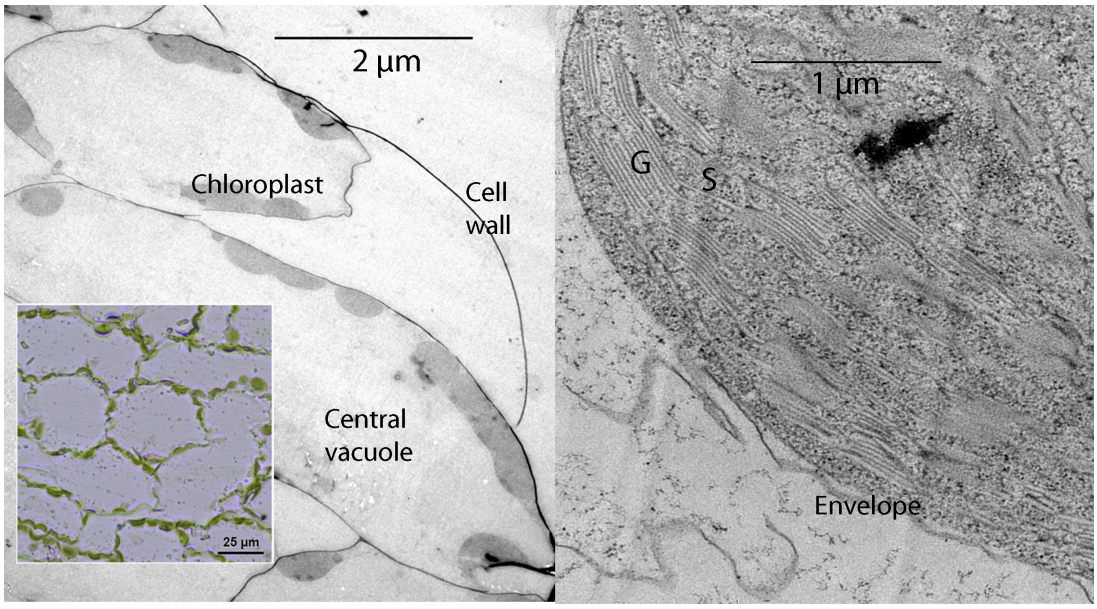

Figure 1.2: TEM images of high-pressure-frozen and freeze-substituted Arabidopsis Col0 leaf. Images taken during a PhD course in University of Zurich, the center for microscopy and image analysis. G indicates grana thylakoids, S indicates stromal thylakoids. Diagonal lines are marks from a diamond knife cut. Inset: Light microscopy of TEM grid. Chloroplasts (green) and central vacuoles (light blue) are visible. Image taken by Łucja Kowalewska, University of Warsaw, Dept. of Plant Anatomy and Cytology.

1.2.1 Etioplast and prolamellar body

Chloroplast biogenesis in higher plants begins from proplastids in young seedlings even without light exposure. During a continuous plant growth in dark (etiolation), developing pro-plastids increase in size and synthesize membrane sheets. Lamellar membranes (sheets) start to perforate and form tubules; when the tubule arrangement becomes highly regular, an etioplast is fully developed [252]. Every fully developed etioplast contains a large highly ordered regular cubic lipid membrane-protein structure - a paracrystalline prolamellar body (PLB, Fig. 1.3 b, c), from which thylakoids develop upon illumination. 1-2 μm diameter prolamellar body is built from a network of interconnecting hollow tetrapodal units, forming characteristic hexagon layers (Fig. 1.3 b, inset), with a few long emanating prothylakoids (PT) [136]. Bicontinuous cubic prolamellar body structure (most likely of a double diamond type) is probably the most themodynamically favourable organization of NADPH:protochlorophyllide reductase (POR) protein and a large volume of plastid lipids [255]. There are 30-60 etioplasts in a single higher plant cell, their number increases with cell age and plant greening [252]. The formation of such highly-organized PLB structure during plastid development in darkness is not limited to higher plants - PLB has been observed in cyanobacteria [148], *Euglena* [130, 211] or *Chlamydomonas* [71] cells. Chloroplast development can also proceed directly from proplastid to chloroplast - without the etioplast stage.

The volume of a single PLB is ca. 1 μm^3 and it can develop into 43 μm^2 + 41 μm^2 (from PLB + from PT) area membrane sheet, which has a very large lipid/volume ratio [90, 37]. As soon as the PLB is exposed to light, a light-dependent POR protein converts protochlorophyllide (Pchlide) to chlorophyllide (Chlide) and the cubic structure of PLB disperses into flat sheets within 30 min to 5 h. The molecular details of neither PLB formation, nor its photodispersal mechanisms are known. It has been postulated that, as soon as exposed to light, NADPH-Chlide-POR complex disassociates/splits and POR protein detaches from the membrane (or redistributes), what finally leads to PLB structure disintegration and dispersion [280, 230, 272]. This hypothesis is currently challenged, as it neither can explain why PLBs recrystallize after light exposure, when low amounts of PChlide are present, nor the examples of light-stable PLBs [148, 6, 271]. As lipid self-assembly alone is not enough to maintain PLB hexagonal structure [273], current hypotheses suggest that the association of POR oligomers - both of light-dependent and light-independent POR variants - can take part in maintaining PLB structure [255, 5, 74], but this needs to be proved experimentally. The physiological role of PLB is unknown - most probably PLB structure serves as a lipid-storing scaffold for thylakoid membrane development; hypothesis of PLB as light-capturing photonic crystal has recently been disproved [59].

As PLB cubic structure disintegrates in light (Fig. 1.3 c, etio-chloroplast stage), prothylakoids elongate. The synthesis of photosynthetic proteins, protein import into chloroplast, their insertion into thylakoid membrane/lumen, followed by protein megacomplex assembly, begins. Later, several prothylakoids align in parallel, approach each other

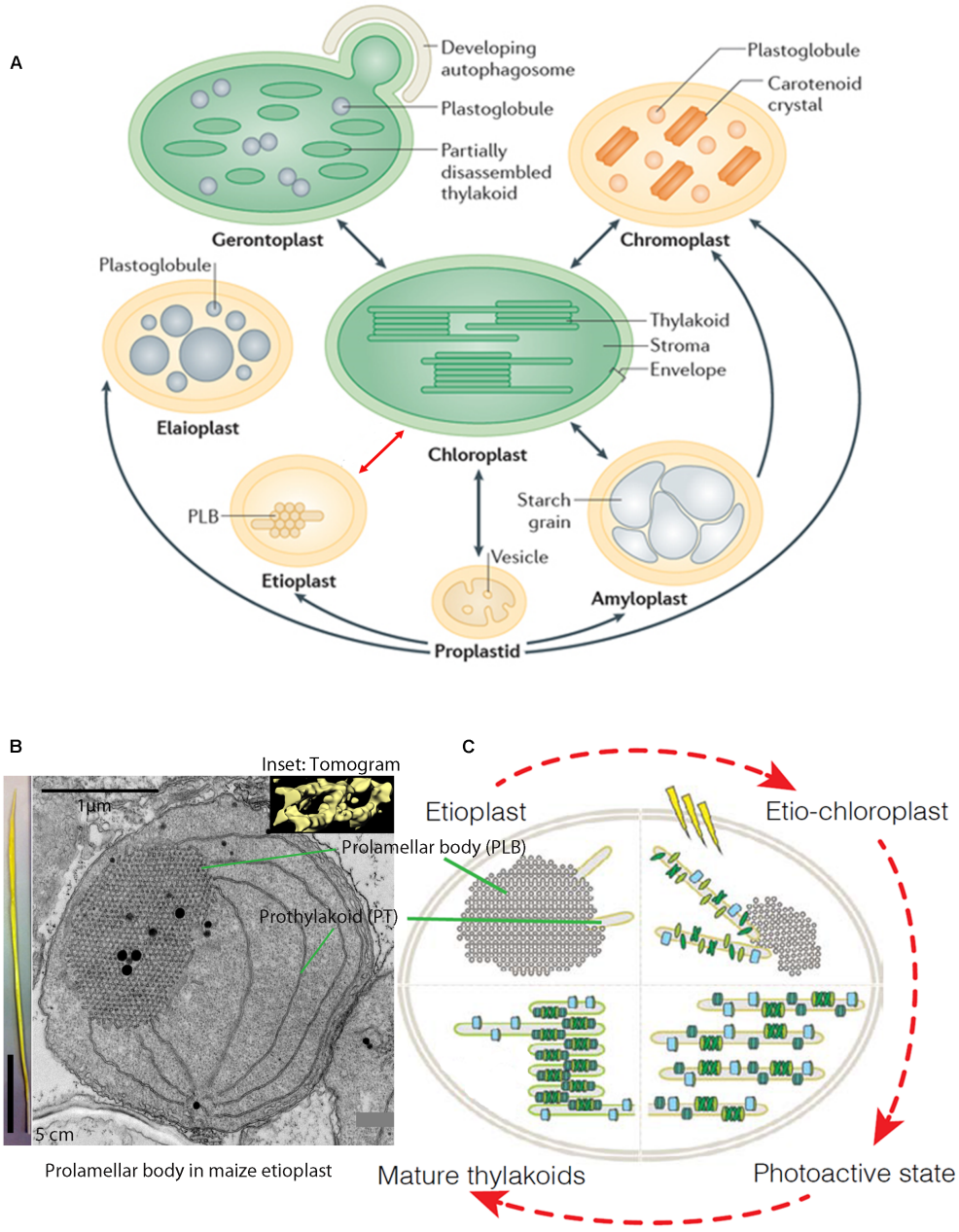

Figure 1.3: a) Plastid development and interconversions [111]; b) Etiolated maize seedling and TEM image of etioplast. A single PLB and several PTs are visible. Inset: tomographic reconstruction of cubic PLB structure. Tomography series and image alignment performed in Department of Histology and Embryology, Medical University of Silesia; c) Etioplast development stages. PSI (blue), PSII (light green), LHCII (dark green) proteins are indicated. Image adapted from [222].

and compact - thylakoid membranes develop (Fig. 1.3 c, photoactive stage). Additional lipids are incorporated into developing thylakoid membranes [222]. Mature higher-plant thylakoids with distinct grana stacks and interconnecting stroma thylakoids are formed. The characteristic granal-stromal thylakoid membrane arrangement in the higher-plant chloroplast (Fig. 1.3 c, mature thylakoids) is described in the next section.

1.2.2 Thylakoid membrane arrangement

Granal-stromal thylakoids in higher plant chloroplasts

Higher plant thylakoids are arranged into two interconnected regions: stacked granal and single stromal thylakoids. Granal thylakoids (gt, Fig. 1.4 a) exist as 300-600 nm diameter cylindrical stacks of appressed flattened membrane discs, covered by non-appressed grana layers (end membranes) at the top and bottom of each grana stack, as visualized in Fig. 1.4. Individual grana thylakoid layers (Fig. 1.4 b, green) are separated by an inter-thylakoid space (also called stromal gap or partition gap) of around 20-35 Å height [11]; relevant distances of grana stack and dimensions of photosynthetic proteins are given in Fig. 1.7 b-c. Individual granal thylakoids (Fig. 1.4 b, c , red) are connected by the long and flat, fret-like stroma lamellae sheets (st, Fig. 1.4 a), which wind around the outer rim of grana discs - grana margins (Fig. 1.4 b, c, orange) as right-handed helices with an angle of 20–25°. In recent years grana margins have been acknowledged as a separate region, as margins, in contrary to flat granal and stroma thylakoids, exhibit large local thylakoid membrane curvature and contain proteins of curvature thylakoid family (CURT). The CURT protein complexes cause/facilitate thylakoid membrane bending [19, 95].

Although thylakoids are appressed and regularly arranged in leaves, their ultrastructure changes when thylakoids are isolated. When chloroplast stroma is exchanged with isolation buffer, individual granal thylakoids swell due to a reduced osmotic pressure (Fig. 1.4 c). The overall thylakoid stacking depends on buffer ion composition and (especially Mg^{2+}) concentrations, although helical organization of stromal thylakoids (Fig. 1.4 c, red) and additional membrane turn-arounds (Fig. 1.4 c, blue) can still be preserved, as visualized by a tomogram. When isolated thylakoids were washed with Na^+ and Mg^{2+}-free buffer and then NaCl and $MgCl_2$ solutions of various concentrations were re-added, a maximum of 50-60 % thylakoids could restack in 400-1000 mM NaCl or 50-100 mM $MgCl_2$, showing that re-stacking *in vitro* is only partially reversible [121].

Photosynthetic protein distribution between granal and stroma thylakoids is distinct due to spatial restrictions occurring from different degrees of thylakoid membrane appression of granal and stromal thylakoids: 85-95 % of photosystem II and LHCII antenna proteins are located in grana. Contrary, PSI, LHCI and CF_oCF_1-ATP synthase (because of their size incompatibility due to large stroma-facing protrusions) are located in stroma-exposed thylakoids and grana margins. Cytochrome b_6f is almost uniformly located in both grana and stroma thylakoids. In order to maintain a functional photo-

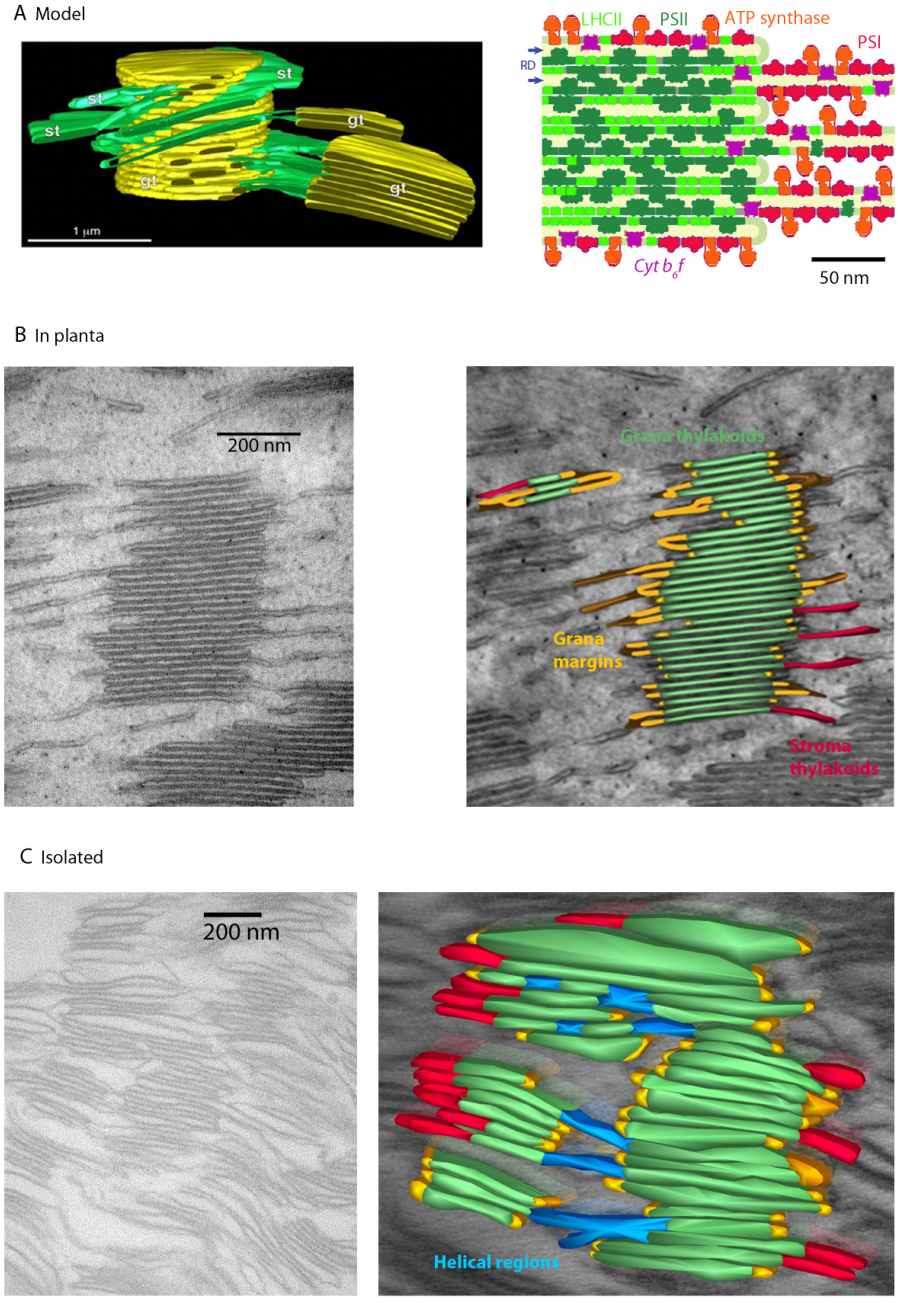

Figure 1.4: a) Tomographic reconstruction of granal-stromal thylakoid arrangement and junctions [21] and relative photosynthetic protein distribution between granal and stromal thylakoids. Blue arrows depict the thylakoid repeat distance [55]; b) TEM picture and tomogram of Arabidopsis oeCURT1A grana and its tomographic reconstruction; c) TEM picture and tomogram of isolated Arabidopsis oeCURT1A thylakoids and their tomographic reconstruction. Helical regions with preserved right-handed rotation join adjacent grana. TEM blocks prepared, TEM images and tomographic reconstruction performed in collaboration with Łucja Kowalewska.

synthetic electron transport, granal-stromal spatial photosystem separation requires that plastocyanin ($40 \cdot 28 \cdot 30$ Å size) shall diffuse hundred of nanometers quickly (within 30-50 μs) inside the lumen - a space, which width (40 - 100 Å) is comparable to plastocyanin size [131]. Plastocyanin diffusion speed and therefore photosynthetic efficiency can be restricted by lumen-protruding oxygen evolving complexes of PSII. Thus, modifying thylakoid appression and changing lumenal width can be a functional possibility to regulate photosynthesis [131].

Grana formation

The mechanism of grana stacking is yet unknown (so the name 'grana enigma', coined by J. Andersson), although it is most probably the result of physichochemical balance between several forces: attractive entropic effects, van der Waals attraction, electrostatic repulsive force and repulsive hydrostructural force [225]. According to the current model, electrostatic repulsion prevents close appression of adjacent negatively-charged granal thylakoids, unless the negative charge is screened by counter-cations; whereas the attractive forces and physical connections between opposing LHCII complexes hold membranes stacked [24, 46, 11]. This complex force balance suggests that granal stacking is not static, but a highly dynamic state, which can be modified by changing the charge balance: via illumination-caused hydrogen influx into the lumen, protein phosphorylations, ion concentration changes and other factors [24, 43, 46, 113, 225].

Although photosynthesis can function without a spatial protein separation - as is *e. g.* in cyanobacteria, granal stacks offer several efficiency advantages, many of which are interrelated: 1. Grana enhances light capture due to a dense pigment packing and large thylakoid membrane area, 2. Interconnectivity of core PSIIs to LHCII antennae allows an efficient exciton tunnelling to reaction centers from antenna megacomplexes both in sunlight and shaded environments, 3. Excitation spill-over from PSII to PSI is limited, 4. Fine-tuning of energy distribution can be regulated by State 1-State 2 transitions (see below), 5. Non-photochemical quenching, occuring in grana, can dissipate excess PSII energy as heat, 6. Photosynthesis efficiency can be regulated by grana structural changes due to transmembrane pH gradient changes, 7. Premature PSII subunit D1 and D2 degradation can be delayed and PSII repair cycle can be spatially restricted to grana margins, 8. Non-cyclic ATP synthesis, occuring from functional full photosynthetic electron transport, can be enhanced and regulated, 9. Possible adjacent OEC association can regulate PSII activity [15, 46].

The logics of large grana formation in low light (LL, in low illumination intensities), such as in deep tropical forests, can be explained by the following: as shorter wavelength light is absorbed by the upper leaves or upper layers of canopy, low light, which reaches ground surface, gets enriched in far-red wavelengths (green light is not absorbed). With its Chl *b* rich antenna, PSII preferentially absorbs a shorter-wavelength light and is functionally inefficient above 680 nm. Contrary, PSI and LHCI antennae are rich in Chl *a* and can efficiently absorb light with the wavelengths beyond 700 nm [224].

Under far-red or low intensity light, PSI works faster than PSII, therefore plants need more PSII to adjust photosynthetic electron transport. Therefore plants grown in low light have grana stacks of large radii and with more layers in a stack. With the use of several herbicides - dihydrostreptomycin [266], chloramphenicol [58, 205, 309, 166], fluorometuron [302], methabenthiazuron [64], bentazon [171], atrazine [169] and lincomycin (chloroplast ribosome inhibitor) [289, 28], large grana can form even in medium and high light conditions in mesophyll cells, this ultrastructure change depends on the inhibitor concentration; lyncomycin effect on grana in bundle sheet cells is less clear [245]. Since these herbicides interfere with electron transfer between PSII and PSI, large grana ensures a sufficient electron transfer to PSI by increasing the amount of PSII [274].

Light harvesting complexes and state transitions in thylakoid stacking

Both PSI and PSII core proteins are laterally associated with extensive peripheral antenna systems - light harvesting complexes LHCI and LHCII (Fig. 1.5 a). LHCII antennae increase spectral and spatial light absorption of photosystems - higher amount of photons of various wavelengths are captured by antennae megacomplexes and subsequently tunnelled as excitons to photosystem reaction centers. LHCI antenna of higher plants consists of Lhca1-4 proteins, which contain approximately 15 Chl *a* and Chl *b* molecules each and efficiently absorb red light. LCHI proteins bind PSI core as two heterodimers Lhca1-Lhca4 and Lhca2-Lhca3, which form a half-moon-shaped belt on top of PsaF-PsaJ subunits [203].

LHCII binding to PSII core is different: minor Lhcb proteins (CP24, CP26, CP29) bind PSII as monomers, major Lhcb1-3 proteins bind PSII as the assembled LHCII trimer (Fig. 1.5 a). An isolated spinach PSII-LHCII complex is C2S2, where C2 is a dimeric PSII core, S2 is two strongly-bound LHCII trimers, two CP26 and two CP29 proteins. This C2S2 assembly contains around 200 Chl molecules. *Arabidopsis* C2M2 contains two additional CP24 proteins, which promote binding of two moderately-bound (M2) LHCII trimers - yielding C2S2M2 stoichiometry. Spinach PSII core can also bind loose (L) LHCII trimer, yielding C2S2ML. C2S2 and C2S2M2 can associate with each other and form megacomplexes and even semi-crystalline arrays (Fig. 1.5 a). *In vivo* these complexes are likely to coexist in different ratios depending on species and light conditions [203, 134]. Recent cryo-EM experiments identified physical connections across the interthylakoid space (stromal) gap between the LHCII complexes from adjacent thylakoid membranes [11].

When algae and plants are exposed to different intensity light, a part of their light harvesting complexes can move and dynamically adapt to altered illumination in order to retain efficient energy distribution between PSII and PSI. This adaptation process, involving thylakoid membrane reorganization, is called state transitions and is indicated in Fig. 1.5. In *Chlamydomonas* and higher plants LHCII is normally bound to PSII (Fig. 1.5 a, State 1). When PSII is over-excited and plastoquinone pool is predominantly reduced, STN7 and STN8 kinases are activated [310]. When PSII core proteins are

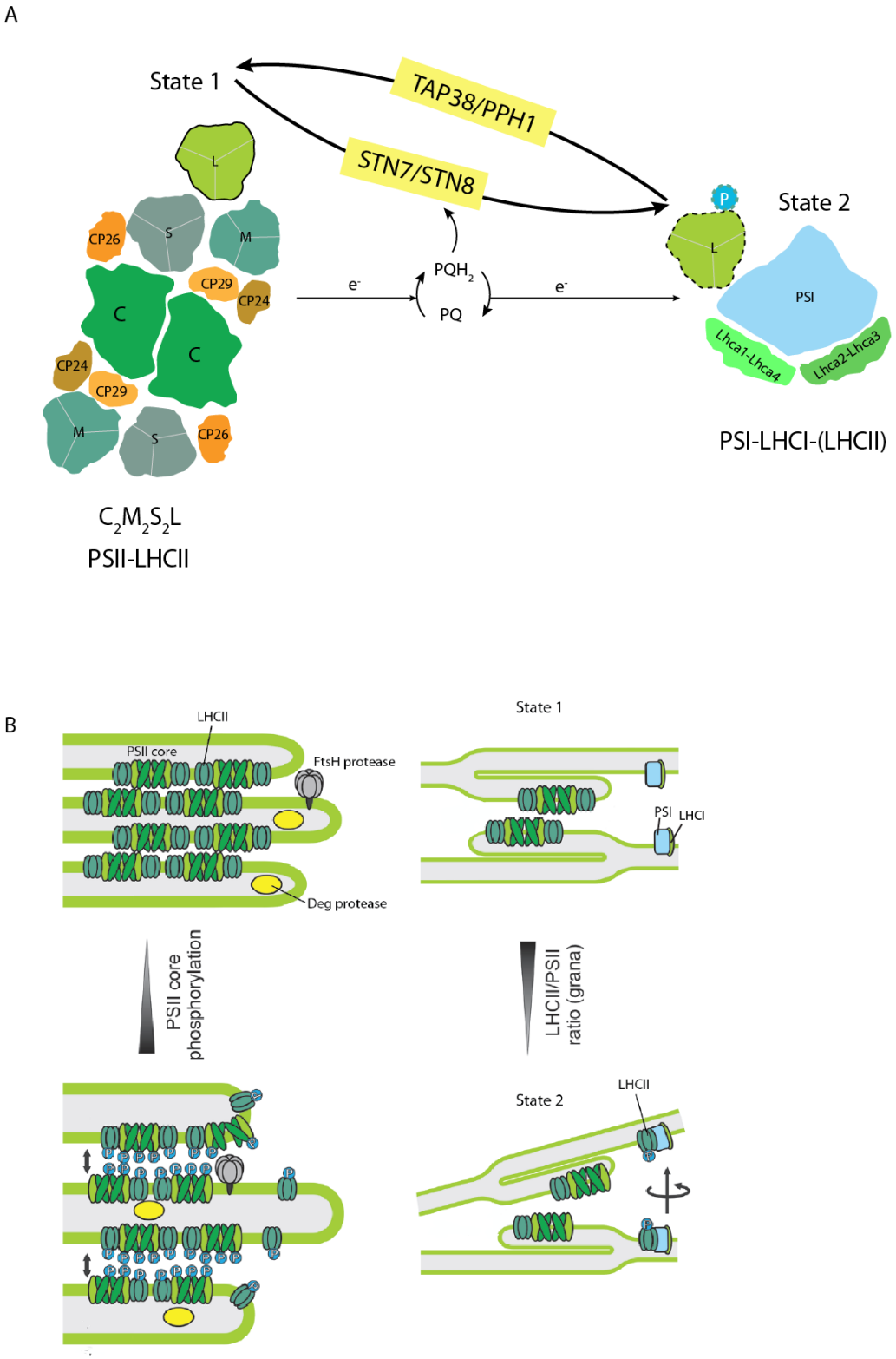

Figure 1.5: a) Schematics of state transitions - vertical plane and top view. Lateral LHCII movement is indicated and partial thylakoid destacking in State 2 is visualized. C - PSII core, S, M, L - strongly, medium and light-bound LHCII trimers. CP24, CP26 and CP29 - small Lhcb proteins; b) LHC-II and PSII-core phosphorylation-induced thylakoid membrane separation. Adapted from [134, 222, 224].

phosphorylated by STN8 kinase, LHCII antenna is further phosphorylated by STN7, after what a fraction of loosely bound LHCII (L-form) detaches from PSII and migrates to stromal thylakoids, where it associates with PSI-LHCI complex, increases PSI antenna cross-section and enables more efficient PSI light harvesting (Fig. 1.5 a, State 2) [224]. Since the excitation energy transfer decreases by the power 10^{-6} of the distance between antenna and photosystem, this reversible LHCII shifting enables plants to regulate the amount of light delivered to PSII or PSI reaction centers [274].

When PQ pool is reoxidized, STN7 and STN8 kinases become inactivated. LHCII is dephosphorylated by TAP38/PPH1 phosphatase, LHCII disassociates PSI and migrates back to PSII. PSII subunits are then dephosphorylated and PSII-LHCII megacomplexes reform again (State 1). Such LHCII and PSII core phosphorylation together with LHCII movement causes a partial grana destacking - the amount of stacked membranes is decreased by 20 % in State 2 [123] (Fig. 1.5 b, right). In *Chlamydomonas*, state transitions are accompanied by switch to cyclic electron transport, what enables to restore cellular ATP levels. It has also been demonstrated by microscopy and scattering, that thylakoids are more loosely arranged in State 2 than in State 1 [203, 197].

Thylakoid stacking is also regulated by LHCII phosphorylation (Fig. 1.5 b, left) [108, 306]. Each N-terminal segment of LHCII contains four positively charged residues, which contrast the overall negative charge of thylakoid stromal surface. Normally, positively charged N-termini bind to negatively charged LHCII regions on opposing thylakoid surface (across the inter-thylakoid space) and promote thylakoid stacking. Under illumination N-termini of LHCII are phosphorylated and negative thylakoid membrane charge increases, what promotes thylakoid unstacking. Unstacking also allows access for bulky lumenal Deg and stromal FtsH proteases to degrade damaged D1 and D2 proteins. Polyamination of stroma-exposed photosynthetic antennae has a similar effect - it minimizes the overall negative thylakoid membrane charge and promotes thylakoid stacking [108].

Mutants with different thylakoid membrane phosphorylation levels have different thylakoid ultrastructures - oeSTN8 mutant, where PSII core proteins are over-phosphorylated, have an increased total grana height, whereas *stn8* kinase mutants have a small grana with long and tightly appressed thylakoids [310]. These findings suggest that reversible phosphorylation of both LHCII and PSII regulates grana activity by varying thylakoid appression under different illumination conditions [203].

Cyanobacterial photosynthesis and thylakoid arrangement

A significant part of the experimental work of this PhD thesis - attached as Manuscript 1 - was carried out using cyanobacteria, therefore their photosynthesis and thylakoid ultrastructures are also described.

Cyanobacteria account for 20-30 % of global photosynthesis, what corresponds to 20-30 Gt CO_2 fixation into biomass and release of 50-80 Gt O_2 into the atmosphere

anually [261]. Cyanobacterial light-dependent photosynthesis reactions are very similar to those of algae and higher plants, what allows using cyanobacteria as model organisms to investigate photosynthesis. Similarly to plants, cyanobacteria oxidize water and use NADPH and ATP to fix CO_2 in Calvin-Benson cycle. Cyanobacterial carbon fixation is carried out in carboxysomes [50] and cyanobacterial RuBP regeneration stage is very similar to plants [287]. Contrary to plants, cyanobacterial oxidative respiration enzymes are localized in the thylakoid membrane [287, 158] (Fig. 1.6 a). Protein content of cyanobacterial thylakoid lumen is not fully characterized [157]

Cyanobacteria contain predominantly Chl *a* - several species also contain Chl *d* and Chl *f* - also carotenoids, phycocyanin, phycoallocyanin and phycoerythrin. Despite the overall functional similarities, there are several ultrastructural differences of cyanobacterial thylakoids if compared to plants. Cyanobacteria do not contain grana stacks and appressed thylakoid membranes, their thylakoids are arranged in the cell cytoplasm as 3-8 parallel layers. Individual thylakoids are approximately 150-250 Å thick and are separated by 300-500 Å cytoplasm layers (inter-thylakoid space) with phycobillisomes.

A specific thylakoid arrangement in the cyanobacterial cell is very species-dependent and is indicated by TEM pictures in Fig. 1.6. In *Synechocystis* sp. PCC 6803 (Fig. 1.6 d) thylakoids radiate from thylakoid centers near cell membrane and are arranged parallel to the cell membrane [155]. In *Synechococcus elongatus* sp. PCC 7942 (Fig. 1.6 b) thylakoids are arranged circularly, there are perforations in thylakoid layers, allowing cytoplasm to be continuous. There are also connections between different thylakoids, indicating that thylakoid membrane and lumen are continuous throughout the cell [202]. *Synechococcus* sp. PCC 7002 (Fig. 1.6 c) exhibits yet another thylakoid arrangement - parallel thylakoids are characteristically arranged as triangles or diamond-shapes if seen perpendicularly, or as long parallel layers if seen from the side [204].

Contrary to plants, there is no strict spatial separation between PSII and PSI complexes in a typical cyanobacterium cell. In cyanobacteral thylakoid membrane PSII dimers are arranged as parallel rows, whereas trimeric PSI are loosely arranged between the rows [182]. In *Synechococcus* sp. PCC 7942, PSI and ATP synthase are predominantly arranged in outer thylakoid layers [260], whereas PSII and cytochrome b_6f are equally spread in all thylakoid membranes, although such protein separation is rather exceptional.

The most different feature, distinguishing cyanobacteria from plants, is their photosynthetic antenna - their composition and dimensions. Cyanobacterial antennae - phycobilisomes (PBS) - are hemidiscoidal phycobiliprotein-pigment structures with a diameter of 300-800 Å and organize as 3-4 core cylinders and 6-10 peripheral stacked rods, which pack between two thylakoid membranes in a zig-zag pattern [265, 208, 45]. They may account up to 24 % of cell dry weight and around 50 % of total cell protein [80]. One of the largest phycobilisomes is the 18.6 MDa intact phycobilisome of *Griffithsia pacifica*, which has dimensions of 680 Å (diameter), 390 Å (height) and 450 Å (depth) [315].

The width of the cyanobacterial interthylakoid space is relatively stable (580±120 Å

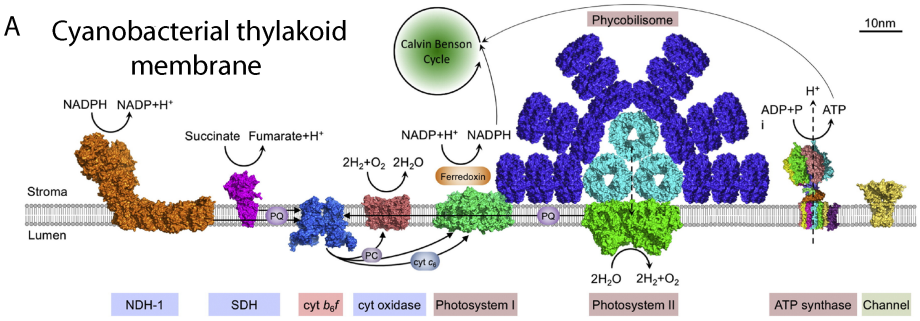

B

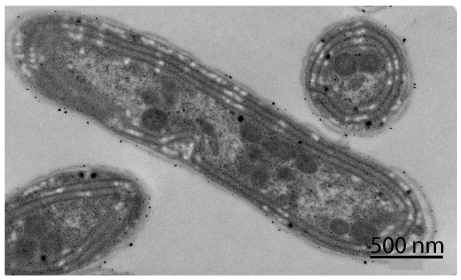

Synechococcus elongatus sp. PCC 7942

C

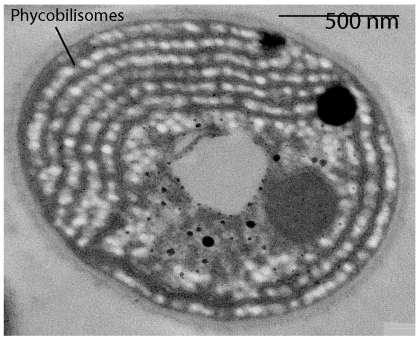

Synechococcus sp. PCC 7002

D

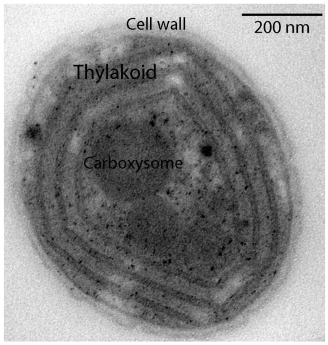

Synechocystis sp. PCC 6803

Figure 1.6: a) Protein complexes in cyanobacterial thylakoid membrane [160]. TEM images of chemically-fixed cyanobacterial cells: b) Synechococcus elongatus sp. PCC 7942, c) Synechococcus sp. PCC 7002, d) Synechocystis sp. PCC 6803. Thylakoids, phycobilisomes, carboxisomes and cell wall are indicated. TEM images taken by Łucja Kowalewska, TEM blocks prepared in Center for Advanced Bioimaging, University of Copenhagen.

for *Synechocystis* sp. 6803, 450±30 Å for *Synechococcus elongatus* sp. 7942, 530±50 Å, 550±60 Å for *Gleobacter violaceus*, 530±50 Å for *Thermosynechococcus vulcanus* [45]) and corresponds to the thickness of the double layer of phycobilisomes.

This also implies that inter-thylakoid space width depends on phycobilisome composition: the smaller the phycobilisome, the lower inter-thylakoid space width. PAL mutant without phycobilisomes has a repeat distance of 340 Å, CK mutant with APC core has a repeat distance of 470 Å [208, 156, 152]. Cyanobacterial thylakoid repeat distance also depends on the level of cell hydration - thylakoid repeat distance in a dessicated state is smaller than in a hydrated state (610±50 vs. 510±290 Å), thylakoid membranes look much more disordered and lumen height is twice smaller in desicatted than in hydrated cells (33±15 vs. 64±25 Å) [63, 62].

Overall, phycobiliproteins comprise around 50 % of total cyanobacterial cellular proteins. Phycobiliprotein composition and content is affected by numerous environmental factors: temperature, CO_2, phosphate, sulphate, iron and nitrogen concentrations, light intensity and light wavelength [51, 159, 80, 265]. Therefore, differences of thylakoid repeat distances can be seen as an indirect outcome of environmental changes, which are species-dependent.

It has been observed that *Synechococcus* sp. PCC 6301 cells grown under low light has longer phycobilisome peripheral rods [51]. For other species, phycobilisome composition, size and shape remains the same, but the number of phycobilisomes per thylakoid area increases in low light and they can compactly aggregate into phycobilisome rows [81, 51, 120]. As a result of aggregation, local phycobilisome concentration between thylakoid membranes can reach 1 mM, which is about 200 g/L (normally, phycobilisome concentration in inter-thylakoid space is around 0.01-0.2 mM) [7]. As discussed in the following chapter, the biological variation in phycobilisome concentration complicates calculations of scattering length densities. Furthermore, phycobilisomes are mobile and can be attached either to PSII (mainly) or PSI depending on light conditions - state transitions in cyanobacteria can occur, albeit they are much less investigated. It is known, that State 2 in cyanobacteria is induced in the darkness [73, 48].

1.3 Photosynthetic membrane behaviour in light

1.3.1 Higher plants

On clear days in open locations photosynthesis in exposed leaves must contend with light intensities that vary over two orders of magnitude from limiting light in early morning/late afternoon versus full sunlight during midday [56]. These changes require an efficient biophysical, biochemical and structural adaptation of photosynthetic apparatus to light environment. It is hypothesized, that expanded lumen yields more efficient photosynthesis due to increased plastocyanin diffusion rate [124]. Therefore optimal photosynthetic conditions - temperature, illumination intensity - can be inferred from

observing ultrastructural thylakoid changes *in vivo*.

However, due to its multilevel complexity, thylakoid membrane behaviour in light is probably the darkest corner of photosynthesis research. Two biochemical processes agreed on are: light-induced lumen acidification and the subsequent photosystem II reaction center protein D1 damage. The impact of illumination on grana architecture changes, especially the behaviour of lumen and inter-thylakoid width, are most probably plant species and experimental condition-dependent [15, 56, 292, 250], what leads to many different interpretations and open questions. They are summarized in Fig. 1.7 a. General characteristics of high-light adapted plants, compared to low-light adapted plants are: higher electron transport and CO_2 assimilation rates, higher Chl a/b and PSII/PSI ratios, smaller PSII antenna size, increased number of chloroplasts per cell and reduced grana stacking [250].

Again, many biochemical and biophysical processes, including several levels of photosynthesis regulation and thus causing ultrastructural changes, occur simultaneously. This topic is currently investigated by different groups and various techniques, involving small angle scattering, however membrane dynamics in a mesoscopic scale is challenging [132]. The prevalent explanations and controversies regarding dark-light thylakoid dynamics are elaborated in this subsection.

In particular, to obtain reliable small angle scattering data in different illumination conditions in the future experiments requires not only having a suitable mathematical model to explain obtained scattering curves, but also suitable growth chambers and controlled experimental environments in large scale facilities for plant pre-adaptation and during the measurement. These requirements are not yet fulfilled, what hinders the future progress of the method application. Furthermore, light-induced thylakoid RD changes by scattering techniques were measured on thylakoid isolates [220, 194], what can differ from thylakoid behaviour *in vivo*. This is accounted for in Manuscript 2, where *in vivo* measurements are performed.

The ultimate goal of light-dependent reactions of photosynthesis is efficient ATP and NADPH production under all illumination conditions - a sufficient proton motive force (pmf) is needed. A proton motive force of -120 mV, required for ATP production, is the sum of electrical (thylakoid membrane potential) and pH-dependent (proton gradient across thylakoid membrane) components, detailed in Eq. 1.2 [52].

$$pmf\ (mV) = \Delta\Psi_{lumen-stroma} + 2.3\frac{RT}{F}\Delta pH_{stroma-lumen} \tag{1.2}$$

where R is universal gas constant and F is Faraday's constant.

From Eq. 1.2, all light-induced thylakoid ultrastructure changes are an indirect outcome of resulting ion movements and their redistribution. That is, ultrastructure changes are governed by ion concentrations, concentration distributions and the total energy partition between the electrical and pH components. The most important ions in photosynthesis are: hydrogen ion, chloride anion and magnesium, potassium cations.

They are included in the models, trying to explain photosynthetic functionality and thylakoid stacking [118, 299, 164, 225].

Two physical constraints, describing ion distribution in the dark steady state (before illumination), are: 1. Intra-lumenal and extra-lumenal osmolarities are equal and 2. Total individual sums of both intra-lumenal and extra-lumenal charges are zero, since no pmf is present [164]. The current approach to explain photosynthetic behaviour is to understand ionic redistributions, to obtain their equilibrium concentrations from mathematical models and to infer the degree of grana stacking together with resulting thylakoid ultrastructure changes [164, 225, 118].

Light induces linear electron transport, what leads to a pmf increase (*i. e.* in the absolute scale pmf becomes more negative). In plants, proton gradient term dominates in high light, whereas both Ψ and ΔpH terms almost equally account for pmf generation in low light conditions. Upon the transition from low light to high light, total pmf increases even more. As photosynthesis is now efficient, decreasing lumenal pH (ΔpH component) can downregulate light harvesting and electron transport from PSII to PSI. This functions as a safety switch and diminishes photosystem over-excitation [18, 52, 137].

As the light is switched on, water splits and additional protons are imported into the lumen. Lumen pH drops from 7.0-7.5 in the dark to 5.8-6.5 in the light. This pH decrease requires an influx of max. 30-60 mM protons into the lumen. However, 99 % of these protons are buffered - they are bound to negatively lysine and carboxyl- residues of thylakoid membrane proteins and buffer groups of lumenal proteins, and therefore cannot decrease lumenal pH 'by their full potential' [168, 2, 221, 137, 61]. Therefore, the exact influx of protons into the lumen is unknown. There is also a physiological lower limit of lumenal pH. Ca^{2+} ion is lost from OEC and Cu atom is lost from plastocyanin in pH below 5.5-6.2. The low pH also inactivates lumenal enzymes and slows down electron transport to PSI, what reduces photosynthesis efficiency. Therefore a large (3 or more pH unit) decrease of lumenal pH is not likely to occur [137, 138].

Proton influx into the lumen is balanced by the action of three ions (K^+, Mg^{2+} and Cl^-), exhibiting antagonistic actions (therefore called counter-ions). How do these counter-ions distribute? It is known, that proton influx into the lumen leads to net anion (especially Cl^-) influx into lumen in order to preserve its electrical neutrality. This is followed by the Mg^{2+} outflux from the lumen into the inter-thylakoid space, what minimizes the overall negative thylakoid membrane charge on the stromal side, as Mg^{2+} binds to negative thylakoid membrane charges.

If ion actions are analysed separately, then the net Cl^- influx into lumen drags water into the thylakoid lumen and would allow thylakoid swelling. K^+ outflux to inter-thylakoid space would promote thylakoid shrinkage and unstacking in concentrations of 5 mM, but thylakoid swelling in concentrations above 50 mM [221, 118]. If simultaneous actions of several ions are investigated, then the situation is concentration-dependent - at low K^+ (< 5 mM), Mg^{2+} efflux dominates (membrane stacking), whereas at $K^+ >$ 5 mM, K^+ efflux dominates (membrane separation), [100, 118]. This ionic balance is

probably what changes the overall 'thylakoid ultrastructural outcome' - stacking versus unstacking. The answer is yet unclear, as it is currently unknown, which counter-ion is dominant in chloroplasts *in vivo*. It is also plausible that different counter-ions behave differently under low light (when Cl^- acts as counter-ion) and in high light (when Mg^{2+} acts as counter-ion) [118]. To illustrate this, *Monstera deliciosa* and even *Arabidopsis* Col0 plants, grown in constant low and high lights behave differently if exposed to high light [56, 250].

It was also demonstrated, that ionic strength increase inside the stroma results in a weakened thylakoid stacking [221], whereas a decrease of stromal pH to about 5.4 (close to thylakoid pI) leads to a spontaneous membrane stacking due to the neutralization of the negative charge of a thylakoid membrane [221]. As the actions of stroma and lumen ions always coexist, it is difficult to predict a final outcome.

The dominant Cl^- influx and the resulting Mg^{2+} outflux would result in less appressed thylakoid packing in light. This has been observed by H. Kirchhoff et al. [124, 132] - they claim that this increase in lumen width alleviates plastocyanin diffusion and thus makes electron transfer more efficient [124, 292]. As outlined in recent works of Kirchhoff and Tsabari, lumenal expansion can be observed both in medium and high-light (saturating) conditions in *Arabidopsis* [124, 292]. Light-induced distance changes, measured in H. Kirchhoff et al. [124] and suggesting lumen expansion, are given in Fig. 1.7 b.

Although this explanation is biologically satisfactory, a variety of other ultrastructural processes have been observed after dark-to-light shift, especially in high-light. In the supplementary material of the same paper, H. Kirchhoff provides light scattering measurements on isolated thylakoids. Here, an increase in light scattering is correlated to particle aggregation. Therefore, an immediate light scattering increase upon illumination could indicate an increased aggregation of the entire thylakoid system, which is restored when the light is turned off [124]. This observation is also supported by scattering data, repetitively showing a decrease of thylakoid repeat distance upon illumination [220, 194].

Lumen expansion is also not uniform along the entire thylakoid width [226]. It is very predominant in grana margins - where adjacent thylakoids bend outwards and their lumens expand, whereas the remaining lumen, especially in the grana core, simultaneously shrinks [226, 313, 311]. Indeed, as exemplified in Nishimura et al. [313], estimating lumenal width is difficult: after 2000 μmol photons $\cdot m^{-2} \cdot s^{-1}$ illumination for 60 min, TEM measurements yield equivocal results - both the thylakoid repeat distance increase and decrease are observed in the same grana, depending on the place of measurement. By measuring the total height spinach grana stacks, consisting of 10 thylakoids in five different cross-sections, Yoshioka-Nishimura *et al.* show that grana total height increases in grana margins (1600 Å to 1620-1660 Å), slightly decreases in two intermediate grana areas (1600 to 1580 Å) and largely decreases in grana core (1600 to 1560 Å) [313, 314]. Taking into account that *Arabidopsis* Col0 grana are not very wide or largely stacked even in darkness [16, 222], and experiments suggesting light-dependent behaviour [250], experimental findings of H. Kirchhoff et al. [124], where average power spectra have been used to calculate repeat distances should be re-evaluated - maybe thylakoid margin

bending simply outdominates grana core shrinkage and shrinkage is therefore simply not observed with TEM. If so, then small angle scattering methods, which simultaneously investigate changes in entire ensemble of thylakoid membranes *in vivo* and do not require sample fixation, are more suitable than TEM methods.

Another hypothesis is the lumenal shrinkage in light. This hypothesis is supported by light scattering increase upon illumination (*i. e.* thylakoid aggregation) and by TEM measurements in a number of articles [185, 279, 184]. Lumen shrinkage is also observed under CO_2 and O_2 deprivation in high light (2000 μmol photons $\cdot m^{-2} \cdot s^{-1}$). A slightly smaller lumen width of 36 Å$\pm$ 6 (lowest lumen width, observed with functional OEC is around 40-50 Å [125]) is observed due to OEC disassembly [292]. Such lumen shrinkage also represses PSII repair by limiting protease access [292]. If so, biochemical implications of lumen shrinkage/expansion need to be reevaluated.

Grana thylakoid behaviours during dark to light transition are summarized in Fig. 1.7 a. It is agreed, that the number of thylakoid layers in granum decreases, grana diameter shrinks and grana partially destacks if a plant is shifted from low to high light, what reduces the excitation pressure on PSII [121, 98]. After destacking, damaged D1 protein can migrate to grana margins and can be degraded by FtsH and Deg1 proteases. Then a newly synthesized D1 can be inserted into a thylakoid membrane and migrate to the grana core [313, 122]. This notion is challenged by a recent paper, claiming that inter-thylakoid gap width decreases in the medium light (500 μmol photons $\cdot m^{-2} \cdot s^{-1}$) suggesting a restricted protease access under illumination [132].

Although presented as individual effects, lumen and inter-thylakoid width changes cannot be analysed independently, as they are correlated, and the total amount of layers in a grana stack is also important. Various experimental findings and conditions are summarized in Table 1.1. Here, available quantitative and qualitative illumination experiments are provided as a reference for detailed investigations in the future. It needs to be said, that a direct comparison between these results is best avoided - since light intensity, light quality/wavelength composition, illumination times and experimental conditions differ. The effect of red light on isolated chloroplasts, illuminated for 5 min with 150 μmol photons $\cdot m^{-2} \cdot s^{-1}$ is not identical to the effect, caused after a white light illumination of 2000 μmol photons $\cdot m^{-2} \cdot s^{-1}$ intensity on intact leaves for 2 h - even if the final ultrastructural outcome is the same. The same is valid for species - thylakoid stacking/unstacking in barley chloroplasts [217] is unique if compared with spinach, pea or *Arabidopsis* [54, 132, 124]. Illumination experiments of Murakami and Packer were performed either with algae thylakoids *in vivo* (low stacking degree) [184] or with isolated spinach thylakoid (higher stacking degree) chloroplasts [183, 185].

In conclusion, investigating the change of one ultrastructural parameter is insufficient to explain the overall changes in thylakoid architecture, as one needs to simultaneously consider illumination intensity and its duration, the resulting flux balance from every ionic species and the magnitude of all biochemical effects (state transitions, NPQ). Therefore, systematic studies of thylakoid dynamics using non-disturbing methods are of high importance. Such studies also require, that illumination spectrum and plant species

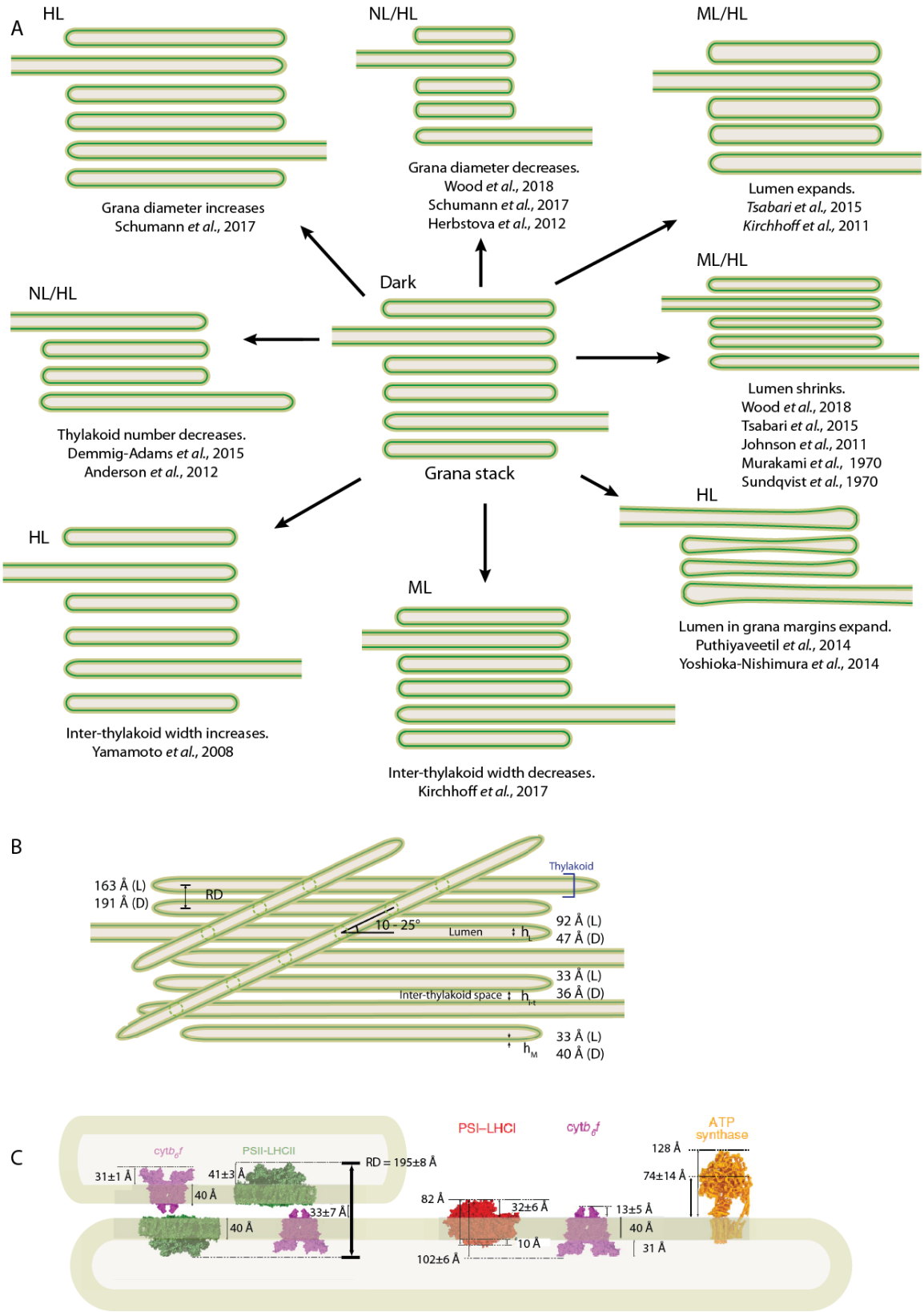

Figure 1.7: a) Examples of possible thylakoid ultrastructural changes during dark-to-light transition; b) Measured grana distances of Arabidopsis Col0 in light and dark, taken from Kirchhoff et al. 2011 [124]. c) Individual thylakoid membrane protein protrusion heights measured by AFM [306].

are known as well as the average degree of grana stacking before the experiment. As a step towards the comprehensive understanding of thylakoid dynamics, the outcome of this PhD thesis - Manuscripts 1 and 2 - investigate thylakoid behaviour of photosynthetic organisms *in vivo* in a non-disturbing way.

Table 1.1: Quantitative effects of illumination

Organism	Entity	RD Dark, AA (Lumen height, D)	RD light, AA (Lumen height, L)	Illumination intensity, color, time	Conditions	Method	Ref.
Plants							
A. thaliana Col0	Leaves	168±4 (46)	186±4 (88)	500 μmol ph·m^{-2} · s^{-1}, White, 30 min	Degassed with buffer: 15% dextran, 50 mM Tricine (pH 7.4)	FS	[124]
A. thaliana Col0	Isolated thylakoids	200±100	213±100	150 μmol ph·m^{-2} · s^{-1}, 640 nm, 5 min [1a]	0.3M sorbitol, 5mM $MgCl_2$, 2.5mM EDTA, 10mM $NaHCO_3$, 20mM HEPES (pH 7.6), 10% BSA	HPF	[49]
A. thaliana stn7	Isolated thylakoids	184±40	220±50	150 μmol ph·m^{-2} · s^{-1}, 640 nm, 5 min [2a]	0.3M sorbitol, 5mM $MgCl_2$, 2.5mM EDTA, 10mM $NaHCO_3$, 20mM HEPES (pH 7.6), 10% BSA	HPF	[49]
A. thaliana Col0	De-enveloped chloroplasts	252±2	316±7 (+ATP), 275±4 (-ATP)	15-200 μmol ph·m^{-2} · s^{-1}, 640 nm, 5-30 min	0.3M sorbitol, 5mM $MgCl_2$, 2.5mM EDTA, 10mM $NaHCO_3$, 20mM HEPES (pH 7.6), 0.5% BSA	ChemF	[47]
A. thaliana Col0	Attached leaves	175[3b]	233±8 (129±13)	2000 μmol ph·m^{-2} · s^{-1}, White, 30 min-2h		HPF	[292]
A thaliana Col0	Attached leaves in N_2	175[4b]	140±6 (60±12)	2000 μmol ph·m^{-2} · s^{-1}, White, 30 min-2 h		HPF	[292]
Spinach	Leaves in 4 °C	162[5c]	190[6c]	2000 μmol ph·m^{-2} · s^{-1}, White, 1 h		ChemF	[313]
Spinach	Leaves	163.1±8.4	147.561±7.0 [7d]	1500 μmol ph·m^{-2} · s^{-1}, White, 1 h		ChemF	[311]
Spinach	Leaf	206±24 (95±20)	192±27 (86±20)	200 μmol ph·m^{-2} · s^{-1}, White, 1 h		ChemF	[306]
Spinach	Leaf infiltrated with D_2O	229, D Re-Ad 223-227	220-224	1700 μmol ph·m^{-2} · s^{-1}, White, 5 min		SANS	[297]
Spinach	Isolated chloroplasts	164±23	146±18	70 klux, R, 2 min	64 mM NaCl, 0.3 mM PMS, 0.5 mM Tris maleate (pH 6.0) and 15 μg Chl/mL	ChemF	[279]
Spinach	Isolated chloroplasts	215±19	175±24	70 klux, R, 30s	64 mM NaCl, 0.3 mM PMS, 0.5 mM Tris maleate (pH 6.0) and 15 μg Chl/mL	ChemF	[279]
Spinach	Isolated chloroplasts	(250)	(150) [8e]	350 μmol ph·m^{-2} · s^{-1}, R; 635 nm, 5 min	0.33 M sorbitol, 5 mM $MgCl_2$, 10 mM KCl, 50 mM HEPES (pH 7.6)	ChemF	[114]
Spinach	Isolated chloroplasts	212±8 (131±10), D Re-Ad: 214±4 (130±9)	144±9 (104±6)	9690 lux, 600-700 nm (R), 3 min	50 mM Tris-HCl (pH 8.0), 175 mM NaCl, 15 μM PMS, 20 μM PMA	ChemF	[185]
Spinach	Isolated chloroplasts	196±4 (129±9)	144±3 (112±10)		175 mM NaOAc (pH 6.7), 15 μM PMS	ChemF	[185]
Spinach	Isolated thylakoids	296, D Re-Ad: 294-298	262-288	170-1700 μmol ph·m^{-2} · s^{-1}, White, 200 s	20 mM Tricine (pD 7.6), 0.4 M sorbitol, 5mM $MgCl_2$, 5mM KCl, 100 μM PMS	SANS	[194]
Pea	Isolated thylakoids	330	270-280	330-1000 μmol ph·m^{-2} · s^{-1}, White, 30 min	0.4 M sorbitol, 5 mM $MgCl_2$, 10 mM KCl, 50 mM HEPES (pH 7.6)	SANS	[220]
Maize WT	Leaves [9f]	Granal thylakoid: 101±7	88±8	1.4 nmol ph·cm^{-2} · s^{-1}, 650±7.5 nm (R), 1 h		ChemF	[189]
Maize WT	Leaves	Granal thylakoid: 101±7	96±8	1.4 nmol ph·cm^{-2} · s^{-1}, 707±8.5 nm (FR), 1 h		ChemF	[189]
Maize WT	Leaves	Stromal thylakoid: 71±6	70±7	1.4 nmol ph·cm^{-2} · s^{-1}, 650±7.5 nm (R), 1 h		ChemF	[189]
Maize WT	Leaves	Stromal thylakoid: 71±6	66±6	1.4 nmol ph·cm^{-2} · s^{-1}, 707±8.5 nm (FR), 1 h		ChemF	[189]
Maize WT	Leaves	Bundle sheet thylakoid: 70±5	69±5	1.4 nmol ph·cm^{-2} · s^{-1}, 650±7.5 nm (R), 1 h		ChemF	[189]
Maize WT	Leaves	Bundle sheet thylakoid: 70±5	71±7	1.4 nmol ph·cm^{-2} · s^{-1}, 707±8.5 nm (FR), 1 h		ChemF	[189]
Carotenoid defficient Maize	Leaves	Mesophyl thylakoid: 73±6	81±12	1.4 nmol ph·cm^{-2} · s^{-1}, 650±7.5 nm (R), 1 h		ChemF	[189]
Carotenoid defficient Maize	Leaves	Mesophyl thylakoid: 73±6	72±6	1.4 nmol ph·cm^{-2} · s^{-1}, 707±8.5 nm (FR), 1 h		ChemF	[189]
Carotenoid defficient Maize	Leaves	Bundle sheet thylakoid: 77±8	79±9	1.4 nmol ph·cm^{-2} · s^{-1}, 650±7.5 nm (R), 1 h		ChemF	[189]
Carotenoid defficient Maize	Leaves	Bundle sheet thylakoid: 77±8	75±7	1.4 nmol ph·cm^{-2} · s^{-1}, 707±8.5 nm (FR), 1 h		ChemF	[189]
Algae							
Porphyra	Cells *in vivo*	150	109±8	9690 lux, 600-700 nm (R), 2 min	100 mM NaOAc, 2.5mM KFeCN (pH 6.6)	ChemF	[184]
Ulva	Cells *in vivo*	198±10	144±6	9690 lux, 600-700 nm (R), 2 min	100 mM NaOAc, 2.5mM KFeCN (pH 6.6)	ChemF	[184]

[9]a) PSI-specific illumination of 740 nm had no effect
[9]b) Estimated from Fig. 2 A
[9]c) Estimated from 3rd picture line in Fig. S1, Partial unstacking in light
[9]d) Estimated from Fig. 4, grana core thickness decrease
[9]e) Decrease of 16-30 %
[9]f) Individual granal and stromal thylakoid thicknesses were measured [189]
[10]g) Isolation buffer: 0.1M sorbitol, 5 mM $MgCl_2$, 15 mM NaCl, 50 mM Tricine-KOH (pH 7.5)

Table 1.2: Qualitative effects of illumination

Plant	Entity	Dark	Light	Illumination intensity, color, time	Method	Ref.
Spinach	Isolated thylakoids [10 g]		Unstacking under HL in vitro	500-2000 μmol ph$\cdot m^{-2} \cdot s^{-1}$, White, 10-60 min	Digitonin fractionation	[121]
Spinach	Leaves	Avg. Grana number in chloroplast lower.	Avg. Grana number in chloroplast higher.	300-1500 μmol ph$\cdot m^{-2} \cdot s^{-1}$, Sunlight, 20 min - 3 h	ChemF	
			Avg. Thylakoid number per grana lower			[233]
A. thaliana Col0 and aLhcb2 mutant	Leaf	Avg. Grana number in chloroplast lower.	Avg. Grana number in chloroplast higher.	150 μmol ph$\cdot m^{-2} \cdot s^{-1}$, Growth light, 1h	ChemF	[16]
		Avg. Thylakoid number per grana higher	Avg. Thylakoid number per grana lower			[16]
A. thaliana Col0	Leaf, LL	No significant changes	No significant changes	1000 μmol ph$\cdot m^{-2} \cdot s^{-1}$, White light, 30 min	ChemF	[250]
	Leaf, NL	No significant changes	No significant changes	1000 μmol ph$\cdot m^{-2} \cdot s^{-1}$, White light, 30 min	ChemF	[250]
	Leaf, NatL	Partial grana restacking after 10 min re-darkening	Light-induced grana unstacking, increase of grana height	1000 μmol ph$\cdot m^{-2} \cdot s^{-1}$, White light, 30 min	ChemF	[250]
	Leaf, HL	Unstacking irreversible after 10 min re-darkening	Light-induced grana unstacking, increase of grana height	1000 μmol ph$\cdot m^{-2} \cdot s^{-1}$, White light, 30 min	ChemF	[250]
Barley	Leaves	Enlarged spherical chloroplasts.	Elipsoid chloroplasts.	130 μmol ph$\cdot m^{-2} \cdot s^{-1}$, White, 3h	HPF-FS	
		Small stacks/unstacked thylakoids, lumen swollen.	Typical grana/stroma arrangement .			[217]
Monstera	Leaves, LL	Avg. Thylakoid number per grana high.	Thylakoid number per granum increases	1500 μmol ph$\cdot m^{-2} \cdot s^{-1}$, White light, 20 min	ChemF	[56]
Monstera	Leaves, HL	Avg. Thylakoid number per grana lower.	Thylakoid number per granum decreases	1500 μmol ph$\cdot m^{-2} \cdot s^{-1}$, White light, 20 min	ChemF	[56]
Monstera	Leaves, LL.	Grana stacked	Grana unstacking	700 μmol ph$\cdot m^{-2} \cdot s^{-1}$, White light, 3 days	ChemF	[56]

1.3.2 Cyanobacteria

Cyanobacterial dark-light changes are less apparent. If cyanobacterial cells are transferred to darkness, light-dependent reactions of photosynthesis cease, cells stop growing, glycogen and ATP is consumed, NADPH/$NADP^+$ ratio decreases [241]. Transcription of around 25 % genes is also downregulated in dark, but metabolic and physiological state of cyanobacteria *Synechocystis* sp. PCC 6803 and *Synechococcus* sp. PCC 7002 does not differ in dark and light [241, 3, 163]. Up to my knowledge, no short-term adaptation ultrastructural changes, such as phycobilisome or thylakoid degradation in darkness, are reported so far.

From scattering experiments, no change is observed in the overall thylakoid structure of WT *Synechocystis* sp. PCC 6803 if dark-adapted cells are illuminated for 10-30 min, as the position of the first scattering peak, corresponding to thylakoid repeat distance is identical in dark-adapted and illuminated samples [156, 192]. Slightly larger changes (of 20-30 Å order) are observed for cyanobacterial phycobilisome truncation mutant CK, in PAL mutant devoid of phycobilisomes and in 3-week far-red light (730 nm) incubated *Halomicronema hongdechloris*, where the thylakoid number decreases from 5-7 to 3-4 and thylakoid RD decreases from 647 to 370 Å [152].

The situation is different in long-term dark adaptation. The number of thylakoids in cyanobacteria in a single 'pseudo-granum' is higher under low light intensities than in high light (0.2-1 klux vs. 7-20 klux, equivalent to 2.7-13.5 vs. 94.5-270 μmol photons$\cdot m^{-2} \cdot s^{-1}$ of cool white fluorescent light [240]) [81]. The total thylakoid area in the cyanobacterial cell is also 40 % higher in darkness than in high-light [81]. If *Synechocystis* sp. PCC 6803 is grown in 300 μmol photons $\cdot m^{-2} \cdot s^{-1}$ for 24 h, thylakoid number in a 'pseudo-granum' decreases and thylakoids become less compact compared to medium light of 40 μmol photons $\cdot m^{-2} \cdot s^{-1}$, a total volume of a cyanobacterial cell does not change [133].

From TEM images published in Sun et al. [278], I have also estimated thylakoid repeat distance for *Synechococcus elongatus* sp. PCC 7942 cells adapted in three different illumination conditions for 24 hours: low light (LL, 10 μmol photons $\cdot m^{-2} \cdot s^{-1}$), medium light (ML, 50 μmol photons $\cdot m^{-2} \cdot s^{-1}$) and high light (HL, 100 μmol photons $\cdot m^{-2} \cdot s^{-1}$). I have obtained (Fig. 1.8 is a rough estimation, since cyanobacterial cells were visualized in low magnification) average RD±SD values of 617±100 Å in LL and 718±100 Å (in ML and HL) with no significant cell volume changes [278].

If dark incubation is prolonged even further, thylakoids in some cyanobacterial species loose their regular arrangement. However, thylakoids are never lost completely [94]. Instead, thylakoids swell and disintegrate, fragmented thylakoids are no longer parallel to each other and are scattered throughout the cyanobacterial cell. Long-term thylakoid swelling in the darkness is suggested to occur due to anoxic conditions. When cellular ATP level and proton flow into the thylakoid lumen decreases, a negative charge of the cytoplasmic side of thylakoid membrane is lowered - thylakoids loose their adhesive properties and thus regularity [27].

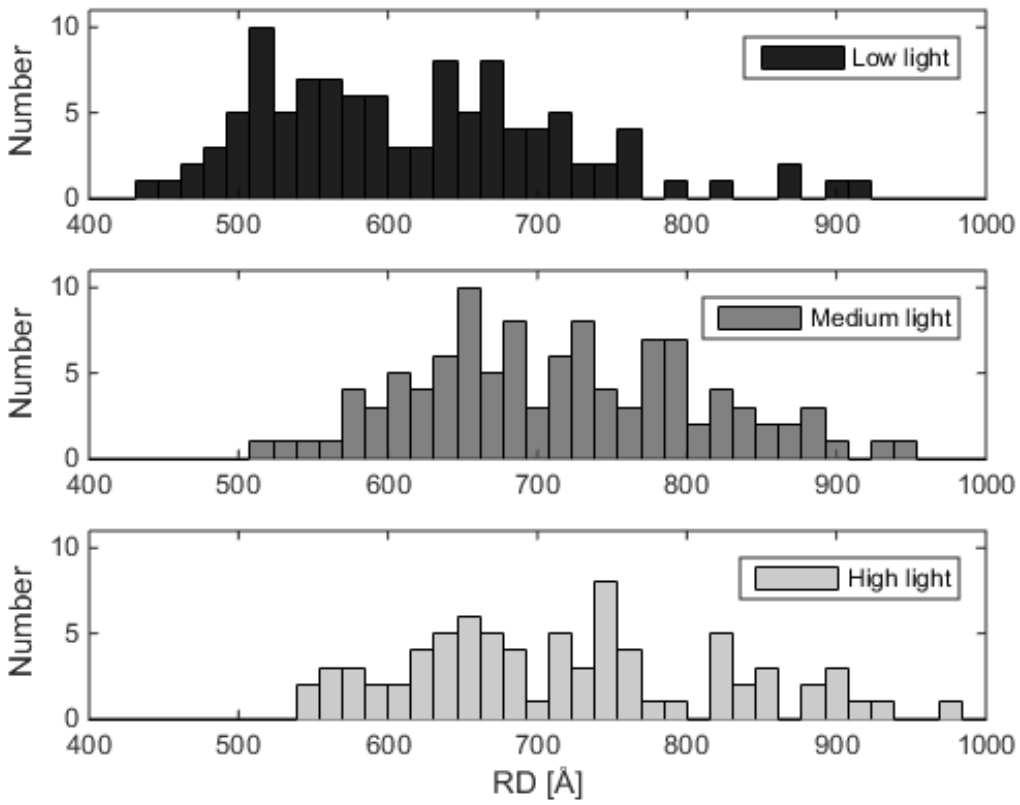

Figure 1.8: Repeat distance measurements of Synechococcus elongatus sp. PCC 7942 in three illumination conditions from Sun et al., Fig. S3 [278].

As described, long-term thylakoid ultrastructure adaptation is also species-dependent. After 2-week light-activated heterotrophic cultivation of *Synechocystis* sp. PCC 6803 in the darkness on glucose, cells have lost the majority of thylakoids (PBS were retained). Thylakoids were reassembled after 8-12 h of white light illumination; changes in cell size or other structures were not observed [26]. Some cyanobacterial species (*Chlorogloea fritschii, Nostoc, Synechocystis* sp. PCC 6714) do not degrade thylakoids - they retain thylakoids even after 3-year heterotrophic growth in the darkness, although thylakoid arrangement is less regular due to a lower adhesion. For *Anabaena variabilis* ATCC 29413, no changes in thylakoid ultrastructure are observed after 1 year dark incubation [81]. This indicates, that preserving and being able to quickly restore functional thylakoid membranes, as they are sole cellular energy producers of the cell, is important - even in the prolonged periods when no photosynthesis takes place or in other cell stress conditions, as the thylakoid membrane synthesis *de novo* is a chemical-energy-intensive process [94].

During the prolonged high-light stress (around 200 μmol photons $\cdot m^{-2} \cdot s^{-1}$), thylakoid ultrastructures of *Synechococcus* sp. PCC 6301 or *Anabena variabilis* 458 are similar to those after prolonged dark-adaptation - thylakoids are swollen, much more undulated and vesiculate, but still remain intact. With light intensities above 250 μmol photons $\cdot m^{-2} \cdot s^{-1}$ thylakoid are disrupted [27]. 1 hour exposure of *Synechococcus* sp. PCC 7002 cells with 900 μmol photons $\cdot m^{-2} \cdot s^{-1}$ and exposure with 250 μmol photons $\cdot m^{-2} \cdot s^{-1}$ for *Synechocystis* sp. PCC 6803 is enough to induce light stress response and related thylakoid changes. Sometimes light intensities of 4500-5500 $\cdot m^{-2} \cdot s^{-1}$, causing photodestruction of cyanobacteria, are also used [27]. During photodestruction, photosynthetic pigments are degraded and thylakoid membrane 'ghosts' are visible in TEM micrographs after 60-180 min [27]. Similarly to high-light stress, high temperature stress for 1 h also yields swollen, disordered and more undulated thylakoids in *Synechocystis* sp. PCC 6803, *Synechococcus elongatus* sp. PCC 7942 and *Synechococcus* sp. PCC 7002 (Fig. 1.9).

Cyanobacterial antennae (phycobilisome) structure also differs, depending on light intensity and light quality. As phycobilisome size can impact thylakoid repeat distance [10, 154, 152], their ultrastructure changes are briefly described below. Phycobiliprotein synthesis is increased in lower light, therefore more phycobilisomes are present in lower light intensities [51]. During the short-term dark adaptation, phycobilisomes remain fully assembled, but can arrange more tightly and form large arrays. During the long-term adaptation, phycobilisome behaviour is species dependent - phycobilisome rods can detach from the core, and only the compact PBS core remains attached to the thylakoid membrane surface (*Halomicronema hongdechloris*), what enables a tighter thylakoid arrangement [152]. Individual phycobilisome rods can become longer (*Synechococcus* sp. PCC 6301) or shorter [51, 265].

In cyanobacterial species which undergo chromatic adaptation, phycobilisome size and composition is also wavelength-dependent. In *Synechocystis* sp. PCC 6701 and in *Calothrix* sp. PCC 7601 phycobilisomes are smaller in red light /or darkness than in green light /or cool white light due to increased phycoerythrin (pigment of the outer part of rods) synthesis [265]. In *Anacystis nidulans* (*Synechococcus*), phycobilisomes become

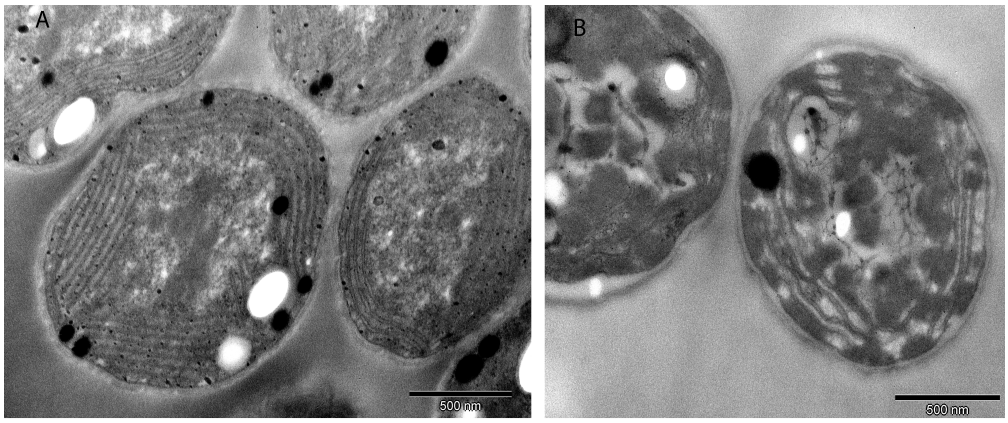

Figure 1.9: a) Thylakoid ultrastructure of Synechocystis sp. PCC 6803 at room temperature; b) Thylakoid ultrastructure of Synechocystis sp. PCC 6803 after 1 h incubation at 60 ° C. An identical effect is observed for Synechococcus elongatus sp. PCC 7942 and Synechococcus sp. PCC 7002 (not shown). TEM images taken by Łucja Kowalewska, TEM blocks prepared in center for advanced bioimaging, University of Copenhagen.

bigger in red light and for some species (*Pseudanabaena* sp. PCC 7409) phycobilisome size does not change [81, 161, 88, 152]. It has been suggested, that phycobilisomes can detach from thylakoid membranes and migrate towards the center of cyanobacteria in high light [286], putatively modifying thylakoid repeat distances. However, this hypothesis is currently questioned and reviewed [4].

To conclude, light intensity changes induce thylakoid membrane ultrastructure changes, including a thylakoid number increase in low light. Thylakoid membrane swelling, membrane undulations and even destruction are also observed under long-term adaptations, high light and high temperature stresses. Light intensity and quality induced changes in phycobilisome ultrastructure are also linked to thylakoid separation distances. A large variety of phycobilisome modification possibilities suggest that the future experiments shall investigate not only on the effect of light intensity, but also on the effect of light quality, with the focus on long-term adaptation. Overall, as cyanobacteria are precursors of higher plant chloroplasts, comparing cyanobacterial and plant thylakoid behaviour *in vivo* as well as thylakoid dynamics is an important direction in photosynthetic research.

Chapter 2

Small-angle scattering

The aim of this PhD thesis is to improve the measurement strategy and analysis methods of small-angle scattering from photosynthetic membranes. In particular, this requires recording scattering patterns *in vivo*, extracting structural information (changes) from scattering using mathematical modelling and relating such changes to underlying biological processes or biochemical phenomena in cyanobacteria (Manuscript 1) and higher plants (Manuscript 2).

This chapter provides an overview of the key concepts and theory of small-angle scattering and critically presents the previous work on photosynthetic membranes in solution and *in vivo* as well as the underlying problematics. Construction of a scattering model, calculation of model parameters and evaluating their biological validity is described in subsequent chapters.

This chapter is divided into three parts. The first discusses the experimental setup and the initial data treatment of a small-angle scattering experiment. The second explains the origin and theory of scattering. The third presents a chronological and critical overview of small angle scattering work on photosynthetic organisms.

2.1 Introduction

Small-angle X-ray (SAXS) and neutron (SANS) scattering are used to probe heterogeneous structures of 10-1000 Å length *in vivo* and in solutions. Small angle scattering (SAS) is routinely used to probe well understood biochemical systems and to extract information on their shape in medium resolution. The aim of applying small angle scattering in biological sciences is to investigate structural changes of the biologic system *in vivo* and correlate them with underlying physiological processes, since scattering experiments, unlike electron microscopy, do not require fixation and thus can be carried out in native-like environments.

In this PhD thesis, both neutron and X-ray small-angle scattering has been used to

study thylakoid membranes: both as isolated entities and in *in vivo* experiments. Even though neutron and X-ray scattering are different, the theory and data interpretation are essentially similar. Therefore the theory described here applies both to SAXS and SANS techniques. The reason for a complementary use of X-rays and neutrons is that different elements and isotopes scatter X-rays and neutrons differently due to differing scattering cross-sections. Such measurements are said to be performed under different 'contrast' situations, visualizing different parts of the sample and yielding a more comprehensive description of the sample. The example is given, how different parts (proteins or lipids) of a photosynthetic membrane can be investigated. In fact, if the system is relatively simple (*e. g.* a polymer dissolved in water or isolated protein in a lipid-water mixture) and its homeostasis does not depend on minute changes of experimental environment (*e. g.* illumination spectrum, temperature), SAXS- and SANS-extracted ultrastructural information can be used simultaneously and complement each other very well. In the *in vivo* case, one obtains useful information from *in vivo* measurements of the entire organism, although simultaneous comparisons or fitting of several experimental datasets shall be performed cautiously, since identical experimental, sample growth, illumination and preparation conditions rarely occur between different beamlines/experiments.

2.2 Scattering theory and experimental considerations

2.2.1 Experiment

A typical small-angle scattering instrument setup used in this work is shown in Fig. 2.1 a. Initially an incident 'white' beam emitted from the source is monochromated and this monochromatic beam is collimated by several slits or pinholes in order to make a highly parallel beam. After the collimation section the beam passes through the sample cuvette exemplified by a green square in Fig. 2.1 a (used sample holders are presented in Fig. 2.1 b), where it is scattered and the scattering intensity is measured by a 2-D position-sensitive detector. A direct (non-scattered) beam of high intensity is blocked by the beamstop (Fig. 2.1 a, red point). If the sample is non-oriented, the scattering pattern is centrosymmetric (such as shown in the picture) and can be radially averaged yielding cumulative scattering intensity as a function of scattering angle 2θ, which is most commonly expressed as vector $q = 4\pi/\lambda\ sin\theta$, described below. If the sample exhibits a degree of orientation (such as in the case of magnetic alignment), registered scattering pattern is non-centrosymmetric and the sectorial average, where signal is averaged only for specific sectors of the 2-D detector is performed. However, estimating the degree of system alignment and further modelling of such partially-oriented systems is non trivial.

The scattering angle 2θ is dependent on the instrument geometry and wavelength of the scattering radiation. To enable comparisons between different measurements (Fig. 2.2), the scattering angle is converted to the wavelength-independent scattering vector q. If an instrument geometry is unknown, the angular calibration is performed to determine q relation to the scattering angle: scattering from a well-ordered standard material

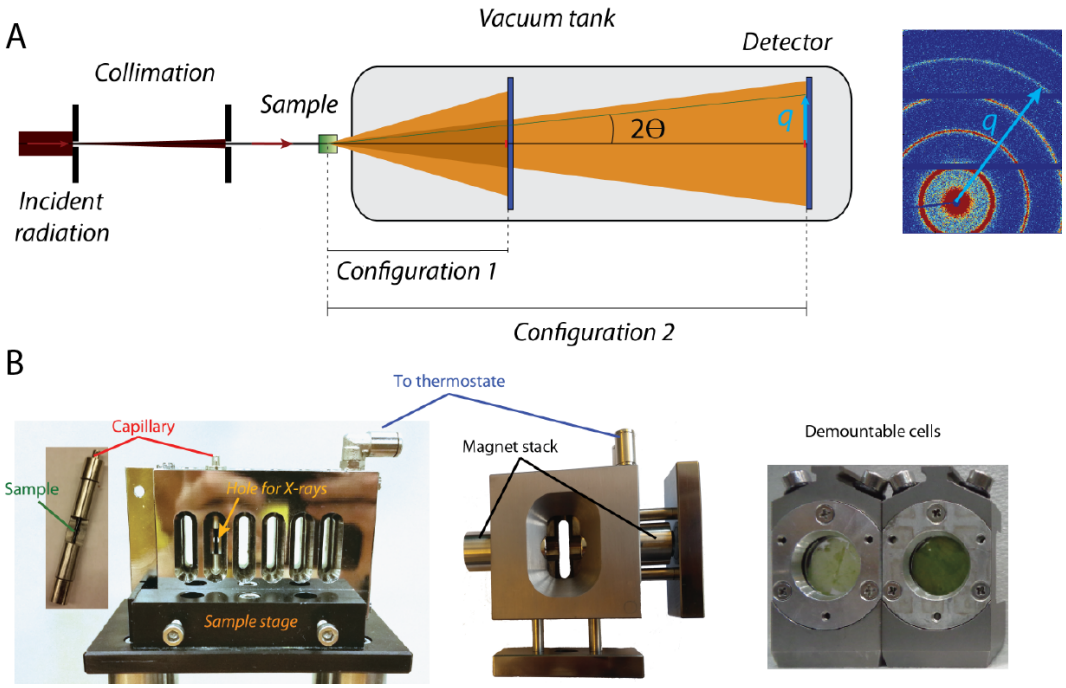

Figure 2.1: a) Small angle scattering setup; b) SAXS capillary holder, capillary magnetic holder and SANS demountable cells.

(e.g. silver behenate) is measured and the scattering angle of the first diffraction peak, corresponding to $d_{001AgBh} = 58.380$ Å ($q = 0.107$ Å^{-1}), is determined.

In order to minimize the beam absorption and air background scattering, many parts of the scattering instrument, especially the detector, is placed in vacuum. Depending on the instrument design, the sample can be placed outside or inside the vacuum tank. If the entire detector tank volume is relatively small and it is possible to reach a vacuum of $\ll 10^{-2}$ mbar quickly, the sample can be put in the air-tight container and remaining air pumped out from the detector tank. This option is used in the in-house SAXSlab 'Ganesha' instrument. In the large-scale facility SANS or synchrotron SAXS instruments, where detector tank volumes are significantly higher and evacuating the tube from air before each measurement is impractical, the sample stage is placed outside the vacuum tank (or in a smaller compartment which can also be evacuated); however detector and other components are placed in a permanent high vacuum (of $\ll 10^{-4}$ mbar [269]).

Three SAXSlab 'Ganesha' instrument configurations were routinely used with the in-house instrument, covering q range of 0.007-2.8 Å^{-1} (Fig. 2.2), the total measurement time was approximately 60+30+10 min. Specifications of all used X-ray and neutron beamlines are given in Table 2.1.

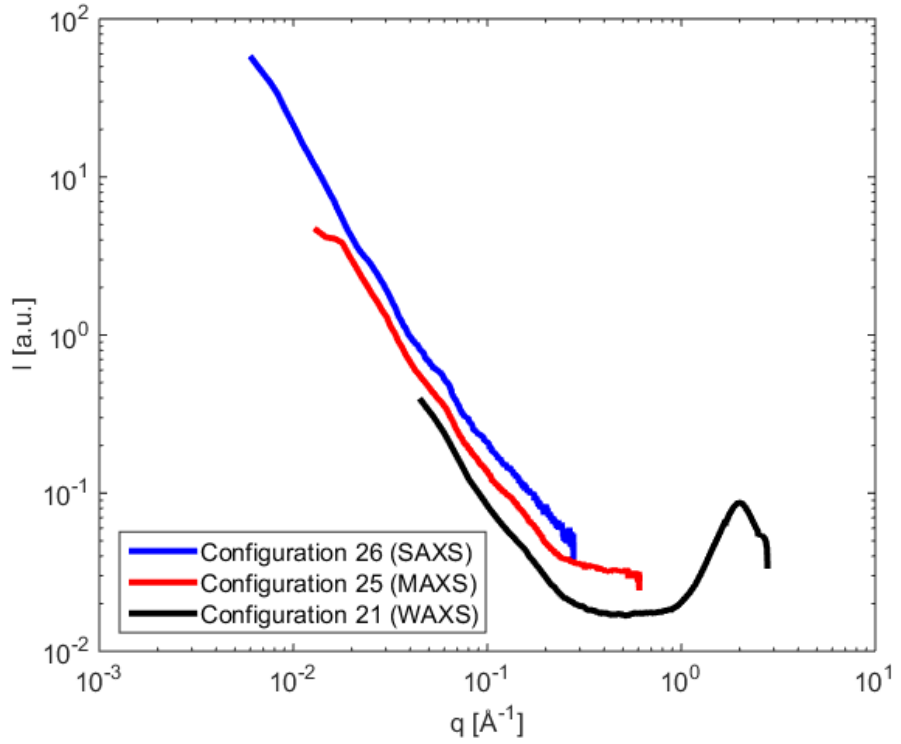

Figure 2.2: SAXSlab 'Ganesha' settings. The curves are vertically shifted for clarity.

Table 2.1: Beamlines and instrument configurations

Configuration	**Sample-Detector distance, mm**	$\mathbf{q}_{min}$, **Å**$^{-1}$	$\mathbf{q}_{max}$, **Å**$^{-1}$	Exposure time, s
Ganesha (SAXS, 26)	1941	0.007	0.18	3600
Ganesha (MAXS, 25)	691	0.015	0.4	1800
Ganesha (WAXS, 21)	101	0.07	2.8	600
PETRAIII (P12)	3000	0.0025	0.5	0.05
ANSTO (BILBY)	10000	0.0038	0.26	3600-7200
SANS-II (PSI)	6000	0.0048	0.03	4800
SANS-II (PSI)	4000	0.013	0.08	2400
SANS-II (PSI)	1500	0.03	0.22	1200

2.2.2 Mathematics

Despite the interaction of X-rays and neutrons with the matter is fundamentally different (practical comparison between X-ray and neutron scattering is given in next chapter), the physics of elastic scattering is described using the same mathematical apparatus. During a scattering experiment, an object is illuminated with monochromatic plane waves travelling in z direction (Fig. 2.3 a): $\psi_{incident} = \psi_0 e^{i\boldsymbol{kz}}$, where a wave vector $\boldsymbol{k}$ has

modulus:

$$k = |\boldsymbol{k}| = \frac{2\pi}{\lambda} \tag{2.1}$$

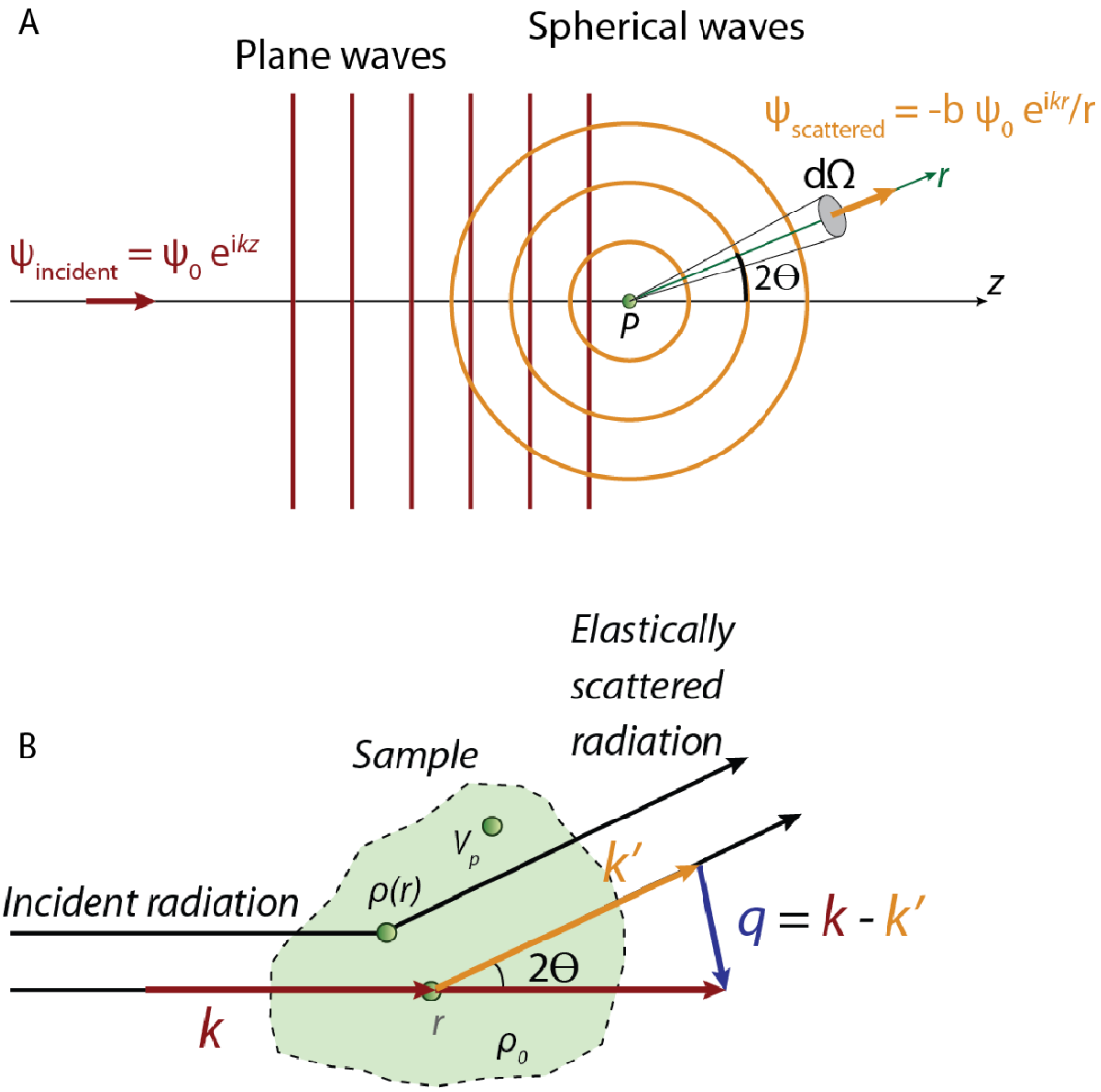

Figure 2.3: Physics of wave scattering. Solution scattering

The atoms (either electron shell or nuclei) within an object interact with incident radiation and become sources of spherical secondary waves. If the scattering is elastic, then in any chosen direction of r: $\psi_{scattered} = -b\psi_0 \frac{e^{ikr}}{r}$ (Fig. 2.3 a). Scattering length b defines how 'well' the object scatters ($I_{scattered} = I_0|b|^2\Delta\Omega$). Here I_0 is the intensity of incident radiation and $\Delta\Omega$ is the small element of solid angle, $d\Omega$ is $\Delta\Omega/r^2$. The

scattering lengths of selected elements are drawn to scale as elemental radii for comparison (Fig. 2.4). In the case of X-rays, b_X depends linearly on the number of electrons (atomic number) Z and is the product of Z and $r_{Thompson}$ - the classical radius of electron (Thomson scattering length, $r_{Thompson} = 2.82 \cdot 10^{-5}$ Å) - b_X has the same sign for all elements and has a magnitude proportional to Z (Fig. 2.4, blue circles). In the case of neutrons, b_N depends on the total nuclear spin distribution and is isotope specific; it does not vary with atomic number in a monotonic simple way (Fig. 2.4, red circles).

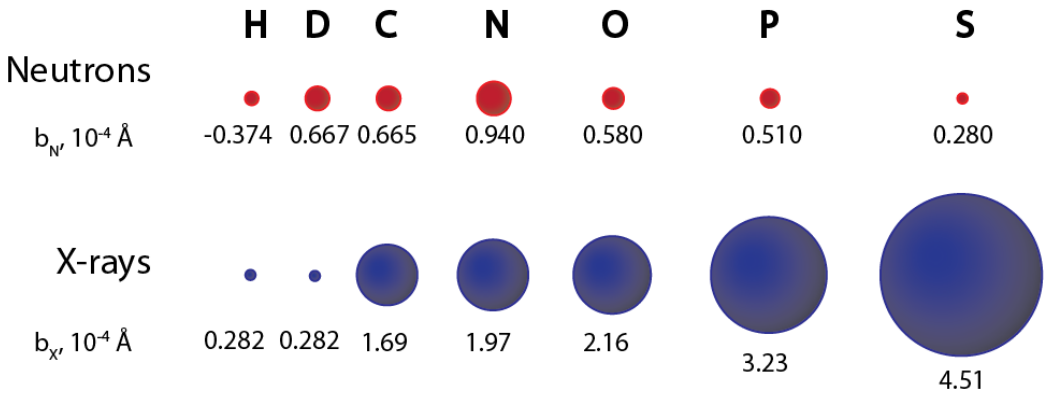

Figure 2.4: a) X-ray and b) neutron scattering lengths drawn as element radii for comparison [105, 104, 251].

As instrument distances are macroscopic quantities compared to Ångstrom order of radiation wavelength, both the incident ($\boldsymbol{k}$) and scattered radiation in any given direction ($\boldsymbol{k'}$) over a solid angle element $d\Omega$ can be considered as plane waves. Since the scattering is elastic, *i.e.* no energy transfer from the incident wave to the object takes place, the modulus of the scattered wave is equal to the incident wave $|\boldsymbol{k'}| = |\boldsymbol{k}|$. The scattering vector is defined as $\boldsymbol{q} = \boldsymbol{k} - \boldsymbol{k'}$. From the scattering triangle (Fig. 2.3 b):

$$|\boldsymbol{q}| = 2|\boldsymbol{k}| \sin\theta = (4\pi/\lambda) \sin\theta \tag{2.2}$$

The scattering length density (SLD) is obtained by summing the coherent scattering lengths of all atoms in the volume element v: $V_{electron} < v <$ particle volume V_p, centered at position $\mathbf{r}$, and dividing by that volume element:

$$\rho(\mathbf{r}) = \frac{1}{v} \sum_{i \in v} b_i(\mathbf{r}) \tag{2.3}$$

Integrating over the volume of the particle V_p and invoking its scattering length density distribution function $\rho(\mathbf{r})$, the unit cell form factor amplitude of an arbitrary

particle is (Eq. 2.4):

$$F(\boldsymbol{q}) = \int_{V_p} \rho(\mathbf{r}) e^{i\boldsymbol{q}\mathbf{r}} d\mathbf{r}. \tag{2.4}$$

If a scattering object is placed not in the vacuum, but in a solvent with a uniform scattering length density ρ_0 (Fig. 2.3 b), the relevant quantity is not the scattering length density of the object itself, but the difference between the object and the solvent: $\Delta\rho = \rho(\mathbf{r}) - \rho_0$. This value is named *contrast* and replaces $\rho(\mathbf{r})$ in equation (2.4). That is to say, if the scattering length difference is zero, the object is invisible (contrast matched-out), since the object and the surrounding medium scatters with the same intensity.

When the scattering object (sample) is composed of identical particles, the measured scattering intensity is proportional to a product of the prefactor term, form factor $P(\boldsymbol{q})$ and a structure factor $S(\boldsymbol{q})$:

$$I(\boldsymbol{q}) = N_p V_p^2 \Delta\rho^2 |F(\boldsymbol{q})|^2 \cdot S(\boldsymbol{q}) \tag{2.5}$$

where N_p is the number of identical particles, each of volume V_p .

The form factor term $P(\boldsymbol{q}) \equiv F(\boldsymbol{q})^2$ describes the overall shape of an individual scattering particle - in the case of this work - lamellae, whereas the inter-particle structure factor term $S(\boldsymbol{q})$ accounts for the local order between scattering particles. In the scope of this work, $S(\boldsymbol{q})$ defines the stacking order of the system and is a composite function with the number of layers in an ordered system, their repeat distance (D) and thermodynamic parameters, such as disorder. The derivations and discussions on contrast, form and structure factor terms is given as the separate chapter of this PhD thesis.

2.2.3 Differences between X-rays and neutrons

Although small-angle X-ray and neutron techniques are similar, yield structures of medium-resolution and can be used complementary, some practical differences between the two techniques are highlighted in this section and summarized in Table 2.2.

The interaction of X-rays and neutrons with matter is fundamentally different. X-rays (high frequency photons) are scattered by the electron shell surrounding the atomic nuclei, while neutrons are scattered by the atom nuclei. The energy carried by the massless X-ray photon and neutron with a mass of $1.67 \cdot 10^{-27}$ kg is different. If we consider a particle of wavelength λ, what corresponds to a wavevector $k = \frac{2\pi}{\lambda}$, then the X-ray photon has energy $E_{photon} = \hbar ck$ and the neutron has an energy of $E_{neutron} = \frac{\hbar^2 k^2}{2m}$, *i.e.* X-ray energy is more than $2 \cdot 10^5$ times higher (12.398 keV *vs.* 81.81 meV for 1 Å). High flux from synchrotron-based X-ray sources requires shorter measurement times (miliseconds) compared to neutrons, however the chance of the X-ray photon is not scattered, but absorbed - and causes sample damage - also increases. Photoelectric

absorption, fluorescent X-ray or Auger emission - all these secondary phenomena quickly ionize and physically damage the sample. If laboratory-based X-ray sources (having lower flux) or neutron sources are used, the sample does not degrade for 24 hours, however a single measurement of sufficient resolution can take from 10 min to 3 hours. During this time, a lot of biological-adaptation processes, which change sample biologically, can take place (due to stress-induced protein degradation, oxygen starvation, slight changes in cellular pH, NPQ), especially if measured *in vivo* on intact organisms. Therefore, one needs to be aware whether scattering from the sample changes through the entire measurement, and to fine-tune measurement times accordingly.

In biological systems, scattering predominantly occurs from low molecular mass atoms (H, C, N, O, P, S). In the case of X-rays, scattering depends of its total number of electrons per unit volume and how different this is from the medium. Knowing that low-Z elements, which ultimately form proteins and lipids, scatter poorly and that the surrounding medium is water (for cyanobacterial cells) or 0.4 M (13.7 %, w/w) sucrose solutions (for isolated thylakoids, required to keep high osmotic pressure and sufficient thylakoid stacking), the overall X-ray scattering contrast (Fig. 2.5 a) is often low and structural features cannot be resolved. A low X-ray contrast is indicated with diffused colors of Fig. 2.5 c). As exemplified by scyatic myelin, membrane SLD profile from X-rays is very different from SLD profile from neutrons - and the overall neutron scattering is smaller in H_2O compared to D_2O (Fig. 2.5 d) [129].

In the case of neutron scattering, different isotopes of a chemical element have their own characteristic scattering lengths (Fig. 2.4). This gives rise to the coherent and incoherent scattering: the coherent scattering interferes and thus gives 'structural' effects, such as correlation between lattice positions, whereas the incoherent scattering occurs from deviations and spin, does not interfere and contributes only to the flat background scattering. Coherent and incoherent neutron scattering of hydrogen (H) and deuterium (D) atoms differ: a coherent scattering cross-section $\sigma_{coh} = 4\pi\langle b\rangle^2 = 4\pi b_{coh}^2$ of D is 3.5 barns larger ($1\ barn = 10^{-24} cm^2$) than of H, whereas incoherent scattering cross-section $\sigma_{incoh} = 4\pi(\langle b^2\rangle - \langle b\rangle^2)$ of H is 78.5 barns larger than of D. This means that the background signal from D is substantially lower that from H and that total neutron scattering lengths for these isotopes differ ($b_{ND} = 0.667 \cdot 10^{-4}$Å vs. $b_{NH} = -0.374 \cdot 10^{-4}$Å, depicted in Fig. 2.4).

These physical properties of H-D are wisely employed during biological SANS measurements. By directly introducing deuterium into a scatterer (or exchanging water with D_2O) one significantly alters the overall scattering - the scattering background is significantly reduced and the total scattering length density is changed. Therefore, by varying the H_2O/D_2O ratio of the aqueous medium the overall contrast can be changed systematically [258, 96] (Fig. 2.5 b). As derived earlier, if the contrast is zero, then the scattering from a particular component is not observed (matched-out). As exemplified by the photosynthetic membrane having both protein and lipid components, they can be separately investigated during SANS experiment, depending on the H_2O/D_2O ratio of the resuspension medium (Fig. 2.5 c). For SANS experiments described in literature,

thylakoid membranes were resuspended in 100 % D_2O and BBY particles in either 40 % or 100 % D_2O [220, 195, 297]. In this PhD work, SANS experiments with leaves and cyanobacterial cells were routinely performed in 100 % D_2O-based medias.

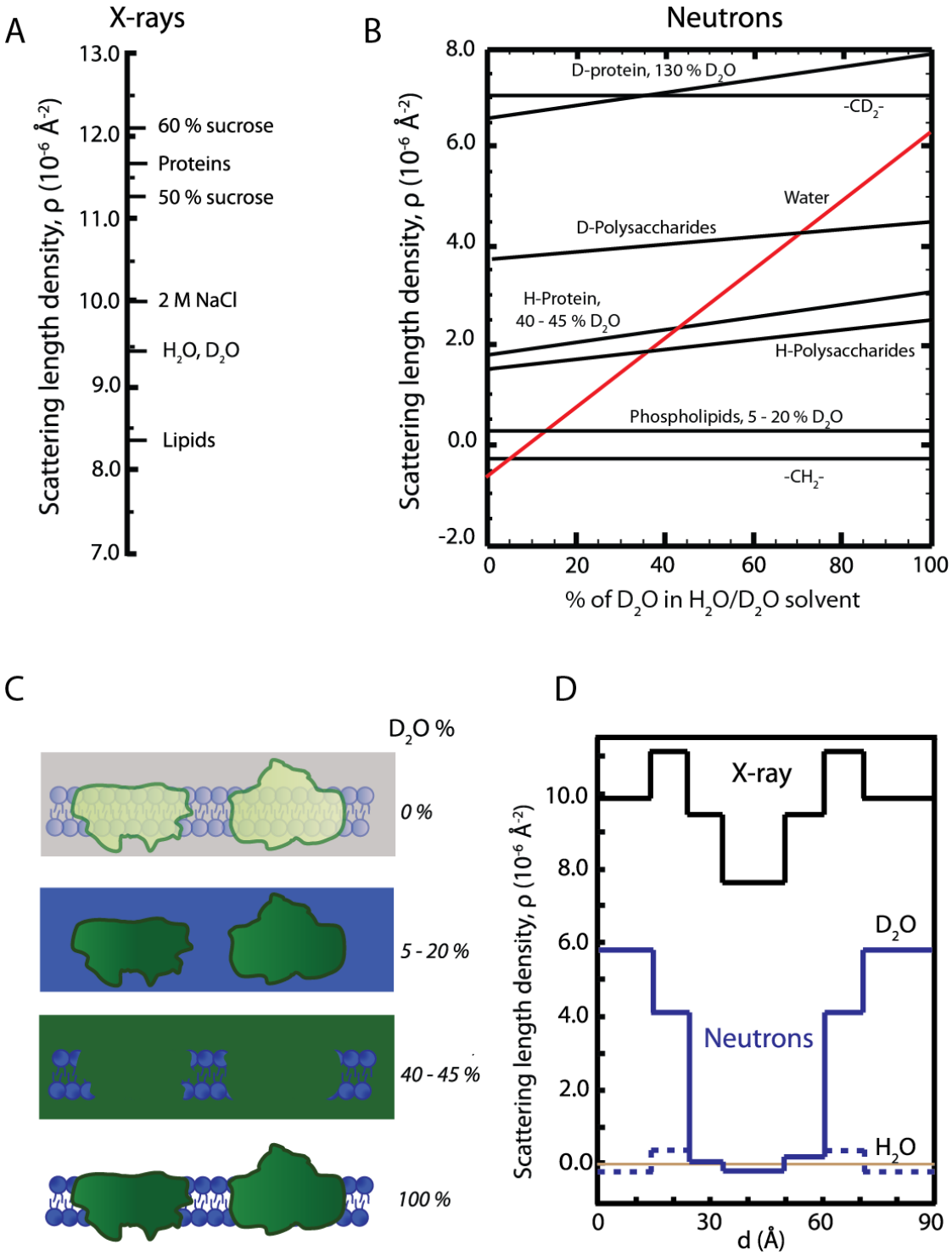

Figure 2.5: a) X-ray and b) neutron scattering length densities; c) Photosynthetic membrane visualization in different contrast conditions; d) Comparison of X-ray (black) and neutron scattering profiles of the same membrane. Neutron scattering is higher in D_2O (violet line) than in water (violet dashed line).

Table 2. Differences and practicalities between SAXS and SANS experimental techniques [288]

	SAXS	**SANS**
Interacting field	Electrons (inhomogeneities in electron densities of the sample)	Nuclei (fluctuations in the nuclear densities of the sample)
Incident beam wavelength, Å	1.0-1.6	4.0-25.0 (thermal: 0.9-10.0)
Flux of the source (particles/s/mm^2)	Medium to high (10^{8-9}-10^{11})	Very low to low (10^5-10^{8-9})
Coherent scattering length, 10^{-4} Å	H: 0.28, D: 0.28	H: -0.374, D: 0.667
Scattering length density, 10^{-6} Å^{-2}	H_2O: 9.47, D_2O: 9.37	H_2O: -5.60, D_2O: 6.33
Incoherent scattering	Low	High
Contrast variation and D-isotope labelling	Rarely used (small or no contrast variation)	Commonly used (large contrast variation)
Sample volumes required in 1-2 mm pathlength cell	20-30 μL	$\gg$ 150 μL
Sample concentration (mg chlorophyll/mL)	5.0-10.0	1.0-3.0
Radiation/Heat damage to the sample	Low for laboratory sources, high for synchrotron sources	Low
Structural information extracted for an individual unit in multicomponent systems	No (electron density average of the entire sample)	Yes (lipid, nucleic acid, protein components can be investigated separately)
Resolution (*vs.* atomic-resolution structures)	Low-Medium	Low-Medium
Experimental facilities	Laboratory and synchrotron radiation sources	Large facilities only
Typical sample counting time	Seconds to minutes	Minutes to hours

2.2.4 The time-of-flight technique

The time-of-flight SANS mode was also used in 'BILBY' instrument in Australian Nuclear Science and Technology Organization (ANSTO) during this PhD, therefore is briefly described here.

Scattering measurements at neutron reactors are generally carried out with a monochromated beam. Monochromatization of neutrons is achieved by the rotating velocity selectors, which allow neutrons of only certain velocity to pass through. To collect data at wide q range, the use of two or three instrument geometry configurations might be needed.

However, this is not the only measurement possibility. Unlike synchrotrons and nuclear reactors with a continuous neutron output, neutrons in spallation sources are produced in short pulses with 10-60 Hz frequency as focused proton bunches periodically hit the target, which then emits neutrons. BILBY is a Time-of-Flight SANS, installed on the reactor source. The neutrons of a wide energy range are selected by rotating disc choppers. The chopper in reactor sources produces a polychromatic pulse of neutrons with a width determined by the time taken by the time to cover distance between the pair of two main choppers, called a double-pair. This neutron pulse cross the chopper at the same time t_0. On BILBY, neutron wavelength range of 2-20 Å (what means a neutron velocity spread of 2000-200 m/s) are used, which allow to cover the necessary q range. As neutrons travel beyond the chopper and are scattered by the sample, they characteristically spread out with faster neutrons arriving to the detector first (Fig. 2.6). The energy and wavelength of each elastically scattered neutron from a single pulse can be determined based on its arrival time (time-of-flight between the point of origin and the detector) using the de Broglie expression:

$$\frac{h}{\lambda_{neutron}} = m_{neutron} \cdot v = m_{neutron}\frac{L}{t}$$

$$t(\mu sec) = 252.78 L(m) \cdot \lambda(\text{Å}) \tag{2.6}$$

$$\frac{\Delta\lambda}{\lambda} = \frac{\Delta t}{t}$$

where t is the time (time-of-flight, ToF) at which an elastically scattered neutron is detected at a given flight distance L. BILBY wavelength resolution in ToF mode is determined by the time resolution of the detector (5-18 Å; q range: 0.01-0.3 Å^{-1}) and is 5 %, whereas if 6 Å wavelength is pre-selected by the velocity selector (same q range), the wavelength resolution is 10 % (Fig. 2.6 b). To further widen the q range several detectors can be placed in different L positions.

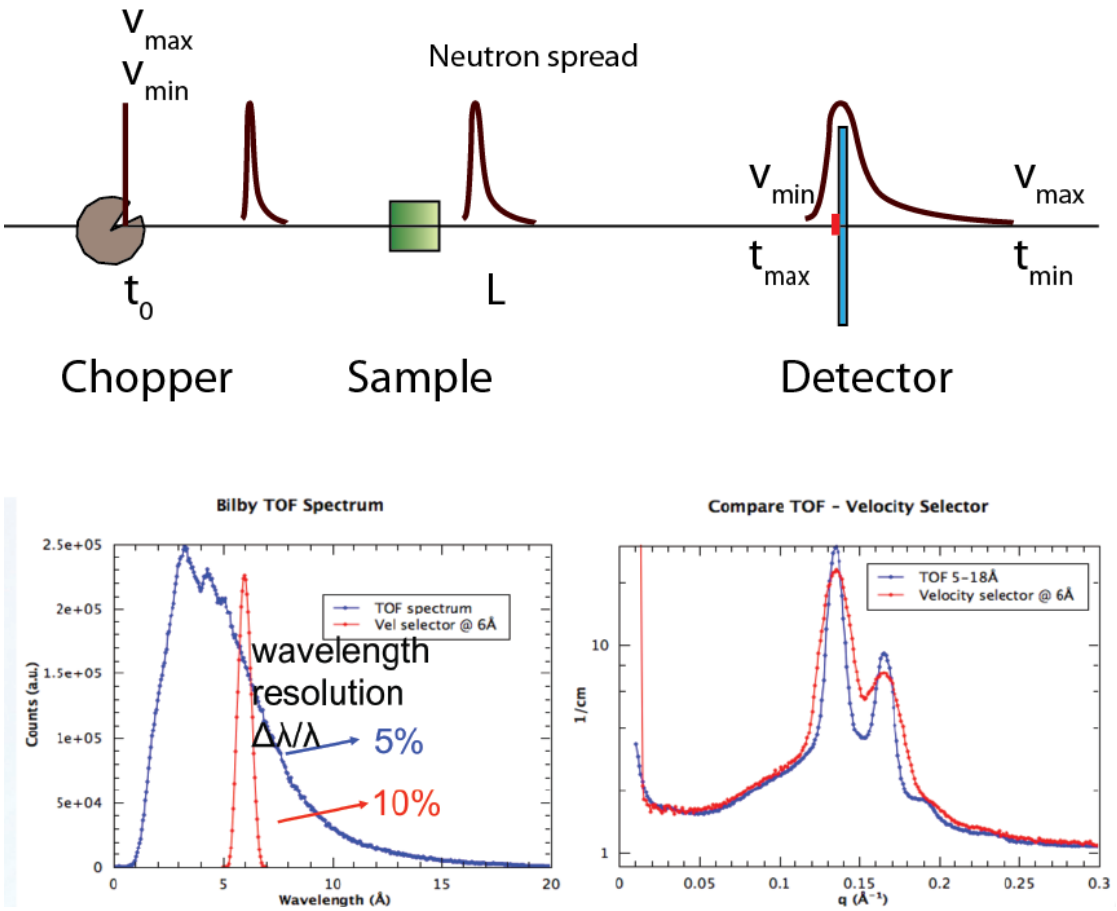

Figure 2.6: Neutron wavelength spread during ToF SANS experiment. Comparison of wavelength and resulting q resolutions in ToF chopper mode (blue) and velocity selector (red) mode [270]. Improved resolution (5 % in TOF mode vs. 10 % in vs mode) enables to distinguish scattering features, which would be smeared at worse resolution.

2.2.5 Resolution

In a small-angle X-ray scattering experiment the beam is monochromatized by Bragg scattering from a crystal, mirrors or filters. The radiation spectrum from an X-ray source is continuous and the wavelength spread $\Delta\lambda/\lambda$ is determined by the mosaic spread, or Darvin width of the monochromator, and beam collimation. For both conventional and synchrotron X-ray source the wavelength spread is typically smaller than 10^{-3} and can be neglected [215]. X-ray photons, contrary to neutrons, move with the speed of light and are massless, therefore are not affected by gravitational effects.

The situation is different in a neutron scattering experiment. Due to relatively low neutron flux available, monochromators with a large wavelength spread (wavelength spread

contribution) and large (cm) apertures (geometry contribution, divergence contribution) are used to retain flux. Furthermore, a neutron has mass and falls while flying. This gravity effect is also accounted for in resolution and is more evident for longer sample-detector distances and for slower (higher wavelength) neutrons; for 6 Å, neutrons fall by ca. 0.5 cm in 13 meters, whereas for 20 Å the fall is already 4 cm [93].

In a ToF instrument, the resolution is determined by uncertainty in the distance traversed by the neutrons between the neutron source and the detector (ΔL), the uncertainty in the corresponding time of flight (Δt) and the uncertainty in the scattering angle ($\Delta 2\theta$) [305]. More precisely, the sum of geometric, wavelength spread and gravity contributions affects SANS data q resolution - q resolution variance σ_q in x and y directions is non-zero, gravity effect term is present in only in σ_{qy} term; elaborate derivation of these formulae is given in Part D of Hammouda (2008) [93].

$$(\sigma_{qx})^2 = \Big(\frac{2\pi}{\lambda L_2}\Big)^2 \Bigg\{ \Big(\frac{L_2}{L_1}\Big)^2 \cdot \frac{R_1^2}{4} + \Big(\frac{L_1+L_2}{L_1}\Big)^2 \cdot \Big(\frac{R_2}{4}\Big)^2 + \frac{1}{3} \cdot \Big(\frac{\Delta x_3}{2}\Big)^2 \Bigg\} + q_x^2 \cdot \frac{1}{6}\Big(\frac{\Delta\lambda}{\lambda}\Big)^2$$

$$(\sigma_{qy})^2 = \Big(\frac{2\pi}{\lambda L_2}\Big)^2 \Bigg\{ \Big(\frac{L_2}{L_1}\Big)^2 \cdot \frac{R_1^2}{4} + \Big(\frac{L_1+L_2}{L_1}\Big)^2 \cdot \Big(\frac{R_2}{4}\Big)^2 + \\ + \frac{1}{3} \cdot \Big(\frac{\Delta y_3}{2}\Big)^2 + \Big(L_2(L_1+L_2)\frac{g m_{neutron}^2}{2h^2}\Big)^2 \cdot \lambda^4 \cdot \frac{2}{3} \cdot \Big(\frac{\Delta\lambda}{\lambda}\Big)^2 \Bigg\} + q_y^2 \cdot \frac{1}{6}\Big(\frac{\Delta\lambda}{\lambda}\Big)^2 \tag{2.7}$$

where L_1 is collimation (source-to-sample) length, L_2 is sample-to-detector distance, R_1 is source aperture radius, L_2 is sample aperture radius, $\Delta x3$ and $\Delta y3$ are sides of the detector, $\Delta\lambda$ is the wavelength spread assuming a triangular wavelength distribution.

In order to analyse such neutron data, pinhole aperture sizes and instrument distances (collimation length, sample-to-detector distance) as well as wavelength spread ($\Delta\lambda/\lambda$) needs to be known beforehand for every instrumental setting and σ_q is calculated for every q value of the data (this is called the resolution function). When SANS data are being fitted, either data de-smearing, or smearing the fitting model function (most commonly), that is adding resolution function to the theoretical scattering model, is performed.

The smearing can be automatically done by the modelling program 'WillItFit' if physical parameters are provided [216]. In short, if experimental SANS data are radially averaged to a 1-D curve, 1-D convolution smearing integral, containing the 1-D Gaussian resolution function with the standard deviation σ_q, is added to theoretical form-structure factor model - in this way, characteristic data smearing is obtained. Calculation of ToF resolution is more complex, since the wavelength distribution is not triangular and each

pixel of each detector registers the entire neutron velocity spectrum at different times. ToF q resolution is calculated per each detector pixel using the Mildner and Carpenter equation and can be significantly better, if compared to velocity selector mode (Fig. 2.6 b) [176, 223]:

$$\begin{aligned}(\sigma_q)^2 = \frac{4\pi^2}{12\lambda^2}\{3(\frac{R_1}{L_1})^2 + 3(\frac{R_2}{L_3})^2 + (\frac{\Delta R}{L_2})^2\} + q^2 \cdot \frac{\sigma_\lambda}{\lambda})^2 \\ \frac{1}{L_3} = \frac{1}{L_1} + \frac{1}{L_2} \\ (\sigma_\lambda)^2 = (\Delta\lambda)^2/12 + (\sigma_{moderator})^2\end{aligned} \tag{2.8}$$

where L_1 is collimation length, L_2 is sample-to-detector distance, R_1 is source aperture radius, R_2 is sample aperture radius, ΔR is virtual ring width on the detector, $\sigma_{moderator}$ is the variation in time for the moderator to emit neutrons of a given wavelength. In practice, σ_q is provided separately for each q value after data reduction and can be imported directly in 'WillItFit' modelling program [216]. Small angle scattering data modelling is elaborated in the next chapter.

2.3 Small-angle scattering in photosynthesis research

Scattering studies on photosynthetic membranes can be broadly divided into two periods: before 1980s scattering studies, in parallel to TEM, were aimed to elucidate the lamellar nature and interior structure of a single membrane bilayer as well as their phase behaviour - temperature and water content necessary for lamellar structure. Many types of highly layered biological membranes have been investigated: myelin, collagen, photosynthetic membranes of *Euglena*, purple membranes of *Halobacterium halobium*, photoreceptor membranes of retinal rods, stacked erythrocyte membranes, *Escherichia coli*, *Mycoplasma* membranes, sarcoplasmic reticulum membranes, muscle, synthetic lecithine bilayers [303, 177, 44, 129, 312, 308, 307]. Isolating membranes and measuring their scattering allowed elucidating electron density profile of the bilayer (hydrophyllic outside, hydrophobic inside), bilayer thickness and even membrane bilayer protein/lipid composition ratio of 0.5/0.5 [303, 127]. Experiments of the 'second period', started by G. Garab and T. Javorfi in 1998, began to examine thylakoid ultrastructure changes in light [112] and thylakoid membrane organization in mesoscale (grana stacks) [103].

Compared to nerve myelin or synthetic membranes, photosynthetic membranes are much less ordered, less oriented and give a much more diffuse scattering. The first scattering study on photosynthetic membranes was performed in 1953 by Finean *et al.* - small-angle reflection band at 250 Å from isolated *Aspidistra elatior* chloroplasts in sucrose buffer fixed with OsO_4 correlated with the repeating unit of the layers obtained from TEM [65, 181] (Fig. 2.7 a). Two problems became immediately apparent: scattering peaks were diffused due to a system disorder and repeat distances, obtained from scattering,

were higher than of TEM. To reduce system disorder, isolated *Euglena* chloroplasts were centrifuged on a thin mica, dried to 90 % humidity and measured at 0 °C for 24 hours - a more biological lamellar periodicity of 165-170 Å was obtained; Sadler *et al.* was aware that lamellae swell in > 90 % humidities and this reduces the overall system order [236]. Importantly, this work was expanded by measurements *in vivo*. The first electron density profile of 'thylakoid membrane-lumen-thylakoid' was proposed, although high membrane protein content was not taken into account [236]. In parallel, protein and pigment arrangements inside a single membrane as well as individual thylakoid lipid scattering was investigated, leading to the 'ball and plate model of thylakoid' (Fig. 2.7 b) - lipids and porphyrin region facing inside, proteins facing outside membrane.The two adjacent thylakoid membranes should be separated by a 100 Å thick water layer. Because the total repeat distance *in vivo* was 250 Å and the entire thylakoid membrane thickness was 150 Å, the resulting water layer thickness should be 100 Å [142, 143]. This needs to be clarified - a single membrane was already known to be 40-50 Å thick (from TEM), therefore a 150 Å 'thylakoid membrane thickness' would actually mean the thickness of two thylakoid membranes and a separating water layer between them. The aqueous lumenal compartment, although already hypothesized, was not resolved at this stage [214] (Fig. 2.7 b).

The structure and form factor equations of thylakoid membrane, required to calculate the electron distribution of a thylakoid membrane, were also derived at this point [145, 144, 146, 141, 140, 142, 143, 236, 214, 101, 57]. The work on isolated thylakoid membranes was expanded with measurements *in planta*: if plant leaves were oriented perpendicularly to X-ray beam, green leaves with normal thylakoid ultrastructure exhibited lamellar scattering, but white leaves, where chloroplasts have no lamellar structure, yielded no ordered scattering. This implied that cell wall and other components does not scatter in an ordered manner, only thylakoids (Fig. 2.7 b).

Another solution to increase scattering intensity was introduced by N. E. Gecintov and D. Sadler in 1976, when they partially aligned isolated thylakoid membranes using external 1 T magnetic field and got an increased ordered scattering signal [78, 235] (Fig. 2.7 c). From the chlorophyll *a* fluorescence polarization in magnetic field *in vivo* they hypothesize, that thylakoid membrane alignment in magnetic field occurs due to anisotropy of magnetic susceptibility of 'some cell components' - thylakoids (and maybe individual chlorophyll molecules) are preferentially oriented perpendicularly to magnetic field and show that this alignment is relatively small at low magnetic field (< 0.2 T), linearly increases in intermediate magnetic fields (0.3-0.5 T) and reaches saturation in high magnetic field strengths (1-3 T). It is also noted, that *Euglena* cells did not reach saturation of fluorescence polarization even after applying 10 T magnetic field [78] and that 7 T is required to orient oblate cyanobacterial *S. lividus* cells perpendicularly to magnetic field [290]. Although biophysically possible to perform, using such high fields question the biological validity of *in vivo* experiments and magnetic alignment has only been used for isolated thylakoids.

When the first SANS measurements on magnetically oriented intact chloroplast

isolates in 100 % D_2O medium were performed, the idea of 'hydrophilic partition' - *i. e.* the existence of two aqueous compartments: lumen and stroma, which separate single thylakoid membranes, was finally introduced [237]. Sadler *et al.* have shown, that thylakoid orientation by centrifugation and dehydration decreased repeat distances and periodicities greater than 180 Å are lost after centrifugation, compared to distances after to magnetic alignment (165 vs. 250 Å); magnesium ion removal also severely decreased ordered scattering [238]. It has been inferred, that the extensive isolation procedures and the manipulation of divalent ion concentrations in the medium modify thylakoid ultrastructure, favouring measurements in *in vivo*-like conditions. This work, employing contrast variation, also showed that scattering was severely reduced in 30 % D_2O, although no information about membrane protein-lipid composition was inferred. Measuring additional SANS in different contrasts (5-80 %) on isolated thylakoid membranes of *Rhodophseudomonas sphaeroides*, the structure of thylakoid membrane was introduced, as we know it today, disproving the 'ball and plate' model of Kreutz *et al.* [143]. From scattering experiments, a single thylakoid membrane was shown to have thickness of 50 Å, be symmetrical in scattering density and have 0.75 protein:0.25 lipid (v/v) ratio. It has been suggested that individual proteins interrupt lipid sheet and extend beyond it [237, 151]. Thylakoid membrane thickness measurements from TEM and different physical methods yield 34-75 Å [151, 85, 124], what is well comparable to thylakoid membrane thickness measured by scattering methods.

Knowing membrane composition allowed measuring osmolarity effects on isolated spinach thylakoids: thylakoid swelling was observed at low-salt conditions and low sucrose concentration (159 - 227 Å); lumen swelling was inferred from electron density profile changes, whereas no individual membrane thickness changes were observed [57, 75]. It has been also shown, that isolated PSII membranes shrink in low hydration [193, 218].

Later scattering studies on isolated plant thylakoids confirmed the thylakoid shrinkage in higher osmolarities and light-induced thylakoid membrane reorganizations were investigated [75, 112, 85, 103, 195, 196, 275]. As higher plant thylakoids, which contain grana and stroma thylakoids, were investigated, a construction of ultrastructural model with separate granal and stromal unit cells had been pursued, with the aim to extrapolate membrane and lumen thicknesses of granal and stromal unit cells and number of thylakoids in a granum from fitting the entire scattering curve. The model, however, was never practically applied [103, 128, 220]. Repeat distances of stromal unit cell were latter attributed to grana unit cell, since thylakoids were isolated and thus swollen [297].

A quick (of the order of minutes) thylakoid repeat distance decrease was observed upon illumination of isolated, magnetically-aligned thylakoids [194]. This shrinkage has been diminished by adding uncouplers, suggesting that proton influx into lumen (transmembrane Δ pH) upon illumination causes the effect. It has also been shown that repeat distance decreases if thylakoids are resuspended in pH 5, compared to pH 8 [296].

However, no information regarding lumen or membrane thickness changes can be inferred, since a prevailing explanation takes into account only peak q value and does not model the entire scattering curve [297, 295, 296]. In order to observe illumination

effect *in vivo* in simpler systems (*i. e.* to 'avoid' a complex grana-stroma arrangement of higher plants), light responses of photosynthetic organisms with more simple thylakoid arrangement were investigated: cyanobacteria [195, 154, 156, 152], diatoms [196] and algae [197] had been used. Similar light-induced effects were observed, indirect indications that thylakoid membrane is more flexible in the dark than in the light were observed [197, 276] although the underlying cause of these observations is yet unclear.

In vivo illumination studies have been recently expanded to plant leaves - a slight RD shrinkage has been observed [297]. This system, however, embodies all inherent complexities: scattering signal is low because chloroplasts are not oriented, granal, stromal and other coherent scattering from cellular components is combined, scattering length densities of thylakoid membrane, lumen and stroma are unknown, vary in time and in space. A synopsis of small-angle neutron scattering and electron microscopy results on photosynthetic systems is provided in Table 2.3 and experimental/measuring conditions are briefed. Overall, although some structural information can be inferred from scattering repeat distances, no structural model, which fully explains the scattering curve of photosynthetic organisms is currently available.

In the context of plant biology, small-angle scattering is not yet a stand-alone technique - it complements various microscopic techniques: transmission electron microscopy (TEM) [173, 213, 274, 217], scanning electron microscopy (SEM) [188, 222], cryo-EM [70, 124], cryo-electron tomography (ET) [262, 21, 53, 69], atomic force microscopy (AFM) [277, 283, 89, 115, 210]), live cell imaging [110, 109], coherent X-Ray diffraction imaging (CXDI) [285, 284] or neutron diffraction [218]. Up to now, small-angle scattering has been used to investigate structure and dynamic changes of thylakoid membrane systems of plants [237, 57, 103, 128, 195, 194, 297, 296], protists [237], diatoms [195, 196], cyanobacteria [156, 295, 276, 152, 62], phycobiliproteins [82], algae [195, 196, 197], bacterial (RC-LHC) and plant (LHCII) light harvesting complexes [288, 41], photosynthetic proteins [83, 150], higher-plant prolamellar bodies (PLB) [254, 304] or plant cell wall cellulose microfibers [167].

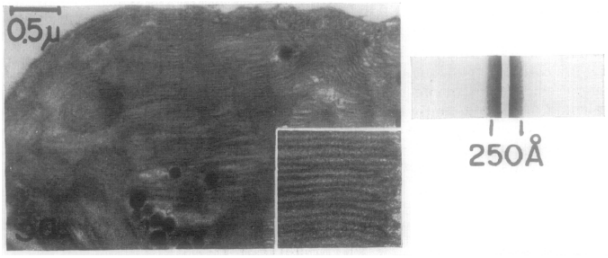

Finean *et al.*, 1953. First low-angle X-ray diffraction measurement on chloroplasts

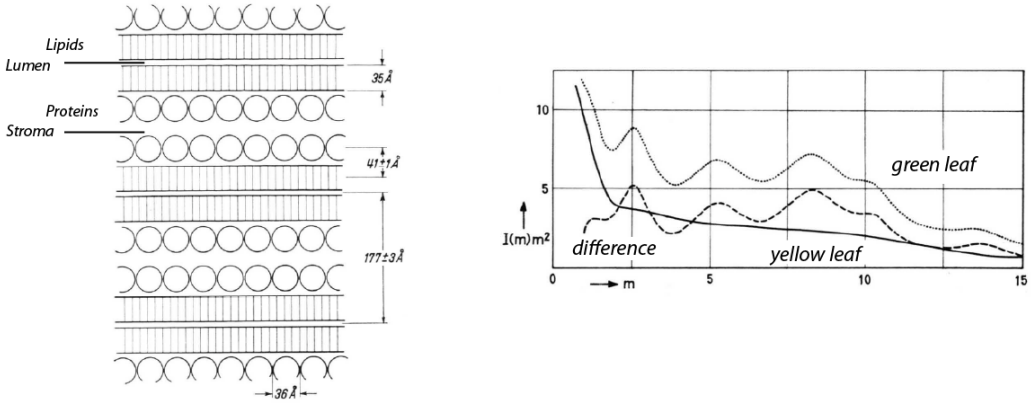

Kreutz et al., 1962 - 1970. Ball and plate model. In vivo scattering

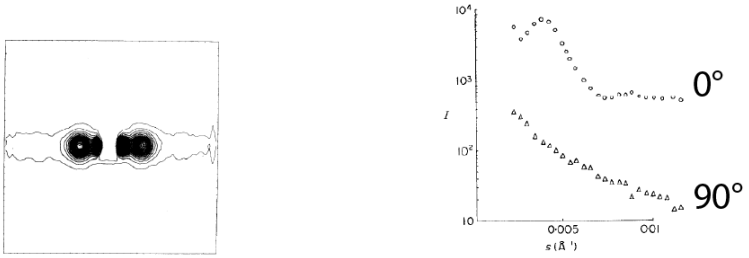

Sadler *et al.*, 1982. SANS. D_2O medium. Magnetic field of 1.7 T

Figure 2.7: Selected small angle scattering studies, contributing to understanding of thylakoid membrane composition and ultrastructure of thylakoid lamellae.

Table 2.3: RD comparison from scattering and EM experiments. Sample type, buffer composition or other experimental conditions are indicated. L - light, RL - red light, WL - white fluorescent light, D - dark, D Re-Ad - dark re-adapted

Species		SANS RD, Å	EM RD, Å	Conditions	Reference
Plants					
Nicotiana tabacum	Leaf	231±5	189± 23 , 193-205	Non-treated leaf	[297], Fig. 30a of [91], cited from [103]
	Leaf	223 ± 7	200 ± 16	D_2O infiltrated	[297]
	Isol. thyl.	314	294	400 mM sorbitol + 5 mM $MgCl_2$ + 5 mM KCl + 20 mM Tricine (pD 7.6)	[297]
	Isol. thyl.	240	208±10	300 mM NaCl + 5 mM $MgCl_2$ + 5 mM KCl + 20 mM Tricine (pD 7.6)	[297]
	Isol. thyl.	349± 11		400 mM sorbitol + 5 mM $MgCl_2$ + 5 mM KCl + 20 mM Tricine (pD 7.6)	[194]
	Protoplasts	251		400 mM sorbitol + 5 mM $MgCl_2$ + 5 mM KCl + 50 mM Tricine (pD 7.5)	[297]
Pisum sativum	Leaf	205	208±16, 205±6, 222	Non-treated leaf	TEM: [297, 77, 257], SANS: [297]
	Leaf	207	209	D_2O transpirated	[297]
	Leaf, average	220 ± 8	224±21	D_2O infiltrated	[297]
	Leaf, + swln end mbrns		211±15 / 230±20	Not infiltrated/D_2O Infiltrated	[297]
	Leaf, - swln end mbrns		205±18 / 206±10	Not infiltrated/D_2O Infiltrated	[297]
	Isol. thyl.	345±11	164±25	400 mM sorbitol + 5 mM $MgCl_2$ + 5 mM KCl + 20 mM Tricine (pD 7.6)	[220]
	Isol. thyl.	342±1 (pD 8.0), 329±1 (pD 5.0)		400 mM sorbitol + 5 mM $MgCl_2$ + 5 mM KCl + 20 mM Tricine	[296]
	Isol. thyl.	235±1 (pD 8.0), 219±1 (pD 5.0)		300 mM NaCl + 5 mM $MgCl_2$ + 5 mM KCl + 20 mM Tricine (pD 5.0)	[296]
	Isol. thyl.	330-355 (D) → 280 (300 μmol L for 30 min) or 271 (1000 μmol L) → 296-306 (D, Re-Ad)		400 mM sorbitol + 5 mM $MgCl_2$ + 5 mM KCl + 20 mM Tricine (pD 7.6)	[220]
	Isol. thyl.		195±4 (D) → 172±3 (50 lux L) or 152±4 (2000 lux L)		[178]
Spinacia oleracea	Leaf	232	157, 144-243, 170-200	Non-treated	TEM: [54, 55, 103]), SANS: [297]
	Leaf	239 ± 6		D_2O infiltrated	[297]
	Isol. thyl.	285-300 (293±7)		400 mM sorbitol + 10 mM $MgCl_2$ + 10 mM KCl + 20 mM Tricine (pD 7.6)	[195]
	Isol. thyl.	314	302 ±35	400 mM sorbitol + 5 mM $MgCl_2$ + 5 mM KCl + 20 mM Tricine (pD 7.6)	[297]
	Isol. thyl.	240	208 ±10	300 mM NaCl + 5 mM $MgCl_2$ + 5 mM KCl + 20 mM Tricine (pD 7.6)	[297]
	Isol. thyl.	279		400 mM sorbitol + 100 mM NaCl + 5 mM $MgCl_2$ + 5 mM KCl + 20 mM Tricine (pD 7.6)	[297]
	Isol. thyl.	273		400 mM sorbitol + 300 mM NaCl + 5 mM $MgCl_2$ + 5 mM KCl + 20 mM Tricine (pD 7.6)	[297]
	Isol. thyl.	241		400 mM sorbitol + 500 mM NaCl + 5 mM $MgCl_2$ + 5 mM KCl + 20 mM Tricine (pD 7.6)	[297]
	Isol. thyl.	307		0 mM sorbitol + 10 mM $MgCl_2$ + 10 mM KCl + 20 mM Tricine (pD 7.6)	[220]
	Isol. thyl.	297		100 mM sorbitol + 10 mM $MgCl_2$ + 10 mM KCl + 20 mM Tricine (pD 7.6)	[220]
	Isol. thyl.	294±7		400 mM sorbitol + 10 mM $MgCl_2$ + 10 mM KCl + 20 mM Tricine (pD 7.6)	[194]
	Isol. thyl.	286±1		400 mM sorbitol + 10 mM $MgCl_2$ + 10 mM KCl + 20 mM Tricine (pD 7.6)	[220]
	Isol. thyl.	277		1000 mM sorbitol + 10 mM $MgCl_2$ + 10 mM KCl + 20 mM Tricine (pD 7.6)	[220]
	Isol. thyl.	269	159±18	2000 mM sorbitol + 10 mM $MgCl_2$ + 10 mM KCl + 20 mM Tricine (pD 7.6)	[220]
	Isol. thyl.	332		100 mM sorbitol + 1 mM $MgCl_2$ + 10 mM KCl + 20 mM Tricine (pD 7.6)	[220]
	Isol. thyl.	297		100 mM sorbitol + 10 mM $MgCl_2$ + 10 mM KCl + 20 mM Tricine (pD 7.6)	[220]
	Isol. thyl.	317		1000 mM sorbitol + 1 mM $MgCl_2$ + 10 mM KCl + 20 mM Tricine (pD 7.6)	[220]
	Isol. thyl.	277		1000 mM sorbitol + 10 mM $MgCl_2$ + 10 mM KCl + 20 mM Tricine (pD 7.6)	[220]
	Isol. chloroplasts		252±26	50 mM sucrose + 44 mM NaCl + 12.5 mM Tris-HCl (pH 7.9)	[185]
	Isol. chloroplasts		172±5	500 mM sucrose + 44 mM NaCl + 12.5 mM Tris-HCl (pH 7.9)	[185]
	Leaf	229 (D) → 227 (D Re-Ad for 5 min) → 224 (1700 μmol L for 5 min) → 220 (1700 μmol L for 10 min) → 223 (D Re-Ad for 10 min)		D_2O infiltrated	[297]
	Isol. chloroplasts	180 → 167	212±8 (L) → 144±9 (RL) → 214±4 (D Re-Ad)	175 mM NaCl + 15 μM PMS + 20 μM PMA + 50 mM Tris-HCl (pH 8.0)	[185]
	Isol. chloroplasts		196±4 (D) → 144±3 (RL)	175 mM CH_3COONa (pH 6.7) + 15 μM PMS	[185]
	Isol. chloroplasts		206±15 (pH 7.7, D) → 143±6 (pH 4.7, D) → 236±24 (pH 7.3, D)	100 mM NaCl	[185]
		288 (150 μmol L for 200 sec) or 286 (330 μmol L for 200 sec) or 272 (650 μmol L for 200 sec) or 262 (1200 μmol L for 200 sec) → 294-298 (D, Re-Ad)		400 mM sorbitol + 5 mM $MgCl_2$ + 5 mM KCl + 100 μM PMS + 20 mM Tricine + (pD 7.6)	[194]
Arabidopsis thaliana	Leaf		D: 163±6 (TEM) 168±4 (freeze-substituted) L (500 μmol for 30 min): 191±5 (TEM) 186±4 (freeze-substituted)	Non–treated leaf	[124]
	Leaf	225		D_2O infiltrated	[99]
	Isol. thyl.	269		400 mM sorbitol + 5 mM $MgCl_2$ + 5 mM KCl + 20 mM Tricine (pD 7.6)	[99]

Continued on next page

Table 2.3 – *Continued from previous page*

Species		SANS RD, Å	EM RD, Å	Conditions	Reference
Lactuca sativa	Leaf		235±7	Non-treated leaf	Estimated as the sum of grana + inter-thylakoid space [262]
	Leaf	222		D_2O infiltrated	[297]
Monstera deliciosa	Leaf	222		D_2O infiltrated	[297]
Hedera helix	Leaf	216		D_2O infiltrated	[297]
Shefflera arboricola	Leaf	227		D_2O infiltrated	[297]
Euphorbia pulcherrima	Leaf	215		Non-treated leaf	[297]
	Leaf	220		D_2O infiltrated	[297]
Epipremnum aureum	Leaf	219		Non-treated leaf	[297]
	Leaf	224		D_2O infiltrated	[297]
	Isol. thyl.	314		400 mM sorbitol + 5 mM $MgCl_2$ + 5 mM KCl + 20 mM Tricine (pD 7.6)	[297]
	Isol. thyl.	241		300 mM NaCl + 5 mM $MgCl_2$ + 5 mM KCl + 20 mM Tricine (pD 7.6)	[297]
Common grass	Leaf	254		Non-treated leaf	[297]
Zea mays	Leaf		110-157	Non-treated leaf	Fig. 21f of [91] cited from [103]
	Isol. thyl.	310		400 mM sorbitol + 5 mM $MgCl_2$ + 5 mM KCl + 20 mM Tricine (pD 7.6)	[297]
Lolium multiflorum	Leaf		172-200	Non-treated leaf	Figs. 2,3 of [38] cited from [103]
Avena ventricosa	Leaf		189-227	Non-treated leaf	Fig. 21c of [91] cited from [103]
Phaseolus vulgaris	Leaf		156±16	Non-treated leaf	[234]
Hordeum vulgare	Leaf		162±5	Non-treated leaf	[267]
Cyanobacteria					
Synechocysis sp. PCC 6803	Bacterial cells	627.1 (D)	550	*in vivo*, in BG-11	[156]
	Bacterial cells	800		*in vivo*, in BG-11	[295]
Synechocysis sp. PCC 6803 CB	Bacterial cells	529.7 (D)	480	*in vivo*, in BG-11	[156]
Synechocysis sp. PCC 6803 CK	Bacterial cells	419.9 (D)	470	*in vivo*, in BG-11	[156]
	Bacterial cells	483		*in vivo*, in BG-11	[295]
Synechocysis sp. PCC 6803 PAL	Bacterial cells	356.9 (D)	340	*in vivo*, in BG-11	[156]
	Bacterial cells	419		*in vivo*, in BG-11	[295]
Halomicronema hongdechloris	Bacterial cells	647.4 (WL), 369 (FR)	430 (WL), 270 (FR)	*in vivo*, K+ES medium, FR - 730 nm, light intensity 20 μmol	[152], RDs from TEM estimated as the sum of Thyl width+inter-thyl width
Leptolyngbya ohadii	Bacterial cells	870/NA (hydrated/dessicated)	610±5/510±29	*in vivo*, in YBG-11	[62, 63]
Other photosynthetic organisms					
Chlamydomonas reinhardtii	Cells	190 (FR)	224±13	*in vivo*, TAP medium, 15 min FR light of 720 nm 1 mW/cm^2; TEM grwth cond N/A	[193, 60]
Phaeodactylum tricornutum	Cells	170 (D), 179 (L), 185 (HL)		4 min WL light of 150 μmol or 1500 μmol	[196]

Chapter 3

Modelling thylakoid membrane scattering

The aim of this chapter is to build up a mathematical apparatus of form factor $P(q)$ and structure factor $S(q)$, which are necessary to explain experimentally measured scattering patterns. The actual scattering for randomly-oriented membrane stacks is described by Eq. 2.5: $I(q) \propto \frac{P(q)}{q^2} \cdot S(q) = \frac{|F(q)|^2}{q^2} \cdot S(q)$ [317]. A series of scattering length density profiles of increasing complexity are constructed and their form and structure factors derived, ultimately aiming to build a complete thylakoid unit cell model for cyanobacteria (Manuscript 1) and higher plants (Manuscript 2). Finally, X-ray and neutron scattering length densities of thylakoid membranes in cyanobacteria and higher plants, and stroma, are calculated using thylakoid lipid, protein compositions and lipid/protein ratios.

3.1 Form factor

3.1.1 Thylakoid form factor derivation

To construct complex thylakoid unit cell form factor $F(q)$, the system is simplified and the "square box" model is build as the first step. As visualized by TEM, a single thylakoid can be well approximated as a flat cylinder with the diameter ($2R$) of 300-600 nm and the overall thickness (h) of approximately 17 nm ($2R \gg h$), as shown in Fig. 3.1 a). Since the granal radius is larger than the q window of small-angle scattering observation, we argue that a single grana layer (flat vesicle) can be simplified to a one-dimensional "box" function of infinite diameter, accounting for scattering length density difference variations only in one direction z.

This assumption is verified by using the methodology of direct 3-D simulations of [128] using different cylinder radii, which show that simulations with sufficiently large radii can be well approximated with a one-dimensional 'box' model, which is independent

of cylinder radius. As shown in Fig. 3.1 b), the form factor of a one-dimensional box (which is effectively identical to a disc of the infinite radius) is already identical to the form factor of a cylinder with $\geq$ 500 Å radius, so R = 1000 Å is used in later calculations. To explain this argument more stringently, a scattering curve follows q^{-2} decay and there shall be no characteristic scattering feature arising from cylinder dimensions observed in the investigated q range. This is true if condition $q_{min} \cdot R \gg 2\pi$, or $q_{min} \gg 2\pi/R$ is satisfied. When the cylinder radius is small (100 Å), a scattering feature - inflection point - at $q \cong 0.01$ Å^{-1} can be observed in the black curve. For cylinder of R = 1000 Å, this feature is at $q = 1 \cdot 10^{-3}$ Å^{-1}, which is well out of the range of interest.

Although a large variation between scattering curves is observed in the high q region, this is due to the fact that a high number of simulated points is required to obtain good statistics for direct 3-D simulations. If the cylinder radius R is increased to nR, then the total number of simulation points shall be increased at least by the factor $(nR/R)^2$, what significantly prolongs the computational time. However, this does not significantly improve data point dispersion in the low q region, which is the most interesting biologically, since structural features of an ordered thylakoid system fall in this region. Therefore a sufficient number of simulation points (140000) was used, which is a trade-off between a long computational time and a sufficient resolution.

Consider a simple "single box" function, where a single region of a scattering length density is different from zero (defined as $\Delta\rho$) and has a width of δ, that is symmetrically centered around $z = 0$ (Fig. 3.2 a), scattering length density is zero otherwise. We solve the basic form factor equation (Eq. 3.1) for this centrosymmetric box (Eq. 3.3). The general form factor equation is:

$$P(q) = |\int_{-x}^{+x} \rho_0(z)\ e^{iqz}\ dz|^2 \tag{3.1}$$

and for a symmetric integral we derive:

$$\int_{-x}^{+x} \Delta\rho\ e^{iqz}\ dz = \frac{\Delta\rho}{q} \cdot 2\sin(qx) \tag{3.2}$$

For situation of Fig. 3.2 a) the following expression is obtained [200]:

$$P(q)_{box} = |\int_{\frac{-\delta}{2}}^{\frac{+\delta}{2}} \rho_0(z)\ e^{iqz}\ dz|^2 = \frac{4}{q^2}(\Delta\rho)^2 \cdot \sin^2(q\frac{\delta}{2}) \tag{3.3}$$

As the next step, the "box" function is made to look more like a biological membrane: 1. Two electron densities are introduced: $\Delta\rho_H$ and $\Delta\rho_T$, corresponding to lipid head (referred to as *headgroups*) and lipid molecule chain entities (referred to as *tailgroups*), 2. The "box" is centred that its symmetry axis is located at 0.

The geometrical form factors can be combined in order to yield new and more complex shapes. The form factor amplitude of a small box A_{ab} can be calculated by subtracting

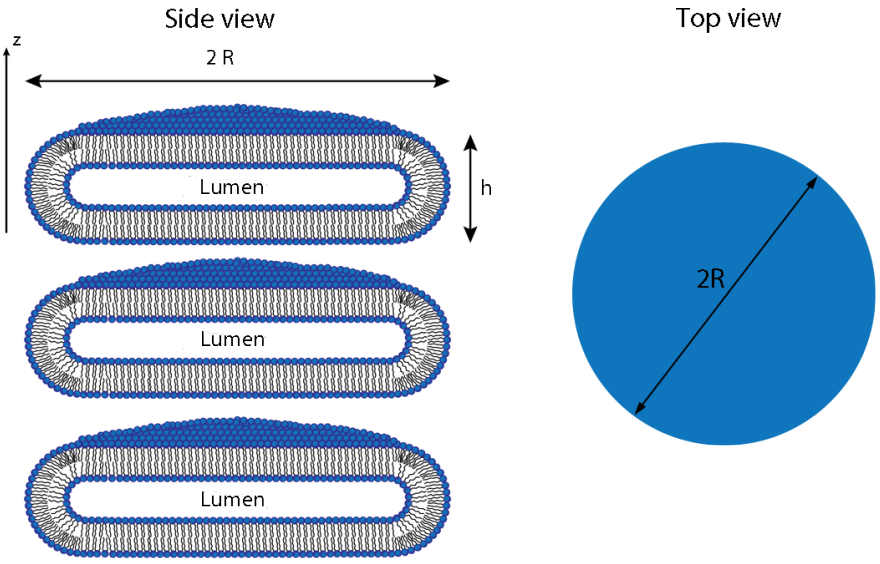

(a)

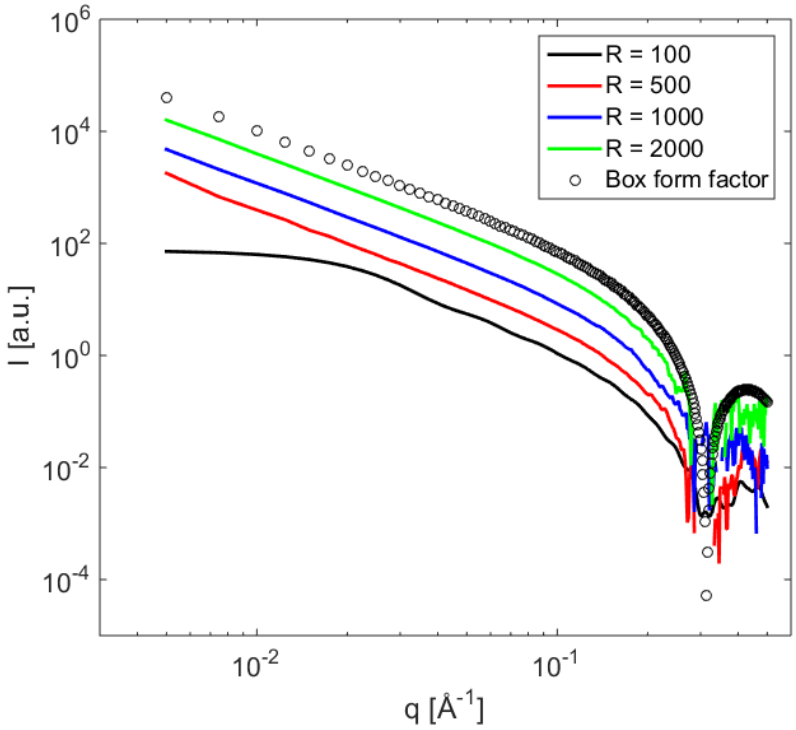

(b)

Figure 3.1: a) Grana stack is approximated as a stack of thin flat cylinders of radii R and heights h. b) Having radii $\geq$ 500 Å the form factor of the cylinder does not change in the low q and can be approximated with radius-independent "box" function. Curves are vertically shifted for clarity.

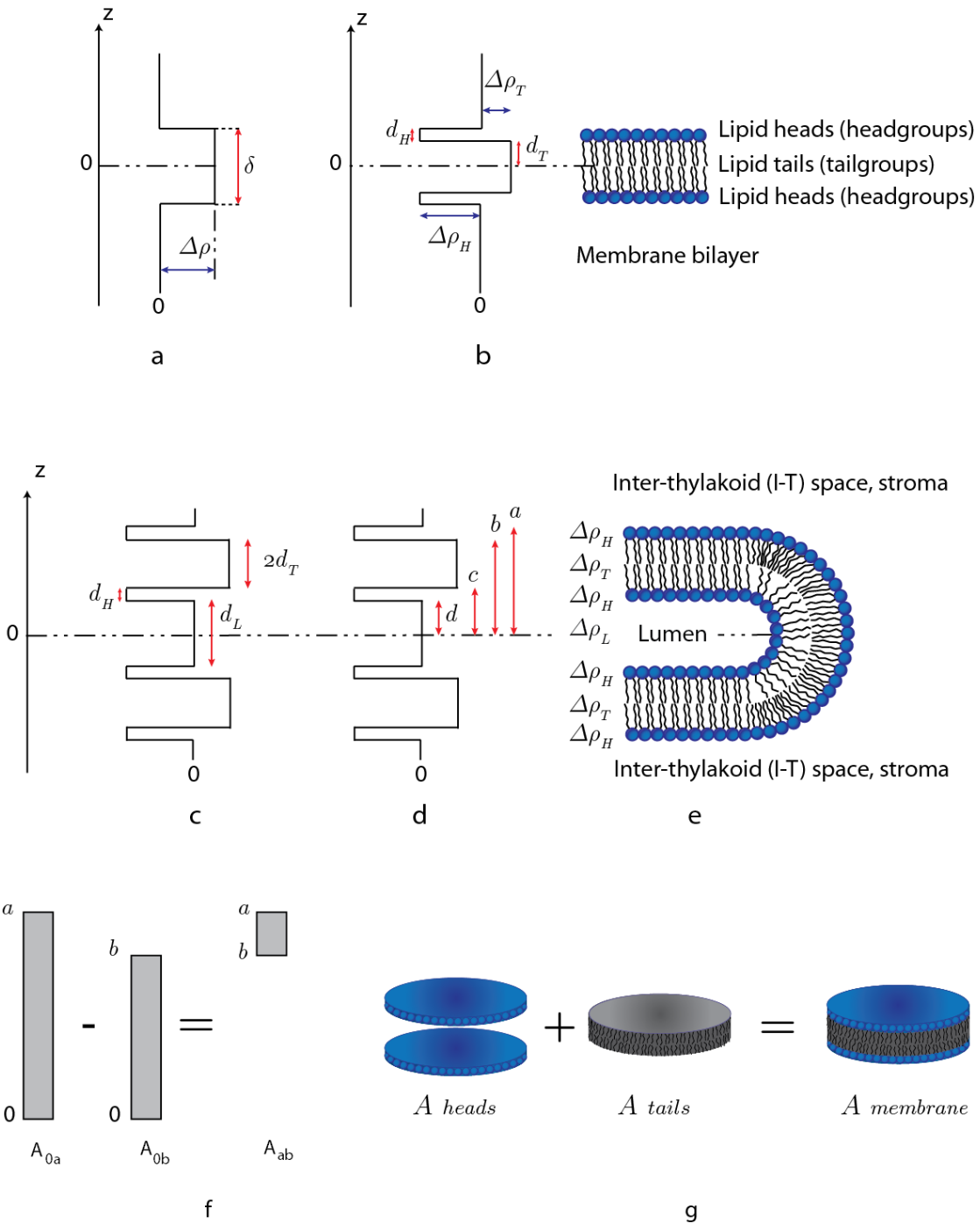

Figure 3.2: Scattering length density (SLD) profiles of: a) Single box with SLD of $\Delta\rho$; b) The "membrane" with SLDs of $\Delta\rho_T$ (tailgroups) and $\Delta\rho_H$ (headgroups). Thickness of tailgroups - d_T, headgroups - d_H; c) Two stacked membranes separated by a lumen of $\Delta\rho_L$ and d_L; d) Distance substitutions of Eqs. 3.6; e) Thylakoid membrane with $\Delta\rho_H$, $\Delta\rho_T$, $\Delta\rho_L$, which is centered around the middle of the lumen; f) Form factor amplitude of the box A_{0b} can be subtracted from the form factor amplitude of the box A_{0a}, yielding form factor amplitude of the box A_{ab}; g) Form factor amplitude of the membrane is the sum of headgroups (A_{heads}) and tailgroups (A_{tails}) form factor amplitudes.

the form factor amplitude of box A_{0b} from the box A_{0a} (Fig. 3.2 f) with the same scattering length density but different height, as shown in Eq. 3.4 [268].

$$\begin{aligned} F_{box\ ab}(q,a,b) &= F_{box\ 0b}(q,0,b) - F_{box\ 0a}(q,0,a) \\ P_{box\ ab}(q,a,b) &= |F_{box\ ab}(q,a,b)|^2 \end{aligned} \tag{3.4}$$

In turn, adding the amplitudes of $2 \cdot F_{heads}$ and $2 \cdot F_{tails}$ and squaring their sum we derive the form factor of a single membrane bilayer of Fig. 3.2 (g). We obtain a situation of Fig. 3.2 b in Eq. 3.5.

$$P(q)_{membrane} = \left(\frac{2}{q}\right)^2 \{\Delta\rho_H[\sin(q\cdot(d_T+d_H)) - \sin(q\cdot d_T)] + \Delta\rho_T \sin(q\cdot d_T)\}^2 \tag{3.5}$$

In order to build a single thylakoid layer: 1. Two membranes are stacked, 2. The lumenal space of thickness d_L and SLD of $\Delta\rho_L$ is introduced between these membranes (Fig. 3.2 c).

To simplify the final form factor formula four substitutions are implemented (Eqs. 3.6) so that all distances start from the same origin - the center of lumen (Fig. 3.2 d). Physical parameters are now as follows: headgroup thickness is $d_H = a - b = c - d$, tailgroup thickness is $d_T = (b-c)/2$ and lumen thickness is $d_L = 2 \cdot d$ (Fig. 3.2 d).

$$\begin{aligned} a &= d_L/2 + 2d_T + 2d_H; \\ b &= d_L/2 + 2d_T + d_H; \\ c &= d_L + d_H; \\ d &= d_L/2; \end{aligned} \tag{3.6}$$

Following the same methodology and using substitutions of Eq. 3.6 (also visualized in Fig. 3.2 d), we derive $F(q)$ for individual thylakoid components (Eqs. 3.7):

$$\begin{aligned} F(q)_{headgroups} &= \frac{2}{q}\Delta\rho_H(\sin(qa) - \sin(qb) + \sin(qc) - \sin(qd)) \\ F(q)_{tailgroups} &= \frac{2}{q}\Delta\rho_T(\sin(qb) - \sin(qc)) \\ F(q)_{lumen} &= \frac{2}{q}\Delta\rho_L \sin(qd) \\ F(q)_{stroma} &= Const. \end{aligned} \tag{3.7}$$

The resulting formula is then Eq. 3.8.

$$P(q)_{thylakoid} = \left(\frac{2}{q}\right)^2 \{\Delta\rho_H[\sin(qa) - \sin(qb) + \sin(qc) - \sin(qd)] + \\ + \Delta\rho_T[\sin(qb) - \sin(qc)] + \Delta\rho_L[\sin(qd)]\}^2 \tag{3.8}$$

In order to calculate these membrane parameters for the real datasets, a Matlab code that derives scattering form factor amplitudes from brute-force calculations with a Monte Carlo point generation [128] has been modified. This simulation was used to calculate form factors of model datasets with known parameters to *a priori* test the functionality of the 'WillItFit' code. In turn, this 'WillItFit' code will be used to fit experimental datasets and to extract physical parameters. We first produce small-angle scattering datasets for form factors (green points in Figs. 3.3 - 3.6) with known parameters by direct 3-D simulation and demonstrate form factor fitting and parameter calculation in 'WillItFit' (black curves) in a step-wise manner - by increasing model complexity:

1. A "single box" model: d_T = 15 Å, $\Delta\rho_T$ = -0.1, remaining distances and scattering length densities equal to 0 (Figure 3.3).

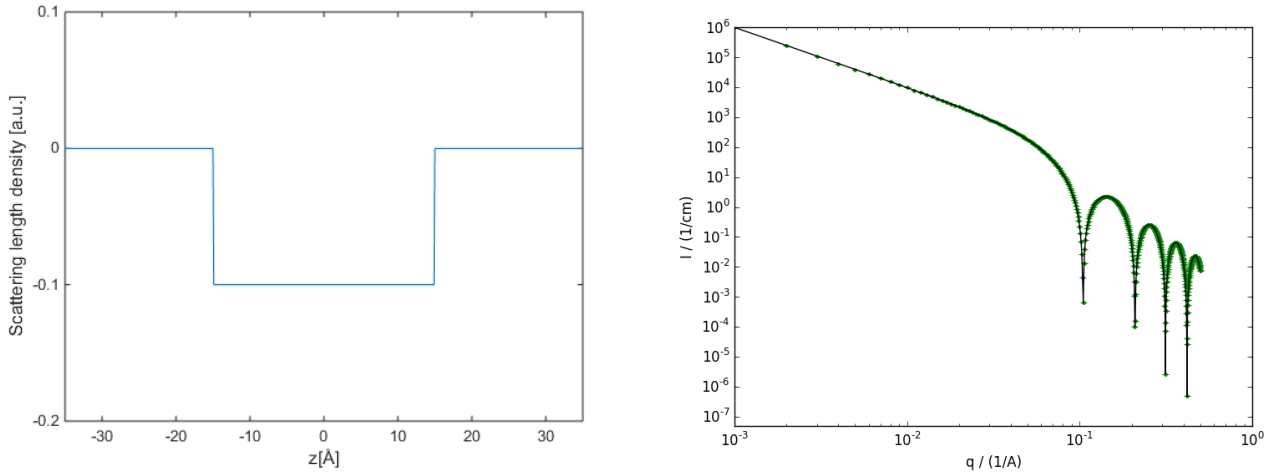

(a) (b)

Figure 3.3: a) SLD profile of a single box, b) Single box form factor calculated by direct 3-D simulations (green points) and fitted in 'WillItFit' software (black line).

2. A "single membrane model": d_H = 10 Å, d_T = 15 Å, $\Delta\rho_H$ = +0.2, $\Delta\rho_T$ = -0.1, remaining distances and scattering length densities equal to 0 (Figure 3.4).

3. A "thylakoid model" with zero lumenal SLD. Distances identical to "single membrane model", d_L = 20 Å, $\Delta\rho_L$ = 0 (Figure 3.5).

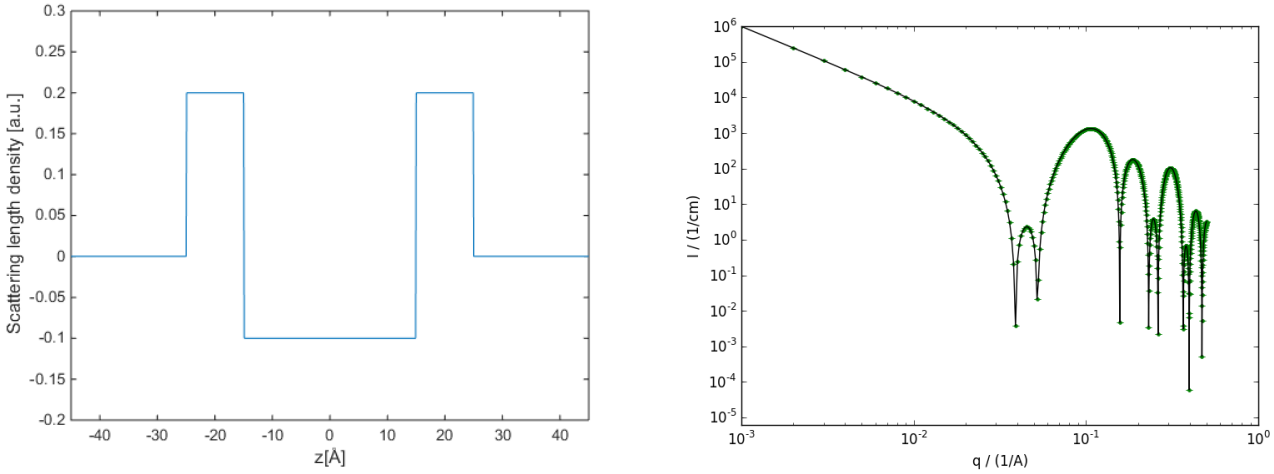

(a) (b)

Figure 3.4: a) SLD profile of a single membrane, b) "Single membrane" form factor calculated by direct 3-D simulations (green points) and fitted in 'WillItFit' software (black line).

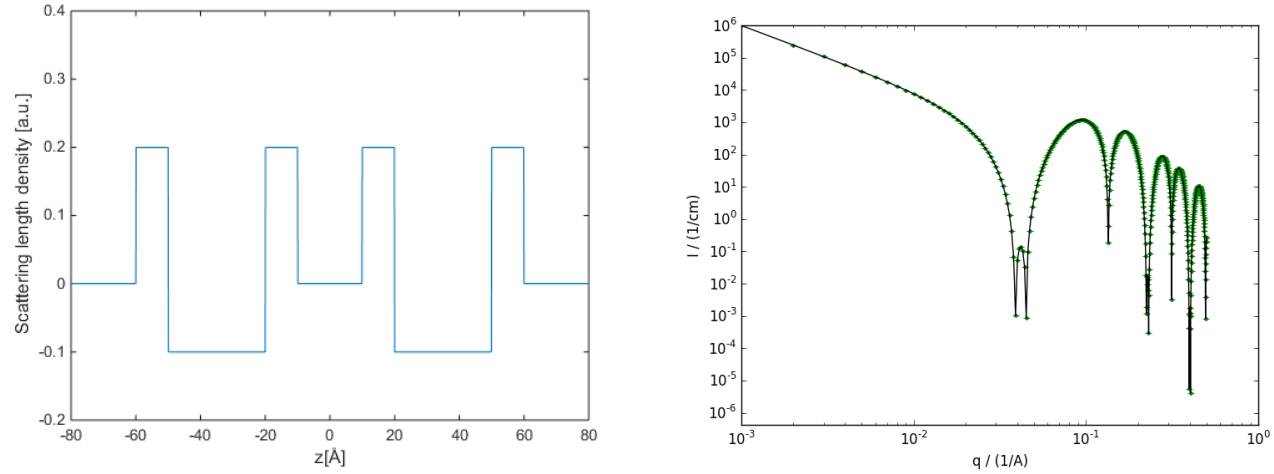

(a) (b)

Figure 3.5: a) SLD profile of a single thylakoid, b) "Thylakoid" form factor calculated by direct 3-D simulations (green points) and fitted in 'WillItFit' software (black line).

4. A "thylakoid" model with non-zero lumen SLD. Distances and SLDs identical to "thylakoid model", except $\Delta\rho_L = +0.02$ (Figure 3.6).

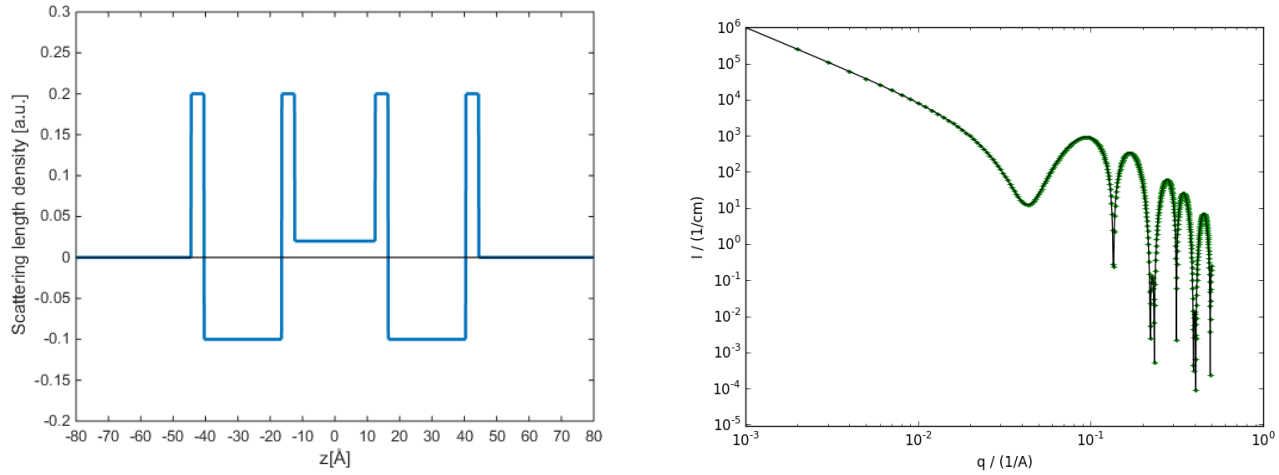

(a) (b)

Figure 3.6: a) SLD profile of a single thylakoid with non-zero lumenal SLD $\Delta\rho_L = +0.02$, SLD = 0 is shown as a black line b) "Thylakoid with a non-zero lumen" form factor calculated by direct 3-D simulations (green points) and fitted in 'WillItFit' software (black line).

3.2 Thylakoid membrane structure factor

As the next step, a stack of thylakoid unit cells is built and modelled using the "double box" form factor model as the form factor of a single thylakoid. This requires an introduction of the structure factor $S(q)$. This is a non-trivial function for lipid bilayers, which are arranged in non-crystalline arrays. We consider a sample, consisting of a stack from N membrane layers, contained in an infinitely wide cylinder of height L along the z direction. On a mesoscale, each membrane is assumed flat with its normal along the z axis of the cylinder, although there are local membrane fluctuations/undulations (Fig. 3.7).

3.2.1 Stacked lamellae structure factor

The lyotropic lamellar phase (smectic A phase) scattering experiments show that a purely geometric model of stacked membranes does not completely describe and account for the scattering features that occur from thermal fluctuations. As shown by experiments, the width of Bragg peaks of such membranes are broadened, additional diffuse scattering

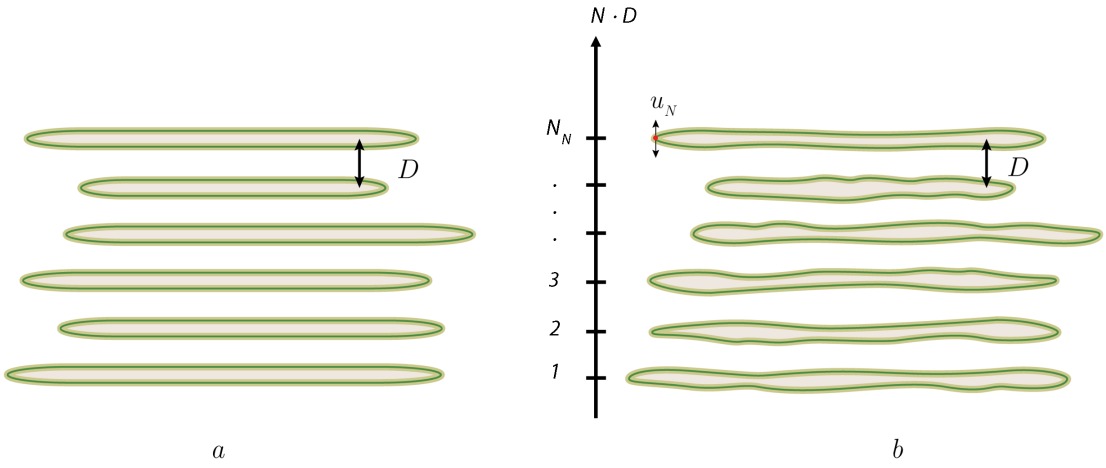

Figure 3.7: (a) - Perfectly ordered thylakoid membrane stack of N layers, separated by a repeat distance D; (b) - Undulated thylakoid membrane stack of N layers, separated by a repeat distance D. Membrane equilibrium position of the N^{th} membrane $N_N \cdot D$ (red dot) and local repeat distance fluctuations/undulations u_N (arrows) are depicted.

at large angles and anisotropic small angle scattering is observed, what makes result interpretation a significantly more complex problem [200]. To overcome this issue, A. Caillé developed a scattering theory, which accounts for bilayer bending and thermal fluctuations in the mean spacing between N lipid bilayers (separated by the repeat distance D in our case). This theory was later modified to take into account a finite size of an ordered lamellar stack (modified Caillé theory, MCT [317]). This physical theory gives rise to broad/wide non-Bragg scattering peaks, what conceal actual scattering intensity and artificially reduce the apparent form factor as the function of the peak order [40, 191]. If the N^{th} layer fluctuates around its equilibrium position $N_N \cdot D$ by the distance u_N and the total number of layers N is $\gg 1$, then the correlation function $\Delta^2 \equiv \langle (u_N - u_0)^2 \rangle$ is defined [40, 200]:

$$\langle (u_N - u_0)^2 \rangle = \frac{\eta}{2\pi^2} \left[\ln(\pi N) + \gamma \right] D^2 \tag{3.9}$$

Here γ is Euler's constant ($\gamma = 0.57721$) and η is the Caillé parameter. The Caillé parameter (Eq. 3.10) is a measure of bilayer fluctuations, which contains the membrane bending modulus K, the bulk compression modulus B (high moduli K and B mean that high impact is needed to deform a membrane) and thermal energy kT. The theory implies that when the Caillé parameter is larger than 1 (either at low q or at low B and K) the diffraction peaks become non-observable. The Caillé parameter becomes higher if temperature increases and becomes lower if: 1. lipid membranes of certain composition are packed closer to each other - membrane D spacing decreases, membranes become more rigid due to increased electrostatic repulsion of adjacent membranes and

their thermal undulations decrease, therefore the compression module B increases, 2. if the lipid volume fraction is high (compression module B increases with dehydration) or 3. proteins/lipids, which make membrane more rigid, are introduced into the membrane (membrane bending modulus K increases).

$$\eta = \frac{q^2 kT}{8\pi\sqrt{KB}} \tag{3.10}$$

In principle, the basis of modified Caillé theory is only adequate for arrays of multiple stacked membrane bilayers [317], but we show that 'Caillé-like theory' can also describe thylakoid data. From literature studies, typical η values for lipid membranes vary between 0.01 and 0.6: for undulating DMPC membranes η varies from 0.2 at 48.5 °C to 0.6 at 95.4 °C, for POPC membranes η varies from 0.05 at 2 °C to 0.09 at 50 °C, for DPPE it is 0.016 at 75 °C; other calculated η values range from 0.03 to 0.19 (with extremes up to 0.25 and 0.41 for DMPC; and even up to 0.8 for diluted dodecane) [239, 227, 316, 84, 191, 212, 209, 79]. These values are realistic for lamellar systems stabilized by electrostatic repulsion between single bilayers, where D is 40-100 Å but η values of the order of 1.3 are predicted for large smectic spacings ($\gg$ 200 Å) [200, 239].

Neither the experimental η measurements of glycolipid-rich membranes, nor for smectic systems with spacings of 200-300 Å have been found in the literature. For model membranes of pentanol/dodecane/SDS in water, η of 0.8 is predicted if the spacing is around 150-200 Å [200, 239]. I argue, however, that η is significantly lower for thylakoid membranes despite a hundred nm-order repeat distance D, as thylakoid membrane contains 50-70 % multi-subunit proteins and is a very rigid membrane. Therefore η value of 0.01 is used as a starting point for modelling.

Again, the modified Caillé theory describes a stack of multiple single bilayers, separated by aqueous layers - the unit cell in this case is a single bilayer thickness and a single water layer. This is not the case for thylakoid unit cell, which is inherently more complex. A thylakoid is comprised of two membranes, separate lumen and stromal water layers. Also, thylakoid membrane contains much more proteins than lipids in the bilayer, individual proteins are very large and can form supercomplexes. Furthermore, negatively charged proteins of adjacent thylakoids also bind cations, forming magnesium bridges (also called 'Mg-sandwiches') and thus exhibit overall stabilizing electrostatic interactions both within a single thylakoid and between adjacent thylakoids. This largely increases thylakoid membrane rigidity and yields a low Caillé parameter value. I conclude, that with these considerations, the modified Caillé theory describes obtained scattering data of thylakoids to a satisfactory extent.

As given above in Eq. 2.5,

$$I(q) \propto \frac{P(q)}{q^2} \cdot S(q) \tag{3.11}$$

The structure factor for an ordered lamellar stack (each composed of N layers) is (Eq.

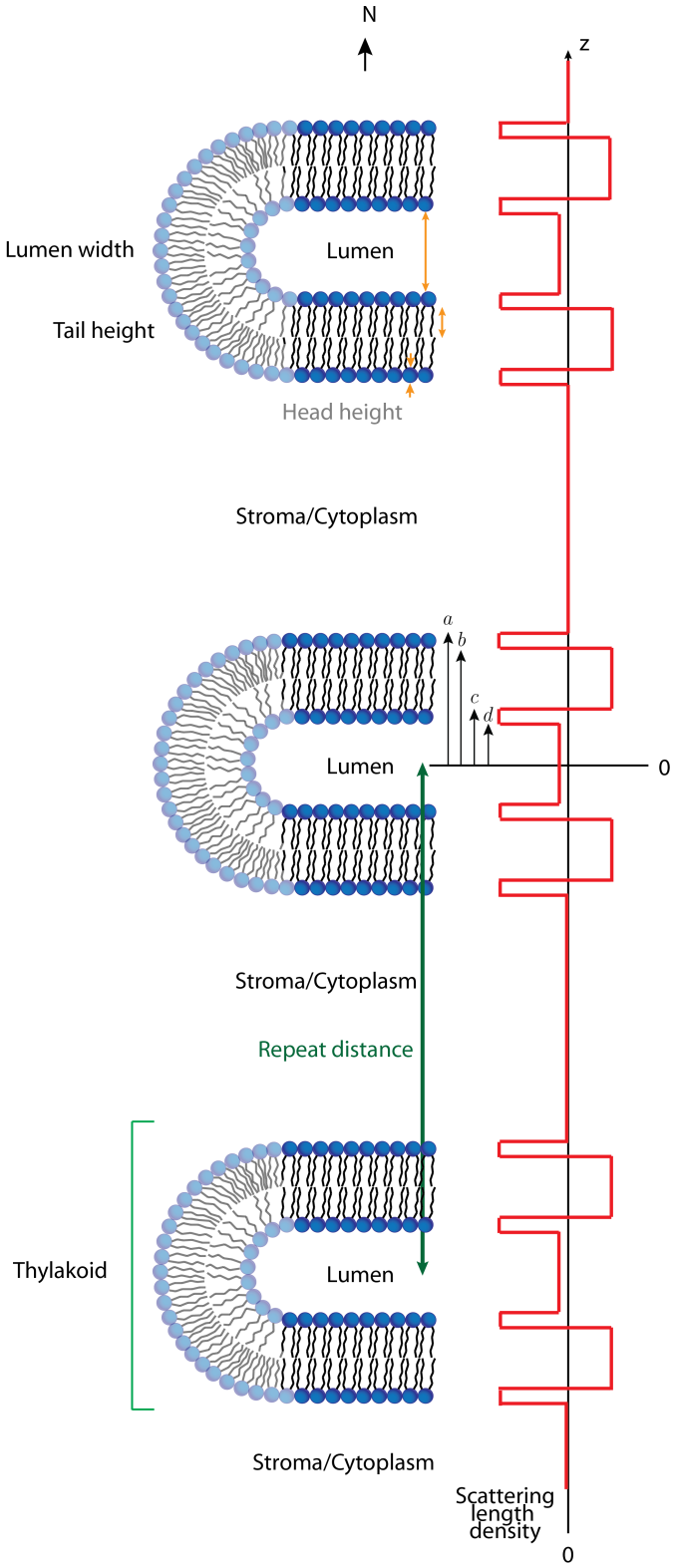

Figure 3.8: Grana stack with relevant distances and SLDs profile of a grana stack indicated. Thylakoid margins (opaque) are only included for better visual separation of thylakoid lumen and stroma compartments (cytoplasm in cyanobacteria) - since we model thylakoids as flat vesicles of infinite diameter, thylakoid magins are not accounted for in the scattering model.

3.12) [200]:

$$S(q) = N + 2\sum_{n=1}^{N-1}(N-n)\cos(qnD)\ e^{-n\Delta^2 q^2/2} \tag{3.12}$$

Keeping the Caillé parameter constant, but increasing the number of layers causes higher and more narrow peaks, the minima between peaks also become more pronounced [72, 200]. Using the substitution $\alpha_N = \frac{\eta}{4\pi^2}\ln[(\pi n)+\gamma]$ and dividing by N (normalizing) we obtain Eq. 3.13:

$$S(q) = 1 + 2\sum_{n=1}^{N-1}(1-\frac{n}{N})\cos(qnD)e^{-q^2D^2\alpha_N} \tag{3.13}$$

Hence the total scattering intensity (including the Lorentz factor for randomly oriented stacks) is given in Eq. 3.11. I leave a proportionality sign, since the data normalization and the introduction of prefactor term is dealt with later.

A set of datasets by 3-D simulation is produced. With already chosen headgroup, tailgroup and lumen thicknesses (d_H = 10 Å, d_T = 15 Å, d_L = 20 Å) we vary the number of membranes from N = 1-6 in a stepwise manner to demonstrate the effect of structure factor (Fig. 3.9).

1. One thylakoid unit cell: d_H = 10 Å, d_T = 15 Å, $d_L/2$ = 10 Å, $\Delta\rho_T$ = +0.2, $\Delta\rho_T$ = -0.1, $\Delta\rho_L$ = 0 (Figure 3.9 a).

2. Two-six thylakoid unit cells with the same parameters (Figure 3.9 b-e).

In the beginning of fitting I assume that granum consists of perfectly flat discs, which do not have membrane thermal undulations, so Caillé parameter η is set to 0 (resulting in $\alpha_N = 0$). The Caillé parameter is included as fitting parameter in the model, so it can be adjusted during the fitting process. I estimate its range of 0.01-0.1 order, which is similar to the range of membrane undulation parameters A from Table 1 of Hodapp *et al.* [101].

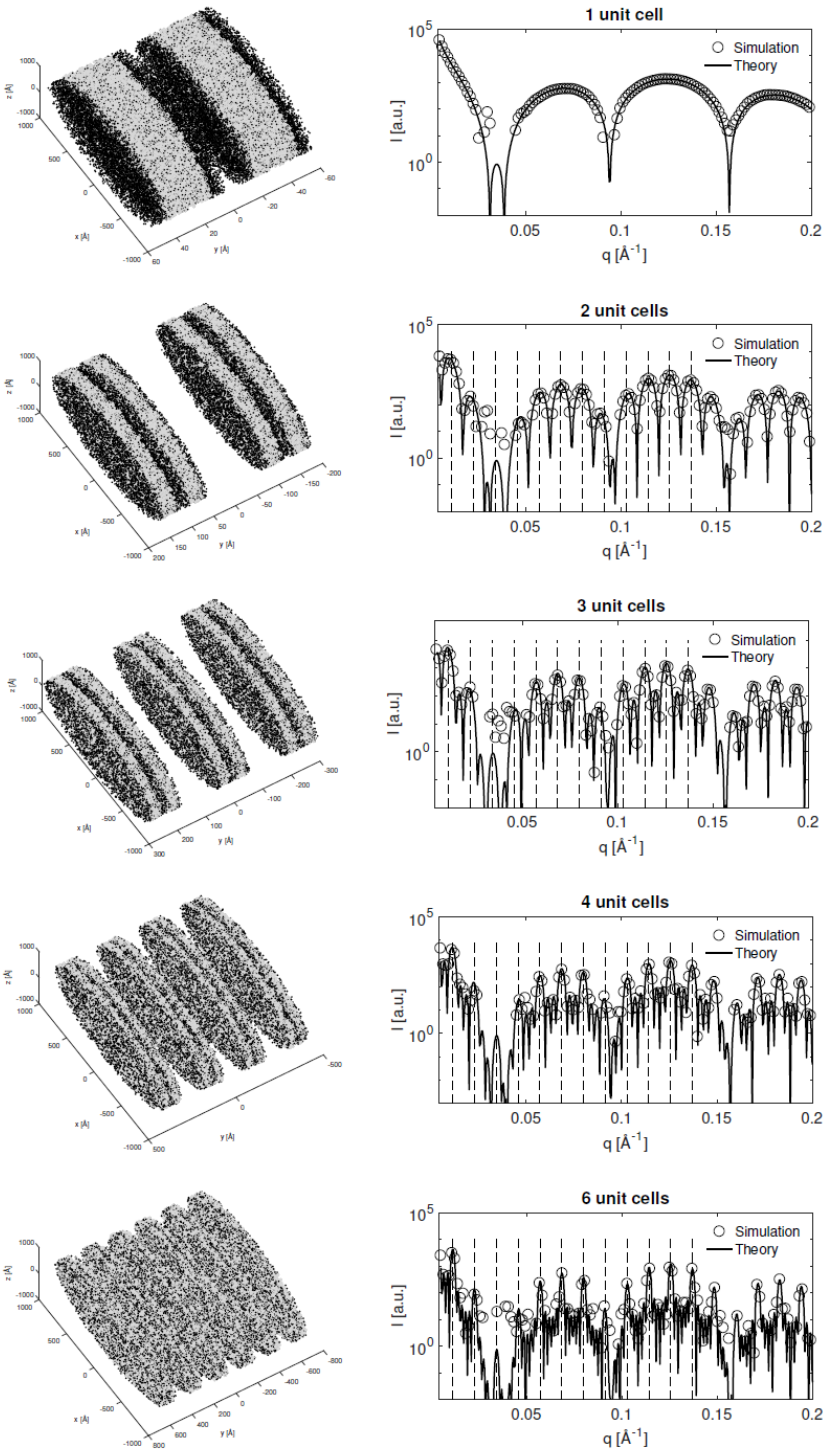

Figure 3.9: a) 1-6 thylakoid unit cells (two bilayers - lipid heads (black) and lipid tails (grey), lumen and stroma (white)) simulated as large discs with $R = 1000$; b) fitting the form factor $P(q)$ for 1 thylakoid unit cell, or $P(q) \cdot S(q)$ for 2-6 thylakoid unit cells. This figure is used in Manuscript 1.

3.3 Polydispersity

A grana stack is not a perfect crystal, where individual thylakoids are arranged in such a way that the center of the lumen is exactly localized at 0, D, $2D$, $3D$ etc. The same applies to lumen - it does not have equal width of d_L in grana thylakoids. There are local variations in both D and d_L. To evaluate the degree of these variations, lumen and repeat distance dispersities are introduced as the final model step. Evaluating uncertainty in parameter variation is also an important step to evaluate overall model quality. Large D and d_L polydispersities of several-hundred-Ångstrom order are higher than the thylakoid membrane polydispersity observed by TEM. Therefore, if the case, such scattering model (however good otherwise) is biologically irrelevant and discarded. On the other hand, a small polydispersity of D is always present, especially in cyanobacterial thylakoids, as thylakoids in cyanobacteria are arranged less compactly. However, although important, small polydispersity cannot be reliably evaluated from TEM pictures, because of fixation/staining-contrast artefacts, an overall small (Å-order) polydispersity scale, and the measurement errors.

We introduce Gaussian polydispersity distribution of mean thylakoid repeat distance (D) and mean lumen width (d_L) and include σ_D and σ_{d_L} as fitting parameters into the mathematical model. We write a double sum in Eq. 3.14:

$$I(q)_{polydisperse} = \sum_i \sum_j f(d_L)_i \cdot P(q, d_H, d_T, d_L, \Delta\rho_H, \Delta\rho_T, \Delta\rho_L)_{thylakoid} \cdot f(D)_j \cdot S(q, N, D)_{thylakoid} \tag{3.14}$$

where i and j are stepsizes in Gaussian distribution and prefactors $f(d_L)$ and $f(D)$ are:

$$f(d_L)_i = \frac{1}{\sigma_{d_L} \cdot \sqrt{2\pi}} e^{-(\frac{d_L\ average - d_{L_i})^2}{2\sigma^2_{d_L}}} \qquad f(D)_j = \frac{1}{\sigma_D \cdot \sqrt{2\pi}} e^{-(\frac{D_{average} - D_j)^2}{2\sigma^2_D}} \tag{3.15}$$

This double sum can be split into two independent sums:

$$I(q)_{polydisperse} = \sum_i f(d_L)_i P(q, d_H, d_T, d_L, \Delta\rho_H, \Delta\rho_T, \Delta\rho_L)_{thylakoid} \cdot \sum_j f(D)_j S(q, N, D)_{thylakoid} \tag{3.16}$$

The effect of polydispersity on a $\frac{P(q) \cdot S(q)}{q^2}$ of a theoretical dataset is visualized in Fig. 3.10, here $d_H = 5$ Å, $d_T = 15$ Å, $d_L = 60$ Å, $\Delta\rho_T$ =+0.2, $\Delta\rho_T$ = -0.1, $\Delta\rho_L = 0.02$, $D =$ 300 Å, $N = 3$. The probability density function of $d_L \pm 3 \cdot \sigma_{d_L}$ (Fig. 3.10 b) exemplifies the probability for each d_L value (Eqs. 3.14) - form factors having values far away from d_L average value are scaled to a lower extent in the sum/integration.

The functional form of scattering intensity, $\frac{P(q)\cdot S(q)}{q^2}$ is plotted in Fig. 3.10 a) without polydispersion (black), with polydispersion in d_L, $\sigma_{d_L} = 5$ (blue), with polydispersion in N, $\sigma_N = 1$ (red), with polydispersion in D, $\sigma_D = 5$ (green) and with polydispersion in d_L and D, $\sigma_{d_L} = \sigma_D = 5$ (cyano). The orders of scattering peaks are depicted as vertical red dotted lines, D of the first order peak is 300 Å.

The number of thylakoid layers N in cyanobacteria is rather constant - it varies from 3-6. From Fig. 3.9, we observed that varying the total number of layers N=3-6 in a 'pseudogranum' had a negligible effect on the appearance of $\frac{P(q)\cdot S(q)}{q^2}$ curve. However, even small polydispersity in N introduces an extensive smearing - one can immediately observe, that polydispersity in N smooths the curve even with $\sigma_{dN} = 1$. Polydispersities of d_L and D have very similar smearing effects, but the minimum around q= 0.1 $Å^{-1}$ is more efficiently smeared with polydisperse d_L. If polydispersities of d_L and D are combined, the effect is similar to D alone, therefore the need of a double polydispersity is questioned. As we elaborate in Manuscript 1, polydispersity in d_L alone can be sufficient to explain the observed SANS data smearing.

We therefore choose to proceed with polydispersity in d_L, which is more important biologically. As suggested by H. Kirchhoff [124], thylakoid lumen thickness varies upon illumination, but thylakoid membrane thickness remains constant - therefore knowing d_L average value as well as its uncertainty is very biologically relevant, as this cannot be straightforwardly evaluated from TEM images.

Polydispersity of D also has a biological relevance as well, however it has never been quantified. Based on TEM analysis, repeat distance variation between thylakoids in different 'pseudograna' in the same bacterial cell can reach 100-200 Å (my rough estimates from [156, 152]). In order to evaluate the magnitude of observed biological changes - e.g. thylakoid repeat distance change upon illumination, dehydration or temperature increase, it is not only important to evaluate the change of the average value, but also its uncertainty.

Finally, although we do not consider N in cyanobacterial case, it is important to emphasize, that variation in N from plant grana stacks (where N reaches 100 in shade-tolerant plants and is 5-7 for *Arabidopsis thaliana* [16]) compared to cyanobacteria (where the average N is 3-6 and is rather constant between species) is higher and this can have a more significant effect. Furthermore, in some plants (e.g. *Arabidopsis*) a number of layers in a single granum can decrease upon illumination, as elaborated in Manuscript 2. N polydispersity is not accounted for in the main text of this PhD thesis, but the importance of polydispersity of all parameters needs to be reconsidered when applied to the thylakoid system of higher plants.

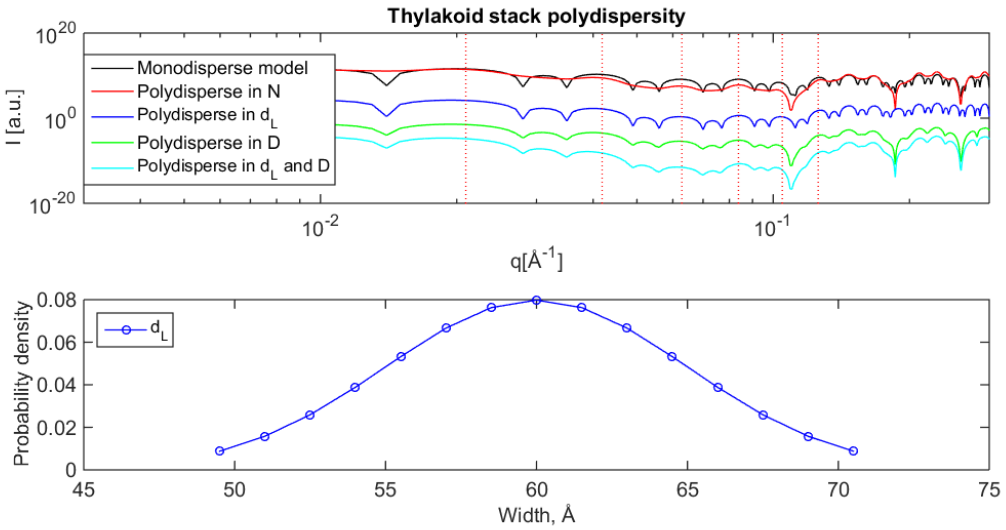

Figure 3.10: a) Thylakoid stack form and structure factor models with no polydispersity (black), polydispersity in d_L (blue), N (red), D (green) and d_L with D (cyano). Curves are vertically shifted for clarity. b) Gaussian probability distribution of d_L.

3.4 Scattering length density (SLD) calculations

In this section realistic estimates of scattering length densities are calculated for different components of thylakoid membrane - lipid headgroups, lipid tailgroups and proteins. These values will be used as a starting point for model fitting in Manuscripts 1 and 2. The logics of SLD derivation, necessary simplifications and considerations, including biological validity, as well as problematics are elaborated in this section. I elaborate and exemplify neutron SLD derivations in the text, as this requires more biological considerations (hydrogen exchange, deuteration levels), but I calculate X-ray SLDs in parallel *sub silentio* - using the same protein/lipid composition and volume fractions.

To my knowledge, X-ray SLD values for thylakoid membrane modelling were chosen using animal cell or synthetic membrane values [128], although X-ray SLDs for thylakoid membrane components were already estimated in 1963-1971 [127]. Indeed, X-ray SLD values for thylakoid lipids were expected to be similar to literature values on other lipids (*e.g.* membranes with scyatic myelin) and protein SLD values similar to other hydrophobic proteins: myelin, rhodopsin or bacteriorhodopsin [33, 32]. As all named lipids have similar X-ray SLDs, similar thylakoid X-ray SLD values were assumed in [128]. Neutron SLD for thylakoid lipids has been estimated in the PhD thesis of Gergely Nagy [192]. G. Nagy calculated thylakoid lipid headgroup SLD 1.67-2.09 $\cdot$ 10 $^{-6}$ Å^{-2} in 0, 40 and 100 % D_2O and thylakoid lipid tailgroup SLD of -0.36 $\cdot$ 10 $^{-6}$ Å^{-2}.

As illustrated in Table 3.1, there is a substantial lipid composition difference between

plants and other organisms. Therefore SLD of thylakoid membrane components - lipid headgroups and lipid tailgroups, were calculated using thylakoid-composing lipids and photosynthetic proteins (using amino acid sequences) in their relative amounts. It is shown SLD of lipid headgroups obtained in this PhD thesis are comparable to G. Nagy's, whereas SLD of lipid tailgroups are very different, as the value of -CH_2- is used as the tailgroup SLD [195]. In the last subsection, I compare mine and G. Nagy's approach and show that if proteins are accounted for, the resulting SLD profiles are generally comparable.

Table 3.1: Lipid composition, % of total lipids by weight. [12].

Lipid	Spinach chloroplasts	Liver cell plasma membrane	Myelin	Mitochondrion (both membranes)	Endoplasmic reticulum	*E. coli* bacterium
Cholesterol	0	17	22	3	6	0
Phosphatidylethanolamine (PE)	3	7	15	28	17	70
Phosphatidylserine (PS)	0	4	9	2	5	trace
Phosphatidylcholine (PC)	7	24	10	44	40	0
Sphingomyelin	0	19	8	0	5	0
Glycolipids	61	7	28	trace	trace	0
Other	29	22	8	23	27	30
Sum	100	100	100	100	100	100

Thylakoid membrane substantially differs from other cellular membranes in three aspects: it is predominately composed of proteins rather than lipids, it contains predominantly poly-unsaturated fatty acids as lipid tailgroups and sacharides (sulfo-) galactose as lipid headgroups. It is therefore argued that using the SLD of the 'average headgroup and hydrocarbon chain density' of animal origin, is an erroneous approach for thylakoids.

Scattering length derivations for biological systems is a complex problem. First of all, the exact composition and ratios of all biomolecules in the system shall be known. Secondly, their molecular volumes, isotope composition and total charges shall also be known. Although maybe trivial for simple small molecules, calculating a total volume of a multi-subunit membrane protein as a total sum of its amino acid volumes - as routinely done in this work - is a simplification. The total protein charge is also unknown and thus not accounted for. Furthermore, protein and lipid molecules have a hydration layer and there are also water molecules in the membrane, but this water is also not accounted for in the following SLD derivations in this PhD thesis. To complicate matters further, it is also not trivial to estimate a degree of H-D exchange for big membrane-embedded and membrane-associated proteins. The absolute maximum H-D exchange after infiltration of big membrane proteins is estimated to be 15 %, however it is more realistically assumed that it is equal to 0 % (as elaborated below). These fundamental problems hinder calculating exact SLD values. Therefore, the range of theoretical SLD values is estimated in this PhD thesis, whereas the 'experimental' SLD values are obtained as fitting parameters from the scattering model, based on the theoretical SLD values.

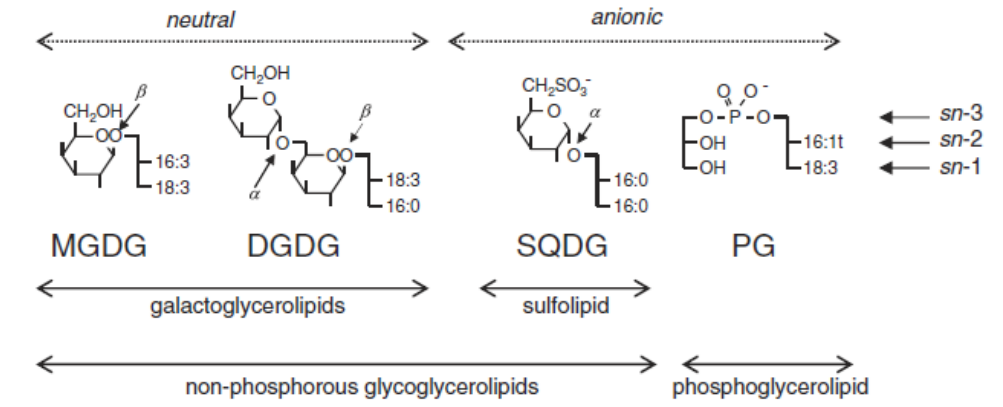

(a)

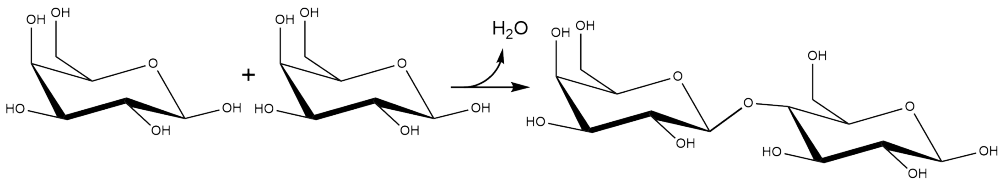

(b)

Figure 3.11: a) Predominant lipid molecules, composing thylakoid membranes of higher plants, exemplified by Arabidopsis thaliana [36]. Fatty acids (lipid tailgroups) occupy sn-2 and sn-1 positions, sn-3 position is occupied by the lipid headgroup; b) Glycosidic bond formation between two galactose molecules and water release.

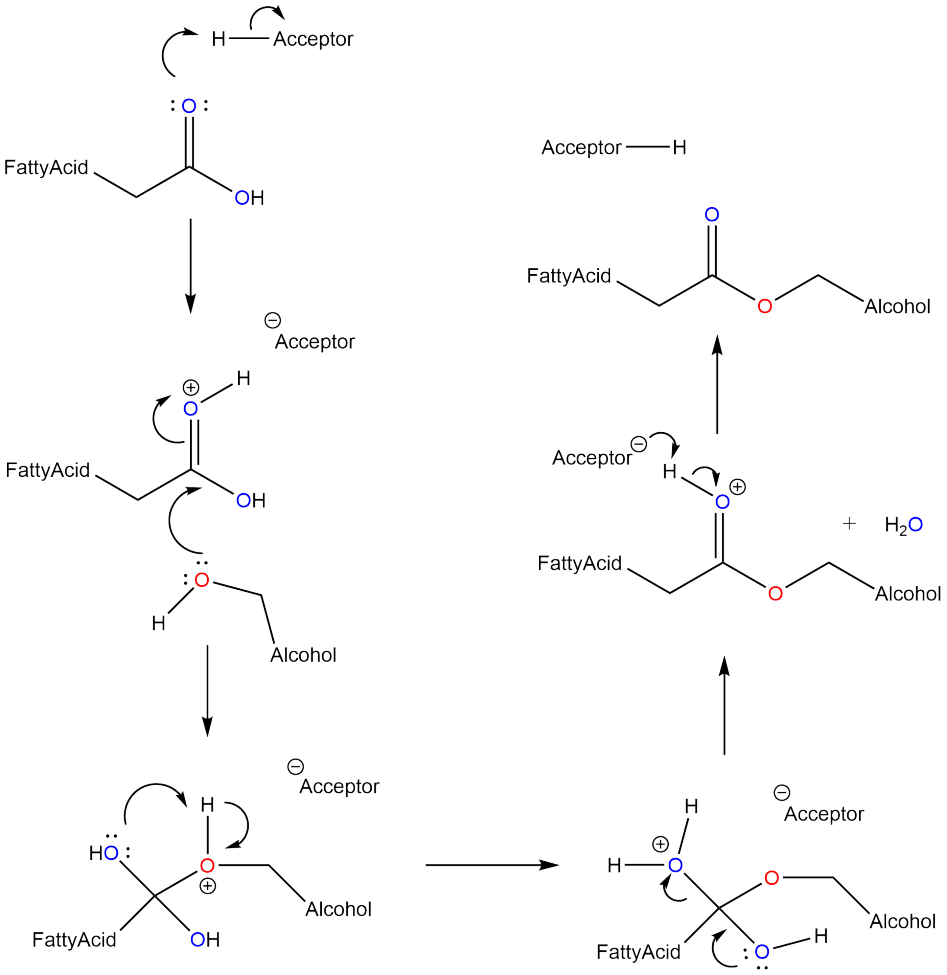

Figure 3.12: Esterification reaction mechanism and water release. Oxygen atoms from fatty acid are depicted in blue, oxygen atom from alcohol is depicted in red.

3.4.1 Lipid tailgroup SLD

Plant lipid tailgroup SLD

Spinach (*Spinacia oleracea*) thylakoid membranes consist of the following lipids: 52 % MGDG, 29 % DGDG, 6.5 % SQDG, 9.5 % PG, 4.5 % PC and 1.5 % PI 3.2 [36, 34]. These lipids normally account for 95 % of thylakoid membrane lipids. This lipid composition is relatively uniform among various species (Table 3.2), and does not change in different illumination conditions (LL, NL, HL and natural light) [250]. Due to their low content, PC and PI are neglected in SLD calculations - also because their presence in thylakoids is currently questioned and these lipid species are sometimes considered experimental-isolation artefacts; furthermore, this simplifies SLD calculations. Therefore, MGDG, DGDG, SQDG and PG are normalized so that their sum is equal to 100 % and not 95 % (this is called the adjusted fatty acid content) in Table 3.3.

*Table 3.2: Plant lipid composition, % of total lipids . [153, 34] * - Lipids neglected in SLD calculations.*

Lipid	Spinach thylakoid membrane	Rice thylakoid membrane	Maize leaf	Clover leaf	*Arabidopsis* plant
MGDG	52	48.4	42	46	48.9
DGDG	26	32.9	31	28	14.5
SQDG	6.5	13.9	5	4	1.6
PG	9.5	4.8	7	6	8.6
PI*	1.5	-	1	1	
PC*	4.5	-	6	7	19.7
PE*	-	-	3	5	6.7
Sum	100	100	100	100	100

When calculating the fatty acid composition for spinach thylakoid membrane in Table 3.3, it is also assumed, that that total fatty acid content is equal to the sum of two predominant fatty acid entities: for MGDG - 50 % 16:3 (sn-2 position) and 50 % 18:3 (sn-1 position), for DGDG - 50 % 18:3 (sn-2 position) and 50 % 16:0 (sn-1 position), for SQDG - 100 % 16:0 (sn-2 and sn-1 positions) and for PG - 50 % 16:1 (sn-2 position) and 50 % 18:3 (sn-1 position), using the fatty acid distribution of *Arabidopsis thaliana* [36]. For the estimations of fatty acid content for maize, pea and spinach leaves, Table 1.1 of [153] is used. For *Arabidopsis*, Tables 3.1 and 3.2 of [117, 180] are used. For AVANTIS lipids, fatty acid distributions from their product descriptions, available on the website, are used. Neutron SLD of individual fatty acids are calculated by internet tools (https://sld-calculator.appspot.com/ or NIST SLD calculator) using fatty acid densities from chemical tables and their chemical formulae.

It is important to note that SLDs are estimated for individual fatty acids and not the compound (headgroup and tailgroup chemically bound together) lipid molecule. When a lipid molecule is formed, a water molecule is lost during esterification reaction between fatty acid and alcohol - therefore fatty acid bound in lipid molecule contains one less hydrogen atom than being unbound (Fig. 3.12). This hydrogen release is not taken into account, since I calculate SLD of fatty acids (if a lipid molecule contains two fatty acids, it is implicit that there are two hydrogen atoms missing). Eq. 3.17 is used to calculate

average-weighted $SLD_{fatty\ acid\ mixture}$:

$$Weighted\ SLD_{fatty\ acid\ mixture} = \sum_i (SLD_{fatty\ acid_i} \cdot Adjusted\ fatty\ acid\ content_i) \tag{3.17}$$

From calculations, weighted average neutron SLD for fatty acids in thylakoids and plant leaves varies from 2.8-3.7 $\cdot$ 10 $^{-7}$ Å^{-2} (Table 3.3). These values are higher than neutron SLDs of saturated alkylgroups ($-CH_2-$) of nanodisc-forming lipids (-2.96 $\cdot$ 10 $^{-7}$ Å^{-2}) [175]). However, as thylakoid fatty acids are predominantly (poly-)unsaturated ($-CH-$) and their SLD is positive, the average-weighted SLD is also positive.

Table 3.3: Plant lipid tail fatty acid composition from different entities. To convert fatty acid content to mol %, multiplication by 100 % is needed.

Fatty acid	Common name	Formula	Adjusted fatty acid content							Density g/cm^3	Neutron SLD Å^{-2}	X-ray SLD (Cu Kα) Å^{-2}
			Spinach thylakoid membrane	Maize leaf	Pea leaf	Spinach leaf	*Arabidopsis* leaf	*Arabidopsis* plant	AVANTIS lipids			
16:0	Palmitic acid	$C_{16}H_{32}O_2$	0.2074	0.08421	0.125	0.1277	0.15	0.05564	0.03587	0.8527	-3.45E-8	8.1493E-6
16:1	Palmitoleic acid	$C_{16}H_{30}O_2$	0.05053	0.0421	0.03125	0.03191	0.038	0.08242	0.02047	0.894	1.2184E-7	8.4925E-6
16:2	Hexadecadienoic acid	$C_{16}H_{28}O_2$					0.011	0.005701		0.9	2.8430E-7	8.4967E-6
16:3	Hexadecatrienoic acid	$C_{16}H_{26}O_2$	0.2766				0.138	0.2011	0.43401	0.9268[1]	4.654E-7	1.0156E-5
18:0	Stearic acid	$C_{18}H_{36}O_2$		0.02105	0.010416667		0.010	0.0103	0.002719	0.9408	-6.7539E-8	9.0048E-6
18:1	Oleic acid	$C_{18}H_{34}O_2$		0.07368	0.020833333	0.07447	0.035	0.001982	0.007931	0.895	7.8055E-8	8.52E-6
18:2	Linoleic acid	$C_{18}H_{32}O_2$		0.08421	0.229166667	0.1702	0.175	0.02441	0.14944	0.9	2.2365E-7	8.5202E-6
18:3	α - Linolenic acid	$C_{18}H_{30}O_2$	0.4656	0.6947	0.583333333	0.5957	0.460	0.6187	0.34956	0.9164	3.7767E-7	8.6266E-6
	Average-weighted neutron SLD of fatty acid mixture, Å^{-2}:		3.03574E-7	2.87755E-7	2.71978E-7	2.68338E-7	2.8173E-7	3.4192E-7	3.69121E-7			
	Average-weighted X-ray SLD of fatty acid mixture, Å^{-2}:		8.9438E-6	1.0277E-5	9.3843E-6	9.6981E-6	9.7338E-8	8.5351E-6	9.4751E-6			

[1]Molar volume of 268.1 cm^3/mol was found in the literature, which was converted to g/cm^3

Cyanobacterial lipid tailgroup SLD

The total lipid content ranged between 10 % and 28 % of cyanobacterial dry weight [259, 244]. Although four major lipid classes in cyanobacteria are similar to other photosynthetic organisms, cyanobacterial fatty acid distribution differs significantly both from plants and algae [244] (Tables 3.4 and 3.3). Cyanobacterial thylakoid membranes do not contain polysaturated fatty acids and are more stiff due to higher saturated fatty acid content [243].

Lipid compositions of two cyanobacterial species - model organism freshwater cyanobacterium *Synechococystis* sp. PCC6803 and a thermophile *Thermosynechococcus vulcanus* - were used to derive their scattering length densities (Table 3.5) in the same way as for plants using Eq. 3.17. To compare them with plant values, X-ray SLD values are very similar, whereas neutron SLD values are slightly lower - due to the fact that more saturated fatty acids, having lower SLDs, are present in cyanobacterial thylakoid membranes.

Table 3.4: Cyanobacterial and algal lipid composition, mol % of total lipids [243, 172]

Lipid	*Synechocystis* sp. PCC6803	*Thermosynechococcus vulcanus*	*Chlamydomonas reinhardtii*
MGDG	37.4	43.5	55
DGDG	20	25.6	20
SQDG	28	24.8	13
PG	13.7	6.1	6
Sum	99	100	94

Table 3.5: Cyanobacterial lipid tail fatty acid composition. To convert numbers to mol %, multiply by 100 %.

Fatty acid	Common name	Formula	Adjusted fatty acid content		Density g/cm^3	Neutron SLD Å^{-2}	X-ray SLD (Cu Kα) Å^{-2}
			Synecocystis sp. PCC 6803 thylakoid membrane	*Thermosynechococcus vulcanus* thylakoid membrane			
16:0	Palmitic acid	$C_{16}H_{32}O_2$	0.5714	0.49078	0.8527	-3.45E-8	8.1493E-6
16:1	Palmitoleic acid	$C_{16}H_{30}O_2$	0.06311	0.1223	0.894	1.2184E-7	8.4925E-6
18:0	Stearic acid	$C_{18}H_{36}O_2$	0.00937	0.04863	0.9408	-6.7539E-8	9.0048E-6
18:1	Oleic acid	$C_{18}H_{34}O_2$	0.10307	0.3383	0.895	7.8055E-8	8.52E-6
18:2	Linoleic acid	$C_{18}H_{32}O_2$	0.12386		0.9	2.2365E-7	8.5202E-6
18:3	α - Linolenic acid	$C_{18}H_{30}O_2$	0.1292		0.9164	3.7767E-7	8.6266E-6
	Average-weighted neutron SLD of fatty acid mixture, Å^{-2}:		7.18668E-8	2.1080E-8			
	Average-weighted X-ray SLD of fatty acid mixture, Å^{-2}:		8.3248E-6	8.3583E-6			

3.4.2 Lipid headgroup SLD

Plant lipid headgroup SLD

Thylakoids of plant leaves are predominately composed of glyco- and sulfoglycolipids. Using the data for spinach thylakoid lipids, 78 % of lipid heads (corresponding to the sum of MGDG and DGDG) is galactose, 6.5 % is sulfoquinovose and 9.5 % is phosphoglycerol. Phosphoinositol, phosphatidylcholine and phosphoethanolamine lipids, which correspond to total of 6 % lipids, are also neglected as in lipid tailgroup SLD calculations. Therefore the sum of galactose, sulfoquinovose and phosphoglycerol lipids is normalized to 100 % and this is called adjusted content. As mentioned in the beginning of the Chapter 3.4, hydration layer of individual lipid headgroups or water content in the membrane are not accounted for.

For pea thylakoids [301], maize and clover leaves [153] lipid headgroup SLDs are derived based on the percentage of individual lipids and knowing their chemical properties - densities and sugar composition (Eq. 3.18). Obtained SLDs are similar between plant species.

$$Weighted\ SLD_{sacharide\ mixture} = \sum_i (SLD_{sacharide_i} \cdot Adjusted\ sacharide\ content_i) \tag{3.18}$$

In principle, DGDG contains two molecules of galactose bound together via α or β junction and H_2O is released upon glycosidic bond formation (Fig. 3.11 b). However for a simplicity in SLD calculations, it is assumed that DGDG contains two galactose molecules that are not bound together. One can consider it the other way (as digalactose) with glycoside bond, but then direct summation of galactose content from MGDG and DGDG cannot be performed. This would further complicate SLD calculations and is therefore ignored.

From calculations, weighted average neutron SLD for lipid heads in thylakoids and plant leaves varies from 1.63-1.68 $\cdot$ 10 $^{-6}$ Å^{-2} (Table 3.6), what are slightly lower values than the average headgroup of nanodisc-forming lipids [175].

Cyanobacterial lipid headgroup SLD

Cyanobacteria contain more negatively charged sulpholipids (SQDG) and phosphatidylglycerol (PG) than plants. In cyanobacteria, PG lipid is necessary to maintain trimeric complex of PSI [246]. The role of SQDG lipid is less clear - the loss of SQDG in the mutant reduced growth and PSII activity for *Synechocystis* sp. PCC 6803 and *Chlamydomonas reinhardtii*, whereas SQDG loss did not impact these parameters for *Synechococcus elongatus* sp. PCC 7942 or *Rhodobacter* [246]. Due to these differences, scattering length densities of cyanobacterial headgroups were derived and are given in Table 3.7. In short,

*Table 3.6: Plant lipid head sacharide composition. To convert numbers to mol %, multiply by 100 %. * cm^3/ mol was found instead of g/cm^3*

Sugar	Formula	Adjusted sugar content				Density g/cm^3	Neutron SLD $Å^{-2}$	X-ray SLD (Cu Kα) $Å^{-2}$
		Spinach thylakoid membrane	Pea thylakoid membrane	Maize leaf	Clover leaf			
Galactose	$C_6H_{12}O_6$	0.8297	0.7222	0.8588	0.8810	1.616	1.611E-6	1.4679E-5
Sulfoquinovose	$C_6H_{12}O_8S$	0.06915	0.1444	0.05882	0.04762	125*	2.133E-6	1.7495E-5
Phosphoglycerol	$C_3H_9O_6P$	0.1011	0.1333	0.0823	0.07143	1.7	1.561E-6	1.5202E-5
Average-weighted neutron SLD of sugar mixture, $Å^{-2}$:		1.6424E-6	1.6800E-6	1.6378E-6	1.6327E-6			
Average-weighted X-ray SLD of sugar mixture, $Å^{-2}$:		1.4927E-5	1.5155E-6	1.4887E-5	1.4851E-5			

despite the differences in lipid composition, weighted neutron and X-ray SLDs of lipid headgroup mixtures of cyanobacteria are very similar to the headgroup SLDs of higher plants.

*Table 3.7: Cyanobacterial lipid head sacharide composition. To convert numbers to mol %, multiply by 100 %. * cm^3/ mol was found instead of g/cm^3*

Sugar	Formula	Adjusted sugar content		Density g/cm^3	Neutron SLD $Å^{-2}$	X-ray SLD (Cu Kα) $Å^{-2}$
		Synecocystis sp. PCC6803 thylakoid membrane	*Thermosynechococcus vulcanus* thylakoid membrane			
Galactose	$C_6H_{12}O_6$	0.541	0.691	1.616	1.611E-6	1.4679E-5
Sulfoquinovose	$C_6H_{12}O_8S$	0.289	0.248	125*	2.133E-6	1.7495E-5
Phosphoglycerol	$C_3H_9O_6P$	0.137	0.061	1.7	1.561E-6	1.5202E-5
Average-weighted neutron SLD of sugar mixture, $Å^{-2}$:		1.7554E-6	1.7378E-6			
Average-weighted X-ray SLD of sugar mixture, $Å^{-2}$:		1.5564E-5	1.5409E-6			

3.4.3 Thylakoid membrane protein SLD

Thylakoid membrane contains around 50-70 % proteins by area [126]. To estimate neutron SLDs of thylakoid proteins predominant thylakoid membrane protein entities have been taken into account: PSII, PSI, cytochrome b_6f and ATP synthase complexes. I have joined the sequences of 23 unique protein subunits of spinach PSII complex (PDB ID: 3JCU) to a single complete sequence, 16 unique protein subunits of PSI complex (from various plants, PDB ID: 2O01) to a single complete sequence, 9 unique protein subunits of cytochrome b_6f complex from *Chlamydomonas* (since no plant sequence was available, PDB ID: 1Q90) to a single complete sequence, 2 spinach ATP synthase (PDB ID: 1FX0) unique sequences to a single complete sequence.

Taking only the unique amino acid sequences into account solves the issue of protein multimerization. If a unique protein sequence is present in a large protein complex N times, the total volume of this sequence will be N times larger. Since SLD depends on the number of particles (unique polypeptides) per volume, SLD will remain constant - as both the total number of polypeptides and the total polypeptide volume increase simultaneously. Also, despite that photosynthetic antennae (for plants - Lhca and Lhcb, for cyanobacteria - phycobillisomes) are prevalent thylakoid proteins (local phycobillisome concentration between two membranes can reach up to 1 mM, which is about 200 g/L [7]), I did not take them into account for thylakoid membrane protein SLD estimations. In the same way, including six-seven additional transmembrane LHC into higher plant protein SLD calculations shall increase the precision, but on the other hand shall not significantly change the average protein SLD. Also, LHCII:LHCI:Photosystem ratio is unknown, can vary in time due to state transitions, what makes it unfeasible to quantify how much LHC is present in the membrane.

Furthermore, as LHC and phycobilisomes are located on top of thylakoid membranes, they account for protein SLD of inter-thylakoid space and not for the SLD of the inner part (lipid heads, lipid tails) of thylakoid membrane. I assume that inter-thylakoid space is composed of proteins and water. Despite the fact that water concentration in inter-thylakoid (or lumenal) space is unknown, it is assumed to be in the molar range (personal communication with Aleksander Tichonov, [13]), what makes the impact of 1 mM phycobilisome proteins (no matter their large protein volume) negligible in SLD calculations of inter-thylakoid space. For the same reason, I also did not take into account chlorophyll and all cofactors that are present inside photosynthetic proteins, since they totally account only for max. 1 % of the chloroplast dry mass.

However, the argumentation of omitting phycobilisomes from $\mathrm{SLD}_{inter-thylakoid\ space}$ calculation due to their 'low concentration' can be wrong. From published data on unicellular red algae *Porphyridium cruentum*, there are 560±20 PBS/μm^2 on the thylakoid membrane under low light (6 W/m^2, corresponding to 29 photons $\cdot$ m^{-2} $\cdot$ s^{-1} - conversion factor 1 W/m^2= 4.80 photons $\cdot$ m^{-2} $\cdot$ s^{-1} PAR [240]) and phycobilisome density is 384±45 PBS/μm^2 in high light (15 W/m^2, corresponding to 72 photons $\cdot m^{-2} \cdot s^{-1}$ [240]) [20]. Using individual PBS dimensions of 600·410·340 Å in high light and 600·350·340 Å in low light, I obtain that the thylakoid membrane surface volume (1 μm^2 area $\cdot$ 550 Å height, which my estimate of inter-thylakoid space average height) is filled with compactly packed phycobilisomes in both illumination conditions: phycobilisome volume fraction in the inter-thylakoid space varies from 68 to 100 % (*which gives the average of 85 %*). The SLD of *Griffithsia pacifica* phycobilisome, calculated from 25 unique protein chains (taken from [315]) in 100 % D_2O and with 90 % labile H-D exchange is $3.12 \cdot 10^{-6}$ Å^{-2}. Similarly, with phycobilisome dimensions of *Synechocystis* sp. 6803 (480·300·300 Å [208]) and its inter-thylakoid space width of 450 Å [208], phycobilisome volume fraction, using *P. cruentum* phycobilisome density in high light (a double layer of phycobilisomes) [20] is also 73.8 %. Therefore, $\mathrm{SLD}_{inter-thylakoid\ space}$ is then $0.85 \cdot \mathrm{SLD}_{phycobilisome} + 0.15 \cdot \mathrm{SLD}_{D_2O} = 3.612 \cdot 10^{-6}$ Å^{-2} - that is, almost 2 times smaller than of pure D_2O. To avoid

possible errors and to simplify calculations, as elaborated later, I subtract the SLD of inter-thylakoid space (which is also called $SLD_{cytoplasm}$ in Manuscript 1 or SLD $_{stroma}$ in higher plants) from SLD of thylakoid membrane headgroups and SLD of thylakoid membrane tailgroups.

To calculate SLD values of photosynthetic proteins, subunit-combined sequences were inserted into Biological SLD calculator (http://psldc.isis.rl.ac.uk/Psldc/, [190]). Parameters used for SLD calculations: proteins were located in 100 % D_2O, 0 % of the non-labile hydrogens covalently bonded to carbon atoms were deuterated, and either 0 % or 50 % of labile hydrogens (bonded to the side chains) could exchange with the deuterium in the solution. Labile hydrogens comprise 20-30 % of total hydrogens of the protein. 90 % labile hydrogen exchange (18-27 % of total hydrogens) is a standard estimate for water-soluble proteins [67]. I have chosen the lower values due to the fact that thylakoid proteins are located in the membrane bilayer *in vivo* and most of their hydrogens (hydrophobic) are buried in the fatty acid tails of the bilayer. Therefore, I assume that the labile hydrogen exchange between D_2O and protein is highly decreased - my chosen minimum value is 0 % and maximum is 50 %; the total hydrogen exchange is then 0-15 %.

For choosing the lower limit of labile hydrogen exchange, I used the information obtained from NMR experiment - that hydrogens buried in the membrane exchange 10^5 times more slowly than in a soluble unfolded protein (personal communication with Jeffrey Brender, [97]). One can argue that this estimate is a bit too low, since hydrogens of stroma or lumen-exposed proteins can exchange more easily than these buried in the membrane.

Choosing the maximal exchange limit is way less concise. I have estimated this in the case that D-diffusion equilibrium is reached after infinite time, as suggested in Henry et al. [97]. However, taking into account that most hydrogens are burried in the membrane or are inside the multi-subunit proteins and that exchange happens slowly, I expect that theoretically possible maximal 20-30 % exchange [67] is substantially lower in reality (personal communication with Zoe Fisher). Therefore 0 % (no H-D exchange occurred) estimate is more realistic than 15 % (if deuterium exchange is 50 % efficient). I calculate both scenarios to compare.

To estimate the total protein SLD of the plant thylakoid membrane from four individual protein entities, I used the Protein/PSII molar ratios of 1, 0.7, 0.5 and 0.7 (for PSII, PSI, ATP synthase, cytochrome b_6f accordingly) [17] and calculated the weight-averaged SLD of total protein in plant thylakoid membrane.

For thylakoid protein SLD calculations of cyanobacteria, a different set of proteins was used: 20 unique subunits of PSII of *Thermosynechococcus vulcanus* (PDB ID: 4UB6), 12 unique subunits of PSI of *Synechococcus elongatus* (PDB ID: 1JB0), 8 unique subunits of cytochrome b_6f of *Mastigocladus laminosus* (PDB ID: 4H13), 11 unique subunits of V-ATPase of *Sacharomyces cerevisiase* (PDB ID: 3J9T). Similarly as for plants, I used the Protein/PSII molar ratios of 1, 0.7, 0.5 and 0.7 (for PSII, PSI, ATP synthase, cytochrome

b_6f accordingly) [17] (a different stoichiometry can also be chosen [42]) and calculated the weight-averaged SLD of total protein in cyanobacterial thylakoid membrane.

To investigate the thylakoid protein SLD parameter variability, I also used different labile hydrogen-deuterium exchange percentages (0 - 100 %). Total protein SLD value varies from 1.83-3.09 $\cdot$ 10 $^{-6}$ Å^{-2}. However, from the previous discussion, the weight-averaged value in 0 % is 1.8188 $\cdot$ 10 $^{-6}$ Å^{-2} and in 50 % is 2.4329 $\cdot$ 10 $^{-6}$ Å^{-2}, which are the values used in further modelling (Table 3.8). These values are slightly lower than 3.41$\cdot$ 10 $^{-6}$ Å^{-2}, obtained for 18-aa amphiphilic water-exposed nanodisc belt peptide [175]. This discrepancy occurs due to the fact that this small peptide can undergo H-D exchange to a much larger degree then membrane-embedded thylakoid protein complexes.

Table 3.8: Neutron and X-ray SLDs for four predominant plant thylakoid membrane proteins.

Protein	Photosystem II	Photosystem I	ATP synthase	Cytochromeb_6f	Weighted averages, Å^{-2}
PDB ID	3JCU	2O01	1FX0	1Q90	
Species	Spinach	Various plants	Spinach	Chlamydomonas	
Protein ratio to PSII (mol/mol)	1	0.7	0.5	0.7	
Chemical composition	$C_{20691}N_{5305}O_{5430}S_{128}H_{31295}$	$C_{16018}N_{4111}O_{3999}S_{80}H_{23828}$	$C_{4831}N_{1328}O_{1400}S_{31}H_{7667}$	$C_{4916}N_{1224}O_{1235}S_{39}H_{7580}$	
Density, g/cm^3	1.34	1.34	1.34	1.33	
Number of residues	4164	3114	1005	981	
Number of exchangable hydrogens at pH 7.0	6637	4979	1721	1501	
Molecular weight, kDa	457.741	345.72	109.08	106.43	
Molecular volume Å^3,	558904	427830	134935	133265	
Neutron SLD (0 % water exchange), Å^{-2}	1.8440E-6	1.8760E-6	1.7830E-6	1.7510E-6	1.8188E-6
Neutron SLD (50 % water exchange), Å^{-2}	2.4601E-6	2.4810E-6	2.4450E-6	2.3360E-6	2.4329E-6
X-ray SLD (Cu Kα), Å^{-2}	1.2202E-5	1.2198E-5	1.2212E-5	1.2133E-5	1.2186E-5

3.4.4 Total SLD of thylakoid membrane

Another different distinction of thylakoid membranes is that, contrary to cell membranes, thylakoid membrane is very protein-rich: 69 ± 5 % of the membrane is composed of proteins [126]; literature values vary from 48-61 % proteins in grana membranes and 23-49 % proteins in stroma lamellae. Using this information thylakoid membrane scattering length density for lipid heads can be calulated as 0.5-0.7 $SLD_{protein}$ + 0.5-0.3 $SLD_{headgroup}$ and scattering length density for lipid fatty acid tailgroups as 0.5-0.7 $SLD_{protein}$ + 0.5-0.3 $SLD_{tailgroup}$. The estimates for SLD variation for spinach thylakoids are provided in Table 3.9, where 0 % and 50 % exchange rate protein SLD data is used. SLD values obtained for 0.7 protein/0.3 lipid ratios are used for modelling (Tables 3.9 and 3.10). I can now visualize SLDs of thylakoid membrane unit cell (Fig. 3.13) and systematically change the SLD of lumen (Fig. 3.14).

In the same way, scattering length densities of thylakoid membrane components were also derived for cyanobacteria using the data of *Synechocystis* sp. PCC 6803 (Table 3.10) using different lipid-protein ratios. Since cyanobacteria contain more non-saturated lipids, their total thylakoid membrane SLDs are slightly different.

Table 3.9: Estimates of neutron and X-ray SLD for lipid heads and lipid tails with different protein/lipid ratios. ***Plants***

Protein/Lipid ratio	SLD of lipid heads, $Å^{-2}$	SLD of lipid tails, $Å^{-2}$	$\frac{SLD_{lipidheads}}{SLD_{lipidtails}}$
With 50 % labile hydrogen exchange. SLD protein used: 2.4329E-6 $Å^{-2}$			
0.0/1.0 (only lipids)	1.6424E-6	3.0350E-7	5.4116
0.4/0.6	1.9586E-6	1.1553E-6	1.6954
0.5/0.5	2.0377E-6	1.3682E-6	1.4893
0.6/0.4	2.1167E-6	1.5811E-6	1.3387
0.7/0.3	2.1958E-6	1.7941E-6	1.2239
0.8/0.2	2.2748E-6	2.0070E-6	1.1334
1.0/0.0 (only proteins)	2.4329E-6	2.4329E-6	1
With 0 % labile hydrogen exchange. SLD protein used: 1.8188E-6 $Å^{-2}$			
0.0/1.0 (only lipids)	1.6424E-6	3.0350E-7	5.4116
0.4/0.6	1.7130E-6	9.0960E-7	1.8832
0.5/0.5	1.7306E-6	1.0611E-6	1.6309
0.6/0.4	1.7482E-6	1.2127E-6	1.4416
0.7/0.3	1.7659E-6	1.3642E-6	1.2944
0.8/0.2	1.7835E-6	1.5157E-6	1.1767
1.0/0.0 (only proteins)	1.8188E-6	1.8188E-6	1
X-rays. SLD protein used: 1.2186E-5 $Å^{-2}$			
0.0/1.0 (only lipids)	1.4927E-6	8.9438E-6	0.1669
0.4/0.6	5.7700E-6	1.0241E-5	0.5634
0.5/0.5	6.8394E-6	1.0565E-5	0.6474
0.6/0.4	7.9087E-6	1.0889E-5	0.7263
0.7/0.3	8.9780E-6	1.1213E-5	0.8007
0.8/0.2	1.0047E-5	1.1538E-5	0.8708
1.0/0.0 (only proteins)	1.2186E-5	1.2186E-5	1

3.4.5 Stromal SLD

Stromal and inter-thylakoid space SLD is used interchangeably in this thesis. Stromal SLD is more biologically correct name for it, since stroma entirely surrounds thylakoids.

Table 3.10: Estimates of neutron and X-ray SLD for lipid heads and lipid tails with different protein/lipid ratios. ***Cyanobacteria Synechoccystis sp. PCC 6803***

Protein/Lipid ratio	SLD of lipid heads, $Å^{-2}$	SLD of lipid tails, $Å^{-2}$	$\frac{SLD_{lipidheads}}{SLD_{lipidtails}}$
With 50 % labile hydrogen exchange. SLD protein used: 2.4704E-6 $Å^{-2}$			
0.0/1.0 (only lipids)	1.7554E-6	7.1868E-8	24.43
0.4/0.6	2.0414E-6	1.0313E-6	1.979
0.5/0.5	2.1129E-6	1.2711E-6	1.662
0.6/0.4	2.1844E-6	1.5110E-6	1.446
0.7/0.3	2.2559E-6	1.7508E-6	1.288
0.8/0.2	2.3274E-6	1.9907E-6	1.169
1.0/0.0 (only proteins)	2.4704E-6	2.4704E-6	1
With 0 % labile hydrogen exchange. SLD protein used: 1.86E-6 $Å^{-2}$			
0.0/1.0 (only lipids)	1.7554E-8	7.1868E-8	24.42
0.4/0.6	1.7991E-6	7.8896E-7	2.280
0.5/0.5	1.810E-6	9.6823E-7	1.869
0.6/0.4	1.8209E-6	1.1475E-6	1.587
0.7/0.3	1.8318E-6	1.3268E-6	1.380
0.8/0.2	1.8428E-6	1.5060E-6	1.223
1.0/0.0 (only proteins)	1.86E-6	1.86E-06	1
X-rays. SLD protein used: 1.2475E-5 $Å^{-2}$			
0.0/1.0 (only lipids)	1.5564E-5	8.3248E-6	1.8696
0.4/0.6	1.4321E-5	9.9777E-6	1.435
0.5/0.5	1.4011E-5	1.0391E-5	1.348
0.6/0.4	1.3700E-5	1.0804E-5	1.268
0.7/0.3	1.3389E-5	1.1217E-5	1.193
0.8/0.2	1.3078E-5	1.1631E-5	1.1244
1.0/0.0 (only proteins)	1.2475E-5	1.2475E-5	1

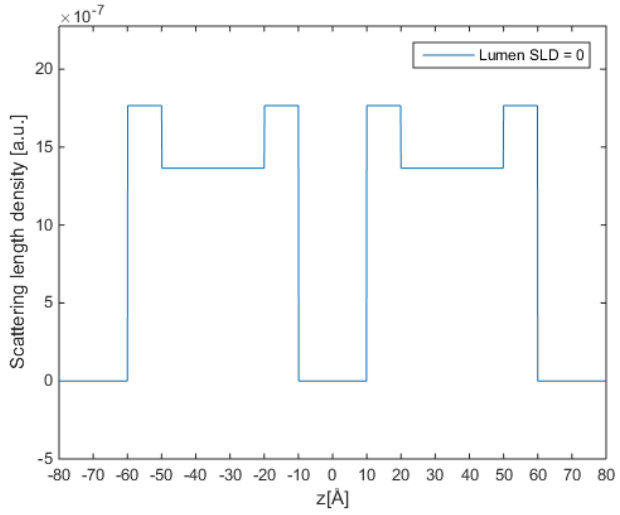

(a)

Figure 3.13: (a)Thylakoid unit cell appearance. SLD estimates of thylakoid unit cell components: $\Delta\rho_H$ *= 1.7659E-6 ,* $\Delta\rho_T$ *= 1.3642E-6,* $\Delta\rho_L$ *= 0.*

However, the only part of stroma which is considered in this PhD thesis is aqueuous environment between two thylakoids - inter-thylakoid space. In cyanobacteria, inter-thylakoid space is filled with phycobilisomes and in plants it is filled with LHC complexes. Therefore, due to large protein content of inter-thylakoid space (as elaborated below), $SLD_{inter-thylakoid\ space}$ can be different from $SLD_{stroma\ average}$.

I calculate a thylakoid membrane form factor relatively to its ambient environment - therefore I assume that stroma has a scattering length density different from water. The absolute scattering length density of stroma can be only roughly estimated - it depends on total protein, ion and water concentrations (which are largely unknown) and substantially varies in space and time. It is estimated that chloroplast consists of 75 % water and 25 % solid material [17]. Similarly to chloroplasts, total cellular water in mitochondria is 72 %, what corresponds to 2 mL water/g dry mass; 61 % of water is not osmotically bound [13].

Therefore I formally calculate heavy water concentration in the chloroplast after exchange (taking volume of 1 dm^3) as $[D_2O] = \frac{750 g/dm^3}{20.02 g/mol} = 37.46$ M. In comparison, pure water concentration is 55.55 M, and light water concentration in chloroplast is 41.66 M. I again emphasize that 41.6 M is an average water concentration inside the chloroplast, whereas local water concentration in inter-thylakoid space and other confined aqueous environments - i.e. if volumes of protein-rich membranes are excluded from total volume - is even higher and can reach 55 M (personal communication with Alexander Tichonov).

An estimate of concentrations for chloroplast solutes (also called free metabolites - ions, sugars, amino acids) were made by Gupta [92] and Kaiser [116]. Total concentration of chloroplast free metabolites is around 300 mM, what is in the same concentration range as in *E. coli* cytoplasm [30].

To calculate absolute SLDs for metal ions, I have used densities of the pure metals, for anions I have used densities of their conjugate acids (HCl, H_2SO_4, H_3PO_4 and HNO_3). I think it is a reasonable assumption, because these strong acids dissociate completely into ions when dissolved in water. On the other hand, the concentration of these ions in water is low enough that the density of deuterated water can be used as the final solution density. In order to avoid over-using water density, I chose to use actual densities of metals and acids from chemical tables (which are all close to 1 g/cm^3).

Using the concentrations of individual solutes (Table 3.11 [116, 92]) and D_2O (personal calculation) in the stroma to estimate the weighted SLDs for each solute (Table 3.12). In comparison with SLD of pure D_2O ($6.39 \cdot 10^{-6}$ Å^{-2}), stromal SLD almost identical, because it is predominantly determined by a 1000-fold higher concentration of heavy water rather than the total concentration of solutes. This result is not very surprising in the light that the majority of plant cell volume (80 %) is occupied by vacuole, which is predominantly water. Chloroplasts, in turn, occupy around 8 % cell volume and are composed of 80 % water-based stroma and 20 % thylakoid membranes [149].

Up to now, I have not consider inter-thylakoid space proteins in the stromal SLD calculations. If exemplified by cyanobacteria, $SLD_{inter-thylakoid\ space}$ is a weighted sum of

$0.85 \cdot \mathrm{SLD}_{phycobilisome}$ and $0.15 \cdot \mathrm{SLD}_{\mathrm{D_2O}}$. Being aware that such stromal SLD estimation is very approximate, I also proceed to calculate chloroplast SLD including more entities: DNA, proteins, lipids in their absolute quantities for comparison.

To sum up, as total solute concentration in the stroma (or inter-thylakoid space) is relatively low, I claim that stromal/inter-thylakoid space SLD can be determined by summing the volume-fraction-averaged water and protein (light-harvesting complex or phycobilisome) SLDs . This is a strong statement per se and its biological validity is elaborated in Manuscript 1.

Table 3.11: Physical properties of stromal components

Solute	Formula	Density, g/cm^3	Neutron SLD, Å^{-2}	X-ray SLD (Cu Kα), Å^{-2}
K^+	K	0.862	4.8727E-7	7.2642E-6
Na^+	Na	0.968	9.2045E-7	7.9585E-6
Ca^{2+}	Ca	1.55	1.0946E-6	1.3377E-5
Mg^{2+}	Mg	1.74	2.3146E-6	1.4798E-5
Cl^-	HCl	0.00149	1.4368E-9	1.2738E-8
$NO_3{}^-$	HNO_3	1.51	3.3305E-6	1.3090E-5
$SO_4{}^{2-}$	H_2SO_4	1.84	2.0997E-6	1.6092E-5
$HPO_4{}^-$	H_3PO_4	1.89	1.9840E-6	1.6533E-5
Reducing sugars – as glucose	$C_6H_{12}O_6$	1.54	1.5356E-6	1.3988E-5
Amino acids – as isoleucine	$C_6H_{13}NO_2$	1.04	5.8107E-7	9.7213E-6

Table 3.12: Estimates of neutron and X-ray SLD of stroma.

Solute	mM Gupta et al.	Weighted neutron SLD, Å^{-2} Gupta et al.	Weighted X-ray SLD, Å^{-2} (Cu Kα), Gupta et al.	mM Kaiser et al.	Weighted neutron SLD, Å^{-2} Kaiser et al.	Weighted X-ray SLD, Å^{-2} (Cu Kα), Kaiser et al.
K^+	53.6	2.61E-8	3.8936E-7	126	6.14E-8	9.1529E-7
Na^+				7	6.44E-9	5.5710E-8
Ca^{2+}	25.0	1.60E-7	3.3443E-7			
Mg^{2+}	21.1	4.88E-8	3.1224E-7	18	4.17E-8	2.6636E-7
Cl^-	58.0	8.33E-11	7.3880E-10	68	9.77E-11	8.6618E-10
$NO_3{}^-$	0.7	2.33E-9	9.1630E-9	26	8.66E-8	3.4034E-7
$SO_4{}^{2-}$	5.1	1.07E-8	8.2069E-8	12	2.52E-8	1.9310E-7
$HPO_4{}^-$	6.9	1.37E-8	1.1408E-7	15	2.98E-8	2.4800E-7
Reducing sugars – as glucose	35.6	5.47E-8	4.9797E-7	18	2.76E-8	2.5178E-7
Amino acids – as isoleucine	94.8	5.51E-8	9.2158E-7	77	5.51E-8	3.5417E-4
Sum of solutes (mM)	300.8			369		
Weighted stroma SLD, Å^{-2}		6.36E-6	9.45E-6		6.34E-6	9.44E-6

3.4.6 Chloroplast SLD

In this section I have used a different - more direct - approach to estimate SLD of the chloroplast. Since cyanobacteria are ancestors of chloroplasts, directly calculating average chloroplast SLD would also yield an average SLD estimate of the entire cyanobacterial cell, which is an important check-up number for Manuscript 1. If measuring cyanobacterial cells *in vivo*, this can also be used in contrast variation experiments. Also, since chloroplasts contain a lot of water as stroma (the question of stromal protein content is again relevant), a rough chloroplast SLD estimate can be compared to stromal SLD values.

I have assumed that chloroplast consists of 75 % D_2O and 25 % of biological material (dry mass): 13.75 % of proteins, 1 % of RNA, 0.03 % of DNA, 7.5 % of lipids and 1.75 % of sugar, 1 % of pigments (do not taken into account, Chl concentration in plant chloroplast is 30 mM or 1 mg Chl/ g fresh wt) [179, 149, 1, 263]. As D_2O density is 1.11 g/mL, there is no problem to define water's volume fraction from its mass fraction - they are practically equivalent. The same argument is not valid for proteins (13.75 % mass fraction), as they are not randomly dispersed in the entire water volume, but are predominantly localized in the thylakoid membrane (photosystems and antennae) and in the stroma (Rubisco). What burdens chloroplast SLD calculations further is that the protein content of lumenal and inter-thylakoid space is unknown. An attempt to derive a realistic lumenal protein content is performed in Manuscript 1.

Therefore, approximations need to be made. Soluble protein SLD was derived similarly as for proteins inside thylakoid membranes. According to Olinares *et al.* [207], 42 % of proteins in *Arabidopsis* have metabolism-related functions and Rubisco alone can constitute up to 60 % of chloroplast proteins (58 % of stromal mass [207]). Ribosomes dorm megadalton protein complexes in stroma and comprise max. 9 % total stromal proteins [207]. In comparison, photosynthesis-related proteins comprise only 6 % of stromal proteins [207]. Therefore, I have taken ribosomes and Rubisco as predominant stromal proteins. 29 unique protein chains of spinach ribosome large subunit 50S (PBD ID: 5H1S) were combined to a single protein chain and 2 unique protein chains of spinach RuBisCO (PBD ID: 1RCX) were combined to a single protein chain.

I calculated SLD for soluble proteins $= 0.5 \cdot SLD_{Rubisco} + 0.5 \cdot SLD_{Ribosome} = 3.3995 \cdot 10^{-6}$ Å^{-2}, where I assumed that 90 % of protein labile hydrogens are exchanged by deuterium, since these proteins are globular and water soluble/water exposed. Therefore, 90 % estimate of D-H exchange is used as a standard for globular water exposed proteins [190].

Since water soluble proteins account only for 20 % of total chloroplast protein, I also used SLD value of thylakoid membrane proteins (from section 3.4.3 with 0 % exchange, $1.8188 \cdot 10^{-6}$ Å^{-2}) and derived total SLD for chloroplast proteins $= 0.2 \cdot SLD_{soluble} + 0.8 \cdot SLD_{insoluble} = 2.07424 \cdot 10^{-6}$ Å^{-2}.

To estimate the SLD of DNA, I used the sequence of chloroplast DNA of *Arabidopsis thaliana* Col0 ecotype (EMBL accession: AP000423.1) and assumed 90 % labile hydrogen

exchange. To estimate rhe SLD of RNA, I have used the combined sequence of spinach 23S, 4.5S and 5S chloroplast ribosomal RNAs (PBD ID: 5H1S) and also assumed a 90 % of labile hydrogen exchange.

To estimate the average SLD of chloroplast lipids, I have used SLDs of spinach thylakoid membrane lipid heads and lipid tails with Protein (0 % exchange)/Lipid ratio of 0.7/0.3, already determined in sections on lipid tailgroup and headgroup SLDs. Finally, I assume that chloroplast lipid SLD = $0.5 \cdot SLD_{heads} + 0.5 \cdot SLD_{tails} = 1.99 \cdot 10^{-6}$ $Å^{-2}$.

To estimate the SLD of chloroplast sugars, I have used average-weighted SLD of spinach thylakoid membrane headgroups, already derived in section on lipid tailgroups. Sugar content in chloroplast is about 1.75 % of weight. Regarding the individual sugar composition of the chloroplast, although thylakoid membranes are mainly comprised of galactose, glucose is also produced in the stroma during light independent reactions, which can then be partially converted to fructose. Luckily, this 'sugar complexity' is easily solved: from the physical point of view all these compounds have the same chemical formula of $C_6H_{12}O_6$, therefore the same SLD can be used for all sugars, including the total chloroplast sugar.

To check what is the total variation of chloroplast SLD, I have also used protein labile hydrogen exchanges of 0 and 50% and varied the percentages of individual biological constituents (proteins and lipids). The overall neutron SLD variation range from many different calculations with different conditions was 5.1-5.5 $\cdot 10^{-6}$ $Å^{-2}$. This value is similar, although slightly lower than the stromal SLD estimate. Again, since water comprises 75 % of chloroplast volume, SLD from biological material has a 'limited influence' to the entire SLD, as the volume fraction distribution of lipids and proteins in different cellular compartments is ignored/averaged out. Therefore, chloroplast protein content (accounted as the volume fraction and not as the mass fraction; this conversion is not straightforward) shall be taken into account more stringently if this calculation is continued or re-evaluated.

Table 3.13: Neutron and X-ray SLDs for predominant chloroplast stroma components

	Ribosome	Rubisco	Chloroplast DNA	Ribosomal RNA
Accession/PDB ID	5H1S	1RCX	AP000423	5H1S
Species	Spinach	Spinach	*Arabidopsis*	Spinach
Chemical composition	$C_{20369}N_{6110}O_{5395}S_{114}H_{33397}$	$C_{3025}N_{817}O_{823}S_{26}H_{4527}$	$C_{1516284}N_{565800}O_{928189}H_{1749126}P_{154478}$	$C_{29092}N_{12057}O_{21020}H_{32837}P_{3037}$
Density, g/cm^3	1.36	1.38	1.66	1.77
Number of residues	4086	598	154478	3037
Number of exchangable hydrogens (at pH 7.0)	8257	1032	286672	9488
Molecular weight, kDa	465.72	68.09	47797	990.39
Molecular volume Å^3,	569127	82108	47771657	858006
Neutron SLD (90 % hydrogen exchange), Å^{-2}	3.105E-6	3.087E-6	3.712E-6	4.427E-6
X-ray SLD (Cu Kα), Å^{-2}	1.2422E-5	1.2543E-5	1.4634E-5	1.5557E-5

Table 3.14: Estimates of neutron and X-ray SLD for chloroplast.

Constituent	Percentage, w/w	Neutron SLD, Å^{-2}	X-ray SLD (Cu Kα), Å^{-2}	Weighted neutron SLD, Å^{-2}	Weighted X-ray SLD (Cu Kα), Å^{-2}
D_2O	75	6.3927E-6	9.4546E-6	4.7945E-6	7.09095E-6
Protein (0.8 insoluble/0.2 soluble)	13.75	2.0742E-6	1.2245E-5	2.8521E-7	1.68373E-6
RNA (90 % exchange)	1.0	4.4270E-6	1.5557E-5	4.4270E-8	1.5575E-7
DNA (90 % exchange)	0.3	3.712E-6	1.4634E-5	1.1136E-8	4.3902E-8
Lipids	7.5	1.995E-6	8.9438E-6	1.4963E-7	6.70785E-7
Sugars	1.75	1.64E-6	1.4927E-5	2.870E-8	2.6122E-7
Average-weighted chloroplast SLD (Å^{-2})				5.3510E-6	9.97599E-6

Impact of lumen SLD

It is also important to estimate, what is the impact of lumen SLD to the overall unit cell scattering pattern. To illustrate this, I use the same membrane model data set as before: d_H = 10 Å, d_T = 15 Å, $\Delta\rho_H$ = +0.2, $\Delta\rho_T$ = -0.1. As neither stromal nor lumenal SLD can be calculated precisely, I set stromal SLD to zero and vary the SLD of lumen $\Delta\rho_L$ from 0 to 0.2 - in relation to the stroma. By this I show that the entire SLD profile can be approximated by a 'single box' model in the conditions $\Delta\rho_L = \Delta\rho_H$ or $\Delta\rho_L = \Delta\rho_T$ (Fig. 3.14 a). If $\Delta\rho_L$ is increased, the form factor of full thylakoid unit cell becomes much more disperse - the 'dips' are less sharp and less pronounced (compare light blue and dark blue curves of 3.14 b).

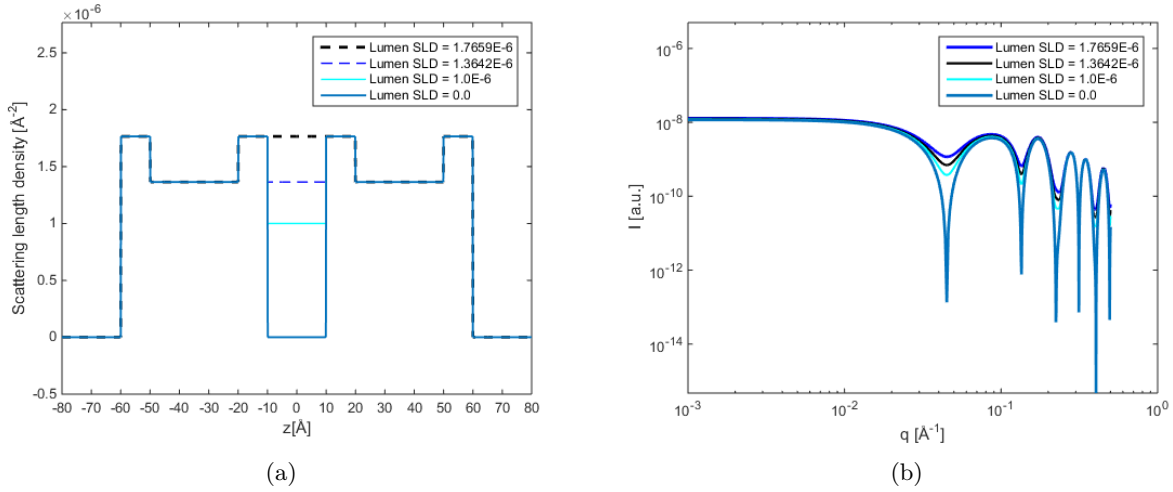

(a) (b)

Figure 3.14: (a) Unit cell appearance with different lumen SLDs. $\Delta\rho_H$ = 1.7659E-6, $\Delta\rho_T$ = 1.3642E-6, $\Delta\rho_T$ as indicated; b) Full thylakoid unit cell form factors with different lumen SLDs

The absolute $\Delta\rho_L$ value can in principle be both positive and negative, both of these situations are depicted in Fig. 3.15. Both situations yield the same form factor (i.e. they are indistinguishable), since the contrast term is squared and sign cancels out. However, these situations have a different biological meaning. In terms of neutron contrast, where $\Delta\rho_S$ becomes $\Delta\rho_S \equiv \rho_S$-$\rho_S = 0$ and $\Delta\rho_L$ becomes $\Delta\rho_L \equiv \rho_L$-$\rho_S$, the negative $\Delta\rho_L$ (calculated relatively to stroma) scenario would mean that there are more proteins in the lumen than in stroma, lumenal proteins are more deuterated or there is less D_2O in the lumen compared to stroma. A positive $\Delta\rho_L$ scenario can also have several explanations: D_2O/H_2O is higher in lumen compared to stroma, degree of protein H-D exchange is higher in lumen, there are less proteins in lumen. This is elaborated in Manuscript 1.

The problems of unknown protein and ion concentrations and volume changes are also valid for lumen - none of these values have been experimentally determined [157].

However, SLD for the inter-thylakoid space ($\Delta\rho_{inter-thylakoid/space}$) is derived as reliably as possible. The $\Delta\rho_{inter-thylakoid/space}$ is set to 0 and $\Delta\rho_L$ is retained as a free fitting parameter in the model. That is, $\Delta\rho_L$ is calculated relatively to the difference between thylakoid membrane scattering ($\mathrm{SLD}_{thylakoid}$ and $\Delta\rho_{inter-thylakoid/space}$, which are slightly easier to calculate) and then the absolute value of SLD_{lumen} is derived by means of scaling. This procedure is elaborated in Manuscript 1.

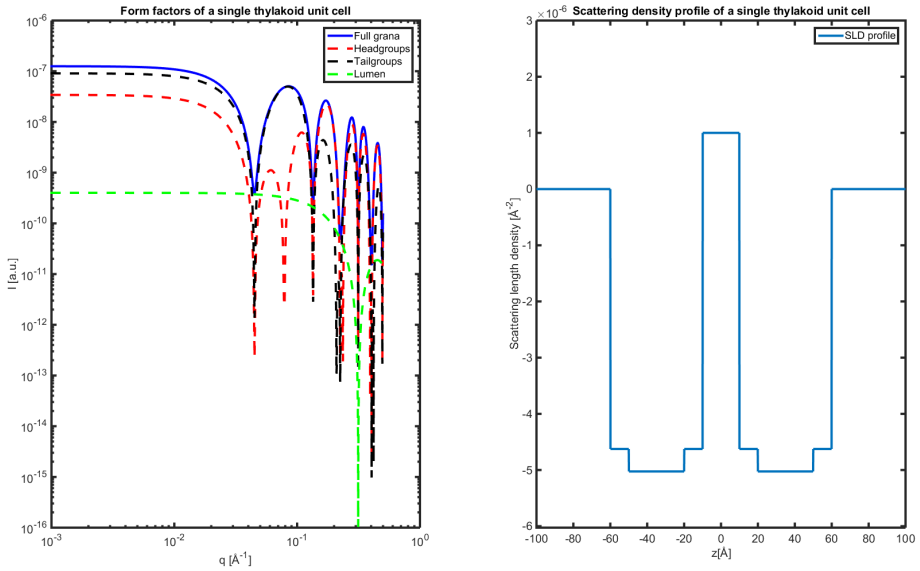

(a)

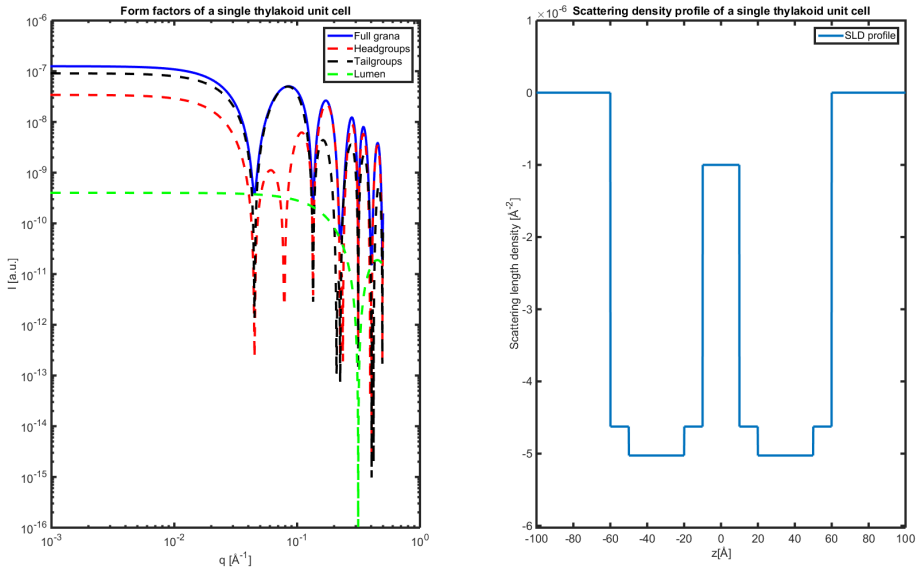

(b)

Figure 3.15: a) Unit cell form factors and scattering density profiles with positive lumen $\Delta\rho_L$ = 1E-6 Å^{-2}; b) Unit cell form factors and scattering density profiles with negative lumen $\Delta\rho_L$ = -1E-6 Å^{-2}

3.4.7 Where does the lipid tail end and the head begin?

A recurrent question is this: the standard neutron SLD of the membrane has a '+-+' profile, where the headgroups have a positive SLD value and the tailgroups have a negative SLD value. As demonstrated from my calculations, I always obtain '+++' membrane profile, in contrary to G. Nagy's '+-+' result. This requires a clarification. The above-raised question seems non-trivial even from the biochemical perspective. The headgroup of thylakoid lipids is added as UDP-Gal (UDP-galactose, one or two times subsequently) or as UDP-SQ (UDP-sulfoquinovose) onto the diacylglycerol molecule (DAG) as the last reaction inside the plastid. The tailgroup is the fatty acid acyl-chain - again with no clear assignment of oxygen atoms of the carboxygroup.

The biochemical differences of G. Nagy's and my calculations are summarized in Fig. 3.16. Ascription of glycerol to the headgroup or tailgroup is not stringently defined. In some modelling papers [60] glycerol is *tacito consensu* considered as a part of a headgroup, but from provided electron density profiles this seems rather an arbitrary choice. For simpler phospholipids, glycerol is also accounted as a part of a headgroup [12], but more stringent biochemical textbooks [201] classify it as a separate entity and **not** as a headgroup. If glycerol SLD is calculated alone ($C_3H_8O_3$, 1.261 g/mL), it has a positive value of $6.13 \cdot 10^{-7}$ Å^{-2}. Due to this inherent uncertaintly of definitions, I do not account for glycerol part (depicted as black arrow in Fig. 3.16) at all in my headgroup-tailgroup calculations. Overall, headgroup definition in this PhD thesis is the molecule part above the green bar and tailgroup definition is the part below the magenta bar in Fig. 3.16, and I consider this to be biochemically correct.

G. Nagy has used a different approach. From the structural perspective, the glycerol part of glycolypid molecule structure is very small. Therefore G. Nagy defined 'headgroup' less stringently. As both galactose and glycerols SLD is positive (although different), he considered both sugar, glycerol and -COO- of the fatty acid parts together as a headgroup (cyano bar in Fig. 3.16). I name this a 'combined galactoglycerol'; using the density of 1 g/mL, it has a positive SLD value. Looking into membrane simulations (Fig. 3.16) from cyanobacteria and higher plants, it is indeed difficult to distinguish a glycerol moiety separately; therefore, its assignment to headgroup is reasonable. In this way, G. Nagy partially avoids ambiguity and has two defined regions - a positive headgroup and a negative tailgroup. If the former is largely acceptable, the second statement is questionable. Fatty acid SLD is simplified to $-CH_2-$, what indeed has a slightly negative SLD value. However, most importantly, fatty acid saturation is not accounted for in G. Nagy's calculations. Indeed, if fatty acid SLD is changed to $-CH-$ (unsaturated carbon), it yields a large positive SLD value both if taken alone and even in largely saturated environment $0.25 \cdot -CH- + 0.75 \cdot -CH_2-$ ($0.045 \cdot 10^{-6}$ Å^{-2}, arbitrary density of 1 g/mL used for this estimation). Since thylakoids contain predominantly unsaturated fatty acids, the overall sign of tails becomes positive, what again supports '+++' profile rather than a traditional '+-+' profile.

The assignment of fatty acid carboxygroup $-COO-$ oxygen atoms to the 'headgroup'

or 'tailgroup' is also a matter of discussion, since one oxygen atom (blue) in the ester comes from the fatty acid and the other (red) comes from the alcohol (glycerol in this case), as shown by reaction mechanism in Fig. 3.12. Therefore, my calculation of $SLD_{tailgroup}$ - if considering applying G. Nagy's approach - can be indeed improved by using R-CO and not R-COO in my $SLD_{fatty\ acid}$ calculations. However, if so, it becomes impossible to determine fatty acid densities precisely (using fatty acid aldehyde densities instead is probably an acceptable solution). In the case when the same density is used for aldehyde and acid, $SLD_{aldehyde}$ becomes lower than SLD_{acid} (exemplified by $-0.161 \cdot 10^{-6}$ vs. $-0.035 \cdot 10^{-6}$ Å^{-2} for palmitic (16:0) and $0.17 \cdot 10^{-6}$ vs. $0.284 \cdot 10^{-6}$ Å^{-2} for hexadecadienoic (16:2) acids) due to oxygen removal, but the overall sign remains unchanged - therefore the overall conclusion of '+++' profile is also unchanged. I did not consider this issue, as I have deliberately omitted glycerol and had to account for both oxygen atoms in tailgroup SLD calculations (as if occurring from fatty acid) in order to make lipid molecule as complete as possible.

Lastly, most of the thylakoid membrane is composed from proteins, having a positive SLD. Therefore, if transmembrane proteins are accounted for ($SLD_{thylakoid\ tailgroup}$= 0.7 $SLD_{thylakoid\ protein}$ + 0.3 $SLD_{lipid\ tailgroup}$), even using $-3.6 \cdot 10^{-7}$ Å^{-2} as lipid acid SLD yields positive overall $SLD_{thylakoid\ tailgroup}$ values. If the absolute SLD values of mine (blue dotted line) and G. Nagy (red dotted line) are compared (Fig. 3.17), the difference between headgroup and tailgroup SLDs is more apparent in G. Nagy's calculations. However, if proteins are accounted for, mine (blue line) and G. Nagy's (red line) SLD values become largely comparable and the profile beholds '+++' character.

3.4.8 The grand SLD summary

Table 3.15 summarizes all calculations of scattering length densities derived above. The SLD values from 0.7/0.3 protein:lipid with 0 % deuteration are used as a starting values for further modelling. Neutron SLD profile of the thylakoid membrane unit cell with absolute values from Table 3.15 is drawn in Fig. 3.14. If the stromal SLD is subtracted from all thylakoid membrane components, the entire SLD profile becomes negative, as depicted in Fig. 3.18. If the lumenal SLD is comparable to stromal SLD, as depicted in Fig. 3.18, the entire SLD profile of a thylakoid is well approximated by the 'double box' model, since SLD difference between the headgroups and tailgroups is not large. From investigating various membrane SLD profiles, it is not uncommon in neutron scattering, that lipid membrane is 'seen' as a single entity - see e.g Fig. 2.5 d) [129].

Importantly, although chloroplast average SLD is slightly lower, it is similar both to stromal average SLD and the SLD of D_2O. This strengthens the argument of exchanging/simplifying stromal SLD with SLD of D_2O in contrast calculations.

To conclude, compared to animal membrane lipids, SLD of individual thylakoid fatty acid chain is higher - due to their predominant polyunsaturation, what yields the average positive tailgroup SLD, especially if it is weight-averaged with proteins. Thylakoid headgroup SLDs derived in this thesis are comparable with those derived by

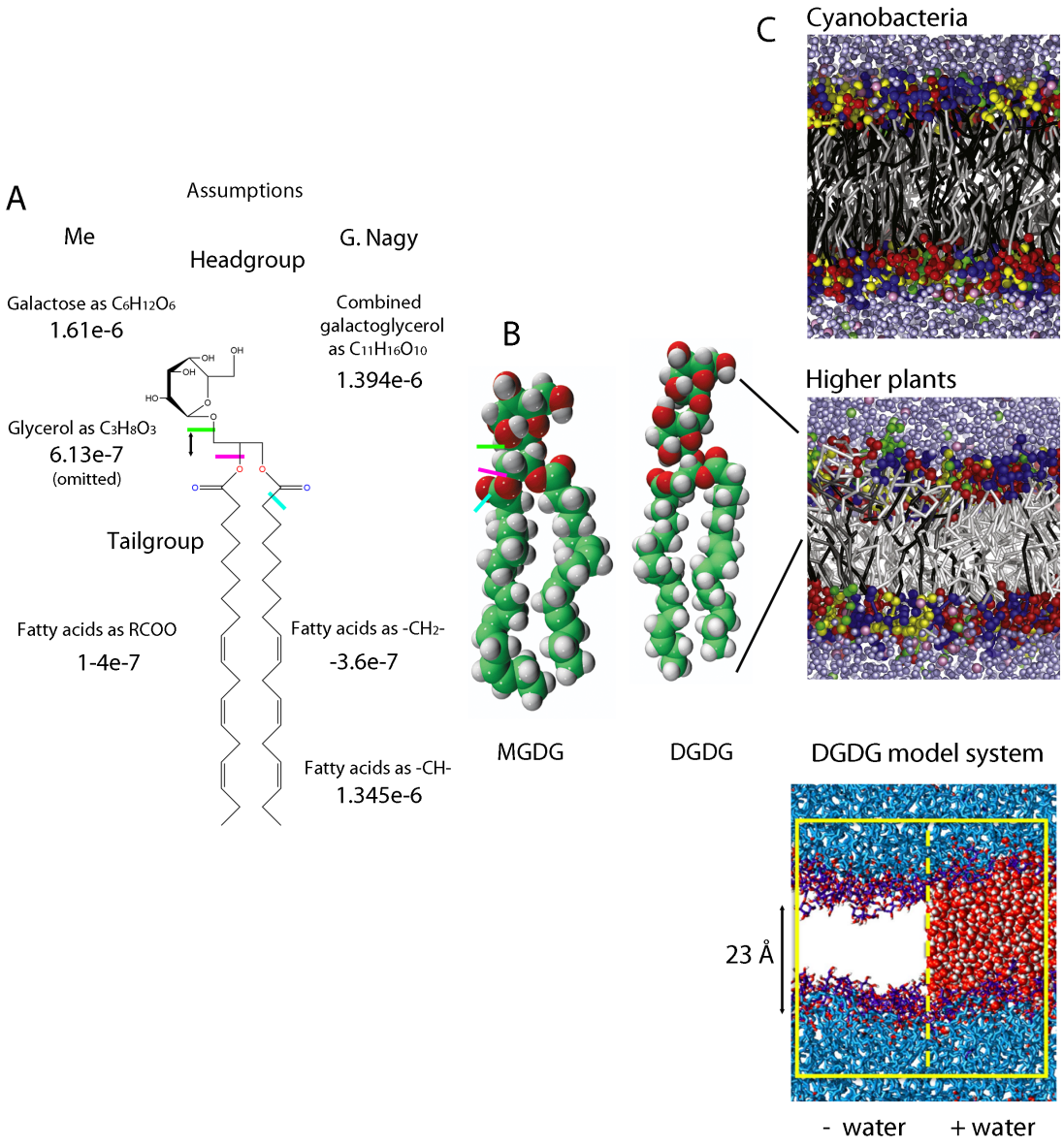

Figure 3.16: a) Comparison of SLD model assumptions from [195] and this work; b) molecular geometries of MGDG and DGDG [23, 22]; c) lipid molecule orientation in cyanobacterial, higher-plant and model DGDG membranes [60, 119].

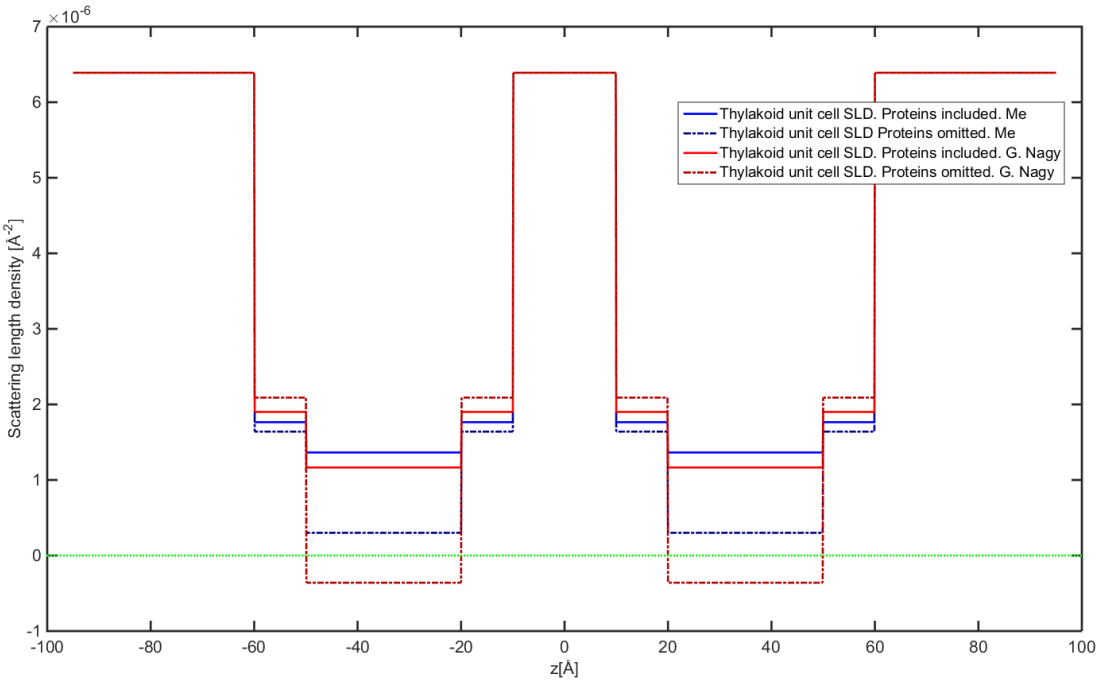

Figure 3.17: Comparison of SLD profiles from G. Nagy and my calculations. Absolute values without proteins - dotted lines, absolute values with proteins - regular lines.

G. Nagy (tailgroups: -0.36 $\cdot 10^{-6}$ Å^{-2}, headgroups: 1.39-2.09 $\cdot 10^{-6}$ Å^{-2} [192]). Overall, G. Nagy uses identical thylakoid lipid composition as a starting point, but his overall SLD pattern with '+-+' resembles membranes of animal origin due to different tailgroup-headgroup definitions - this mathematical conundrum disappears after average-weighting SLD values with proteins. I also argue that the large discrepancy between tailgroup SLDs in derivations is predominantly due to disregarding fatty acid poly-unsaturation in G. Nagy's approach (which is otherwise structurally sound) and needs to be corrected if this approach is pursued.

In conclusion, it is important to emphasize that scattering length densities in this chapter were derived using numerous biologically valid physical simplifications. Therefore obtained numbers are valid as 'the best available estimates', but shall by no means be taken as the absolute constant SLD values. To investigate the issue further, scattering length densities are incorporated as fitting parameters in the scattering model and shall be particularized for individual scattering experiments on cyanobacterial and plant thylakoid membranes.

Table 3.15: Neutron and X-ray SLD values used for modeling

	Neutron SLD, Å^{-2}	X-ray SLD (Cu Kα), Å^{-2}
Lipid headgroups. Plants	1.73E-6	8.98E-6
Lipid tailgroups. Plants	1.36E-6	1.12E-5
Lipid headgroups. Cyanobacteria	1.832E-6	1.34E-5
Lipid tailgroups. Cyanobacteria	1.327E-6	1.12E-5
Inter-thylakoid space average. Cyanobacteria (85/15 % Phycobilisomes/D_2O)	3.612E-6	11.86E-6
Stroma average. D_2O and ions-based	6.36E-6	9.45E-6
Chloroplast average. D_2O and ions-based	5.35E-6	9.98E-6
H_2O	-5.61E-6	9.469E-6
D_2O	6.393E-6	9.455E-6

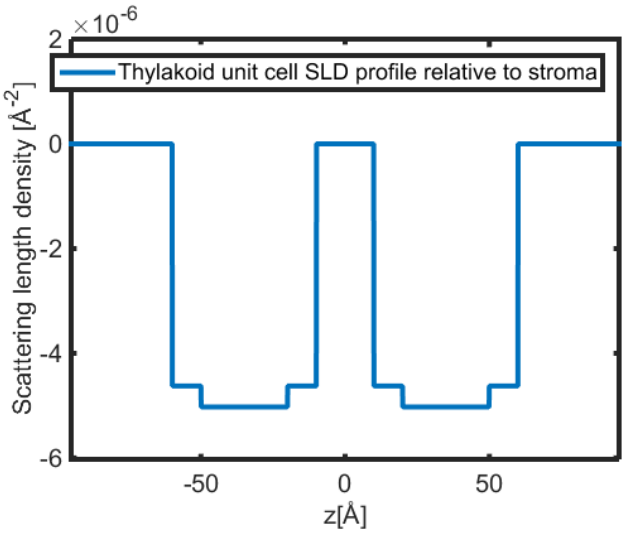

(a)

Figure 3.18: (a) The final model of the thylakoid unit cell, SLD values are relative to stroma: d_H = 10 Å, d_T = 15 Å, d_L = 20 Å, $\Delta\rho_H$ = 1.77E-6 Å^{-2}, $\Delta\rho_T$ = 1.36E-6 Å^{-2}.

Chapter 4

Additional experiments not described in manuscripts

This chapter contains experiments on prolamellar bodies and cyanobacteria, which are not discussed in the manuscripts. The cyanobacterial part of this chapter to a large extent can be considered as supplementary material for Manuscript 1. It provides a detailed statistics on cyanobacterial TEM images, cyanobacterial SANS contrast variation series, the effects of temperature and illumination to wild-type cyanobacterial thylakoid ultrastructure as well as cyanobacterial *Synechocystis* sp. PCC 6803 CURT1 protein mutant studies.

4.1 Investigation of prolamellar bodies

This PhD project started under the name 'Cubic membranes' with a goal to investigate the ultrastructure of prolamellar bodies and their subsequent development to thylakoid membranes by means of scattering. The original project idea was inspired by the earlier works of E. Selstam [304, 254], where SAXS signal has been obtained from PLB isolates, but the exact space group of PLB membrane isolates from maize seedlings experiment could not be ascribed. The original goal was therefore to extend this work: to measure SANS on PLB samples *in vitro* and *in vivo* with the aim to obtain scattering signal from PLBs in D_2O in a much higher resolution, to explain scattering pattern by means of modelling and to extract PLB space group and to calculate its unit cell size unequivocally. The complementary electron microscopy and tomography images on the same samples, would confirm the hexagonal nature of the PLB and provide its ultrastructural information in real space. Furthermore, PLB unit cell dimensions would be calculated from the transmission microscopy images using a Fast Fourier Transformation and the basic lattice motif would be calculated by the help of reverse FFT of the indexed maxima using the MRC software, as described in the poster of Schoefs *et al.* [249]. Unit cell sizes obtained with scattering and TEM techniques in several experimental conditions - e.g. different

pH, salt concentrations, could be compared.

This part of the PhD project led only to a partial success: maize plants, producing paracrystalline PLBs have been selected and cultivated, a subsequent etioplast isolation procedure has been carried out and neutron scattering has been measured. The current isolation protocol is given in detail as Appendix 2 with the aim to further improvements - if considered worthy in the future.

The SAXS signal measured on isolated etioplasts was of insufficient quality, therefore the measurements were uninformative. Such experiments - as I see it now - do require much more concentrated sample, therefore the isolation procedure shall be improved further, maybe including the up-concentration step and drying the PLB pellet. This is easier said than done, as the following steps are needed to perform in the large scale facility in complete darkness and 4-10 ° C, maybe with the use of ultracentrifuge. Overall, some large scale facilities cannot provide a suitable experimental environment for such measurements. Therefore, these seemingly simple practical issues cannot be overcome due to the lack of equipment and/or experimental space.

SANS signal from PLBs, although finally measured and obtained in ANSTO (Sydney, Australia) from both isolated etioplasts and etiolated seedling leaf samples, was also of insufficient quality to unequivocally deduce a space group because of the absence of a clear scattering peak pattern, possibly due to a large peak smearing. Since the PLB space group could not be determined, PLB unit cell size could not be calculated from the q position of the scattering peak, although the peak was observed in *in vitro* samples. Low SANS signal can be caused by the insufficient lipid-protein concentration in the sample or due to inherently worse SANS instrument resolution (7-9 % in SANS vs 0.01 % in SAXS), despite the fact that the contrast between protein-lipid complex of PLB is expected to be higher in 100 % D_2O-based buffers.

Good quality PLB tomograms were obtained and reconstructed with the collaborators from Warsaw University, confirming a hexagonal nature both for PLBs from isolated etioplasts and for PLBs from leaves from etiolated maize seedlings. The FFT analysis of PLB images and unit cell size calculations have not been performed, because the corresponding authors (with the exception of B. Schoefs) of the poster from University of South Bohemia, did not respond to the invitation to collaborate.

The experiments are described in detail below.

4.1.1 Etiolated plant growth conditions

Early vigour maize plants *Zea mays* var. 'Ambition' (Limagrain, Denmark) were selected for experiments. Plant seeds were treated with the antifungal agent mesurol. Seeds were sown in the trays of water-soaked vermiculite and kept in darkness in 27 °C climate chamber with a controlled humidity of 80 % for 10 days. Vermiculite was watered with a tap water once after 5 days. Etiolated maize seedling and the total biomass yield are depicted in Fig. 4.1 a).

For *in vivo* neutron scattering experiments in ANSTO, maize variety Reid's yellow dent and barley (Eden seeds, Australia) were used, additionally coated with the antifungal Thuram. The seedlings of etiolated plants were grown in Brent Kaiser's growth facilities, in ARC Industrial Transformational Research HUB, Centre for Carbon, Water and Food, School of Life and Environmental Sciences, Faculty of Science, University of Sydney, Camden, Australia. The seeds were sown in the trays of water-soaked vermiculite and kept in the darkness, in 28/25 °C (day/night) climate chamber with the controlled humidity of 80/50 % (day/night) and the CO_2 level of 250 ppm for 10 days. Etiolated plant seedlings were transported to ANSTO in a light-impermeable plastic box and kept in room temperature until SANS measurements.

4.1.2 Etioplast/prolamellar body body isolation

PLB isolation protocol from Eva Selstam's lab (Appendix 2) was used to isolate intact etioplasts, and had been subsequently modified. Only the first and second leaves of etiolated maize seedling were plucked. Plucked leaves were stored on ice in aluminium foil- wrapped portions of 50 g, until all leaves had been plucked, the total yield of leaf material was 300-400 g. 50 g of leaves were mixed with 300 mL ice-cold PLB isolation buffer (0.5 M sucrose, 20 mM Tricine, 10 mM HEPES, 50 mM KCl, 5 mM cysteine, pH 8.0). To preserve paracrystalline PLB structure better, Turax/Polytron grinding was not employed. Instead, plant leaves were manually ground using an ice-cold mortar and pestle with the addition of two tablespoons of purified sea sand. Leaf slurry was then filtered with a sandwich of 5 layers of cheesecloth membrane and 2 layers of Miracloth. The filtrate was centrifuged at 3300g for 10 minutes, supernatant discarded. The pellet was resuspended in 40 mL of of isolation buffer and centrifuged again at 4300g for 10 min, supernatant discarded. The pellet was mixed with 0.5 mL of isolation buffer and 5 mL of 0 % sucrose solution (20 mM Tricine, 10 mM HEPES, 50 mM KCl, 1 mM $MgCl_2$, 1 mM EDTA, pH 7.6) was added in order to osmotically break intact etioplasts. Everything was carefully stirred for 3 minutes and 3 mL of 50 % sucrose solution (1.47 M sucrose, 20 mM Tricine, 10 mM HEPES, 50 mM KCl, 1 mM $MgCl_2$, 1 mM EDTA, pH 7.6) was added to restore sucrose concentration. This was diluted with 20 mL of isolation buffer and centrifuged for 20 min at 6000g. The pellet was washed (but not resuspended) twice with a D_2O-based storing buffer (buffer discarded). As a final step, the pellet was resuspended in the D_2O-based storing buffer (50 % sucrose, 20 mM Tricine, 10 mM HEPES, 50 mM KCl and protease inhibitor cOmplete (Sigma-Aldrich), pD 7.6, solvent 100 % D_2O). The samples of isolated etioplasts were flash-frozen in LN_2 and shipped to Australia in 10+ kg dry ice for SANS measurements.

The steps of etioplast pellet treatment with syringe, resuspension in 60 % sucrose buffer (1.7 M sucrose, 20 mM Tricine, 10 mM HEPES, 50 mM KCl, 1 mM $MgCl_2$, 1 mM EDTA, 0.3 mM NADPH, pH 7.6), a subsequent centrifugation in the 46-42-37 % discontinuous sucrose gradient, PLB membrane collection from the 42-37 % gradient interphase, centrifugation at 8100g for 10 min and pellet resuspension in storage buffer

(these steps were present in the original PLB isolation protocol), were omitted. In principle, these steps increase PLB purity, but the final yield is considerably lower, as the PLB pellet in the 42-37 % gradient interphase is very thin. Also, significant part of protein was located in the 46-42 % interphase (visualized by UV fluorescence, Fig. 4.1 b).

Making of the discontinuous sucrose gradient and storage buffer requires 0.3 mM NADPH (2.5 mg/10 mL), what makes every experiment very costly. As elaborated later, 0.3 mM NADPH concentration is too high and can be reduced to 0.1 mM or even omitted (personal communication with Eva Selstam) and there is no documented effect that NADPH preserves the cubic PLB ultrastructure better (see also Appendix 2). Together with the fact that extra NADPH was washed away before SAXS and fluorescence spectrophotometry experiments [253, 253] and paracrystalline structure was observed, the use of excess NADPH in PLB isolation procedure had been discontinued.

Starch content in the leaf slurry filtrate was evaluated after 500g centrifugation for 5 min - no starch pellet was observed, therefore large starch granules were not present the slurry. After etioplast resuspension in final buffer, the remaining pellet was also checked for starch using EtOH-dissolved iodine. Pellet color changed to violet after a prolonged incubation, suggesting that a low concentration of starch was present in etioplast isolates. This is also confirmed by some impurities in the bottom of a discontinuous sucrose gradient (Fig. 4.1 b).

4.1.3 Biochemical studies of isolated etioplasts (prolamellar bodies)

PLB fraction was checked by the Western blot with αPOR and αPSIA antibodies. A qualitative Western blot with a triplicate of isolated etioplast fraction (PLB123) and *Arabidopsis* thylakoid membranes (T) is visualized in Fig. 4.1 c). POR protein was present in etioplasts, but not in thylakoids, whereas PSIA subunit was observed only in thylakoids.

77K fluorescence emission spectrum of isolated etioplasts (Fig.4.2, green) exhibit 633 nm peak (non-photoconvertible POR-PChlide form), 654 nm peak (655 nm correspond to photoconvertible POR-PChlide form), 670 nm shoulder and small 690, 713, 728 nm peaks (correspond to vibrational sublevels) [35]. Etioplasts do not exhibit 688 nm peak (corresponding to POR-Chlide) and no 696 nm peak (Chlide), showing that they were not light-exposed.

Isolated maize PLBs obtained from Eva Selstam, purified around 2008 (Fig.4.2, yellow) and stored in -80 °C were also not light-exposed - the peak of 654 nm, corresponding to a photoconvertible POR-PChlide complex is absent. Instead, their predominant peak is 633 nm. While the photoactive 657 nm Pchlide is a dominant pigment in the prolamellar body membrane and in the soluble etioplast fraction (stroma), the non-photoactive 633 nm Pchlide form is mainly located in the envelope-prothylakoid membranes [135]. This peak becomes apparent after PLB treatment with a high salt concentration or low pH [253], what suggests damage of paracrystalline PLB structure upon prolonged sample

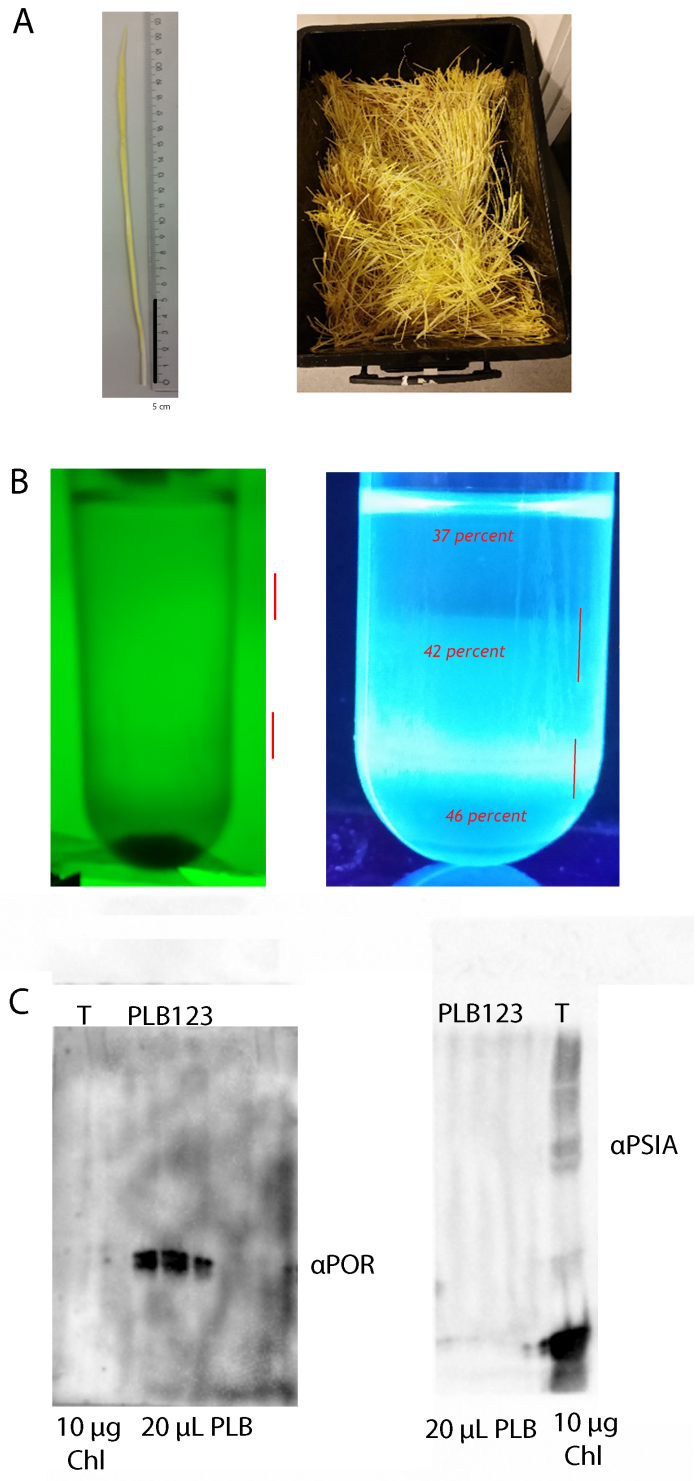

Figure 4.1: a) Zea mays var. 'Ambition' (Limagrain, Denmark) - etiolated seedling and yield of plant material. b) Sucrose gradient with PLBs in safe green and UV light; c) Western blots of PLB and thylakoids with protochlorophyllide oxidoreductase- and PSI-antibodies.